Author's response – Gier et al. bg-2020-170

Response to Anonymous Referee #1

We thank the reviewer for the helpful comments. We have revised the manuscript according to all review comments we have received. A pointwise reply is given below, with the original comments in bold black, and our answers in red.

This is a concise analysis of the current CMIP6-generation emission-driven Earth System Models' ability to reproduce satellite-observed variability characteristics of column-average atmospheric carbon dioxide concentrations (XCO2). The manuscript provides a comparison with the previous generation of models and demonstrates improvement over time as a modeling community. The manuscript also demonstrates that geographic and temporal sampling biases in the satellite observations contribute to an observed negative trend in the amplitude of the seasonal cycle of XCO2. This manuscript is an important documentation of the models' ability to simulate atmospheric CO2 and could be suitable for publication after addressing some of the concerns outlined below.

We thank Referee #1 for the constructive comments which helped to improve the manuscript.

Major Comments:

1. The spatial sampling issues comparing models to satellite obs are addressed in this manuscript, but the temporal issues are only partially addressed. It is not clear what role the presence of cloud cover plays in the results. Satellite observations of column-average CO2 occur over locations with low cloud cover (line 120). One could imagine that some processes – such as stomatal conductance – could vary significantly on cloudy vs. cloud-free days. The model monthly averages however include all model timesteps and are not impacted by the presence of clouds. Some quantitative assessment of this effect is needed to interpret the results of this study. Perhaps reconstructing some monthly averages using a daily or sub-daily cloud mask could help understand whether or not this has a large influence on the comparison between models and satellite observations.

Only monthly frequency CO_2 data is currently available on the ESGF and therefore an analysis as proposed here is not possible at the current time. While it is true that studies have found cloud cover to have an impact on photosynthesis, the response can be fundamentally different for various ecosystems (Still et al., 2009). Cheng et al. (2016) found that "the diffuse light effect from clouds is not as strong of a driver of regional or global ecosystem productivity in temperate ecosystems during the midday as previously suggested in other studies". The satellite data we use is measured at 13:00 local time, which falls into this midday period. Moreover, we would expect a larger effect from the diurnal cycle than the cloud cover with the satellite data measure at 13:00, while the model monthly means are computed using both day and night data. While both of these effects may change the absolute values, their scale should not vary much throughout the years, so that they have no effect on relative changes on growth rate and seasonal cycle amplitude.
We have added this point as a caveat in section 5.3.2. and in the Conclusions as part of the discussion of limitations and future directions.

2. What are the baseline trends in the control simulations for the physical climate and carbon cycle processes that influence atmospheric CO2? Was there an attempt to detrend the models? Why or why not?

We have looked at various variables for a few sample models in the control simulations, and found no significant trend in the physical processes. For CO_2 the trend in the control simulations is negligible compared to the interannual variability, as discussed e.g. by Dunne et al. (2020) for GFDL-ESM4. Therefore, the models have not been detrended. A detailed analysis including all the processes which influence atmospheric CO_2 which you are suggesting here on a per model basis is a study on its own and beyond the scope of this paper.

3. Were multiple model ensemble members from each model considered? The manuscript seems to suggest that only one ensemble member from each model was considered. This point should be clarified and all available ensemble members should be analyzed to get as comprehensive a picture as possible regarding the models' intrinsic variability given the nature of this study and the relatively short time period of analysis.

In CMIP5 only one model performed the future scenario simulations with more than one ensemble member, and therefore we have chosen not to include these. For CMIP6 there are various models with several ensemble members. We have extended Figure 3 (the timeseries) both with additional panels depicting the computed monthly growth rate and detrended seasonal cycle, as well as including all the ensemble members for CMIP6 in it. The multi-model mean shown in this plot only includes the first member for each model. A deeper analysis shows that while there are small differences in the growth rate for different ensembles members, the SCA and its patterns on the map plots are very similar. The inclusion of more ensemble members does not impact the existing analysis and we have therefore elected to only include the first ensemble member for each model in all analysis beyond Figure 3, which gives a good overview of the models intrinsic variability. Using an ensemble mean would average out much of the interannual variability found in each individual member.
We have made this clearer by ending section 2.2 on the model simulations with "For CMIP5, only one model had more than one ensemble member performing the emission driven RCP 8.5 simulation and thus only one ensemble member for each model has been used. In CMIP6, several models have three or more ensemble members. We consider all of them in Figure 3 for the timeseries to show the models' intrinsic variability, but then proceed the analysis with only the first ensemble member for each model, as they perform similarly to each other for the analysis in this paper, and using an ensemble mean would reduce the interannual variability found in each individual member."

4. The conclusions section would benefit from a longer discussion regarding the limitations of the study and future directions. Can the authors make any further recommendations regarding improvements that are needed on either the observational or modeling side to make this comparison better?

We have added a paragraph devoted to the discussion on the limitations and future directions:
"There are several ways to improve on this analysis in the future. With more available future scenario simulations, the analysis can be extended for a longer time series, making use of longer observational timeseries, such as the one introduced in Reuter et al. (2020). Higher temporal resolution of the models would enable studies on the effect of the diurnal cycle of CO_2 on the monthly mean and also allow for the construction of a co-located time series with the Level 2 satellite data. This could help highlight some of the causes of model biases by being able to pinpoint time and space where they occur more precisely. Model biases may also result from the CMIP experimental design, such as requiring the climate state to be in equilibrium in 1850 while the real world may not have been (Bronselaer et al., 2017), or the parametrizations of biological and physical processes not allowing the system to change rapidly enough (Hoffman et al., 2014). Along with a longer time series, newer satellites, such as OCO-2 or the planned Sentinel 7 bring higher resolutions and more data, potentially helping to fill in the gaps and reduce the impact of the sampling we discussed in Section 5.3.2."

Minor Comments:

Line 21: Replace "slightly" with a more quantitative value

Replaced "slightly" with the multi-model mean bias for the growth rate.

Line 40: Unequivocal warming of what? Troposphere?

Changed to "unequivocal warming of the climate system" which was used in the IPCC report used as reference.

Lines 46-48: This sentence has some grammatical issues

Following a suggestion by referee #2 to shorten this part of the introduction, this sentence has been removed.

Line 57: What is meant by "seems to be"

Changed sentence to "Although models do not agree unanimously, the dominant effects are a positive trend in SCA due to the CO_2 fertilization combined with a negative trend due to climate warming."

Line 119: The observational record is already relatively short from a climate perspective. Discarding 2 years seems like a lot. Consider adding in the years if simulations are now available.
While we have been able to add additional models to the analysis, scenario simulations are still not available for all models discussed in this study and have therefore not been included.

Lines 131-133: Consider expanding the discussions as to why these sites were selected
The discussion has been reworded to make the selection process clearer, with stronger critera being mentioned first. "Measurement sites at locations with no available satellite data were excluded from the analysis, which ruled out the four baseline observatories in Mauna Loa, Samoa, as well as the South Pole and Point Barrow sites. Furthermore, sites which did not collect data during the period from 2003–2014 were discarded. From the remaining sites, a sample of five sites was chosen which had the best coverage of different latitudes, and when latitudes were similar, different longitudes were selected for increased spatial coverage. The selected sites are listed in Table 1."

Line 205-206: Consider mentioning these offsets sooner in the paragraph to improve readability.
Swapped this and the previous sentence.

References: Please add data DOIs for all CMIP6 datasets downloaded and analyzed from the ESGF archive.
Data citations with DOIs have been added as the last entry in Table 2 under "References".

Figure Comments:
Figure 3: Is there a way to incorporate linear trend information into this figure?
As mentioned above, we have added additional panels to this figure, showing the growth rate and the detrended seasonal cycle. As the growth rate symbolizes the trend and the mean value with interannual variability is given in Figure 4, we believe this is enough. Adding regression lines and further linear trend information to the time series panel would clutter the figure.

Figures 6a & 6b: Consistent color scale ranges are needed for comparison
Implemented consistent color scale for both CMIP ensembles. We have also changed the color scale to the non-divergent newly implemented one used for the top panels of Figure 6 (formerly 7) for consistency.

Figures 7a and 8a: A non-diverging color scale for the top panels could make it easier to contrast against the information contained in the bottom panels
Changed the color scale to a non-divergent one for the top panels in Figure 6 (formerly 7).

References

Bronselaer, B., Winton, M., Russell, J., Sabine, C. L., and Khatiwala, S.: Agreement of CMIP5 Simulated and Observed Ocean Anthropogenic CO2 Uptake, Geophys Res Lett, 44, 12,298-212,305, 10.1002/2017gl074435, 2017.

Cheng, S. J., Steiner, A. L., Hollinger, D. Y., Bohrer, G., and Nadelhoffer, K. J.: Using satellite-derived optical thickness to assess the influence of clouds on terrestrial carbon uptake, Journal of Geophysical Research: Biogeosciences, 121, 1747-1761, 10.1002/2016jg003365, 2016.

Dunne, J. P., Horowitz, L. W., Adcroft, A. J., Ginoux, P., Held, I. M., John, J. G., Krasting, J. P., Malyshev, S., Naik, V., Paulot, F., Shevliakova, E., Stock, C. A., Zadeh, N., Balaji, V., Blanton, C., Dunne, K. A., Dupuis, C., Durachta, J., Dussin, R., Gauthier, P. P. G., Griffies, S. M., Guo, H., Hallberg, R. W., Harrison, M., He, J., Hurlin, W., McHugh, C., Menzel, R., Milly, P. C. D., Nikonov, S., Paynter, D. J., Ploshay, J., Radhakrishnan, A., Rand, K., Reichl, B. G., Robinson, T.,

Schwarzkopf, D. M., Sentman, L. T., Underwood, S., Vahlenkamp, H., Winton, M., Wittenberg, A. T., Wyman, B., Zeng, Y., and Zhao, M.: The GFDL Earth System Model version 4.1 (GFDL-ESM 4.1): Overall coupled model description and simulation characteristics, J Adv Model Earth Sy, n/a, e2019MS002015, 10.1029/2019ms002015, 2020.

Hoffman, F. M., Randerson, J. T., Arora, V. K., Bao, Q., Cadule, P., Ji, D., Jones, C. D., Kawamiya, M., Khatiwala, S., Lindsay, K., Obata, A., Shevliakova, E., Six, K. D., Tjiputra, J. F., Volodin, E. M., and Wu, T.: Causes and implications of persistent atmospheric carbon dioxide biases in Earth System Models, J Geophys Res-Biogeo, 119, 141-162, 10.1002/2013jg002381, 2014.

Reuter, M., Buchwitz, M., Schneising, O., Noël, S., Bovensmann, H., Burrows, J. P., Boesch, H., Di Noia, A., Anand, J., Parker, R. J., Somkuti, P., Wu, L., Hasekamp, O. P., Aben, I., Kuze, A., Suto, H., Shiomi, K., Yoshida, Y., Morino, I., Crisp, D., O'Dell, C. W., Notholt, J., Petri, C., Warneke, T., Velazco, V. A., Deutscher, N. M., Griffith, D. W. T., Kivi, R., Pollard, D. F., Hase, F., Sussmann, R., Té, Y. V., Strong, K., Roche, S., Sha, M. K., De Mazière, M., Feist, D. G., Iraci, L. T., Roehl, C. M., Retscher, C., and Schepers, D.: Ensemble-based satellite-derived carbon dioxide and methane column-averaged dry-air mole fraction data sets (2003–2018) for carbon and climate applications, Atmos. Meas. Tech., 13, 789-819, 10.5194/amt-13-789-2020, 2020.

Still, C. J., Riley, W. J., Biraud, S. C., Noone, D. C., Buenning, N. H., Randerson, J. T., Torn, M. S., Welker, J., White, J. W. C., Vachon, R., Farquhar, G. D., and Berry, J. A.: Influence of clouds and diffuse radiation on ecosystem-atmosphere CO2 and CO18O exchanges, Journal of Geophysical Research: Biogeosciences, 114, 10.1029/2007jg000675, 2009.

Response to Anonymous Referee #2

We thank the reviewer for the helpful comments. We have revised the manuscript according to all review comments we have received. A pointwise reply is given below, with the original comments in bold black, and our answers in red.

This study used satellite-observed column-average CO2 (XCO2) to evaluate how well the current generation of earth system models reproduces atmospheric CO2 variability. The authors compared spatially resolved model simulations of XCO2 with observed XCO2 in terms of biases, growth rates, seasonal cycle amplitudes (SCA), and trends in SCA. They found that most models overestimate XCO2 and the growth rates of XCO2, but underestimate the seasonal amplitudes of XCO2. The study is novel and interesting, and could be considered for publication after concerns are addressed.

We thank Referee #2 for the constructive comments which helped to improve the manuscript.

General comments

1. The apparent "trend reversal" of SCA in satellite XCO2 caused by the sampling coverage bias raises an important question whether other characteristics of the observed XCO2 were subject to the same bias. It seems that the "sampled" vs. "unsampled" comparison was done only for the trend in SCA. Would this comparison give different results for the growth rate of XCO2?

As mentioned in section 5.2. the spatial variability of the growth rate is small. We did analyze the sampling on the other considered quantities, but found no significant sampling impact on the growth rate. We have also added a panel to Figure 3 which depicts the mean monthly growth rate, and while the change from the satellites is visible in these monthly rates in 2009, this is due to the way in which it is calculated and averaged out in the annual values. The annual growth rates of the satellite dataset have been found to correlate well (correlation coefficient of 0.82) with the NOAA global growth rates (Buchwitz et al., 2018). We have added the sentence "No significant changes to the annual growth rates due to the satellite spatial coverage have been found." in section 5.2 to clarify this.

2. Although the effect of different spatial coverage between the two instruments has been addressed in Figs. 9 and 10, there has been no mention of whether the measurement scales of XCO2 were calibrated between the two instruments. This could be another source of bias. During the overlapping period, did SCIAMACHY and GOSAT measurements agree well with each other?

The joint time series is computed using the Ensemble Median Algorithm (EMMA, Reuter et al. (2013);Reuter et al. (2020)), which includes a bias correction to all products during overlap phases, resulting in a good agreement during the overlap period. This bias correction is shown in Figure 5 of (Reuter et al., 2020).

3. In addition to the spatial distribution of SCA shown in Fig. 6, it would also be interesting to compare the simulated latitudinal gradients (i.e., the zonal mean) of SCA from different models on the same plot.

We have added zonal mean panels to the map plots in Figure 6. They show the increase of SCA with increasing latitude for all models, with growth spurts around the equator and in the midlatitudes for most models.

4. Given that there was no correlation between the growth rate and the growing-season temperature anomaly in the *observations* (Fig. 5), I'm not convinced that a robust emergent constraint relationship can be established for the period of 2003–2014. Note that this is different from Fig. 2 in Cox et al. (2013) Nature in which a clear correlation is seen in the observations. In the absence of a relationship of the same kind in the observations, one could not distinguish a real emergent constraint from an artifact of model assumptions. It may as well exist for a longer period with more data, but we couldn't tell. I suggest moving the paragraph of P8L248–P9L263 as well as Fig. 5 to the supplement.

We agree with this assessment, as discussed in l. 257-259 - “This shows that the time period 2003–2014 is not sufficient to reproduce the emergent constraint, but it might be feasible once CMIP6 emission driven future simulations are available for a longer time overlap between models and observations". We have moved this paragraph and its accompanying Figure to Appendix C.

5. In all figures that show a regression line, it would be better to show both the Pearson correlation and the p-value.

p-values have been added next to the Pearson correlation coefficient in the bottom right of the panels.

6. The study would benefit from a more structured discussion of lessons learned from model evaluation, for example, what the likely causes of model biases in XCO2 and the SCA of XCO2 would be. There are some good points made in section 5.3 and the summary, which could be better organized.

Following a suggestion from Referee #1 we have added a paragraph devoted to the discussion on the limitations and future directions, which should include some of these points.

“There are several ways to improve on this analysis in the future. With more available future scenario simulations, the analysis can be extended for a longer time series, making use of longer observational timeseries, such as the one introduced in Reuter et al. (2020). Higher temporal resolution of the models would enable studies on the effect of the diurnal cycle of CO_2 on the monthly mean and also allow for the construction of a co-located time series with the Level 2 satellite data. This could help highlight some of the causes of model biases by being able to pinpoint time and space where they occur more precisely. Model biases may also result from the CMIP experimental design, such as requiring the climate state to be in equilibrium in 1850 while the real world may not have been (Bronselaer et al., 2017), or the parameterizations of biological and physical processes not allowing the system to change rapidly enough (Hoffman et al., 2014). Along with a longer time series, newer satellites, such as OCO-2 or the planned Sentinel 7 bring higher resolutions and more data, potentially helping to fill in the gaps and reduce the impact of the sampling we discussed in Section 5.3.2.“.

Specific comments

• Abstract: The abstract is quite long and technical. Describe the major findings concisely and leave nonessential details to the main text.

We have shortened the abstract by removing several of the technical sentences which are not required to understand the results.

• P1L20: The multi-model means give a feeling that CMIP6 models had a great improvement relative to CMIP5 models. But a closer look at Fig. 3 would tell that this was mainly because negative biases canceled positive biases. I suggest adding the multi-model standard deviations of the bias (or other statistics that characterize the spread) in parentheses.

We have added the full model spread alongside the means.

• P1L25–32: The “trend reversal” in SCA caused by sampling bias is not clear on a first reading. It would be helpful to write this in a way that is less entangled.

We have rewritten this part as follows to make it clearer: “While the combined satellite product shows a strong negative trend of decreasing effective SCA with increasing XCO_2 in the northern midlatitudes, both CMIP ensembles instead show a non-significant positive trend in the multi-model mean. The negative trend is reproduced by the models when sampling them as the observations, attributing it to sampling characteristics. Applying a mask of the mean data coverage of each satellite to the models, the effective SCA is higher for the SCIAMACHY/ENVISAT mask than when using the TANSO-FTS/GOSAT mask. This induces an artificial negative trend when using observational sampling over the full period, as SCIAMACHY/ENVISAT covers the early period until 2012, with TANSO-FTS/GOSAT measurements starting in 2009.”

• P2L46–60: If the purpose of this paragraph is to introduce SCA, then the first few sentences seem quite redundant. Better get to the point straight away.

We have rewritten this part to be a more concise introduction of SCA: "Photosynthesis causes a net uptake of atmospheric CO_2 and thus declining atmospheric CO_2 concentrations in the growing season. Conversely, atmospheric CO_2 concentrations rise throughout the dormant season when there is a net release of CO_2 from the land due to decomposition of organic matter in soils. This uptake and release of carbon by the terrestrial biosphere throughout the year causes a seasonal cycle of atmospheric CO_2 (Keeling et al., 1989)."

• P2L64: Missing Ciais et al., 2013 in the References.

Fixed issue which resulted in reference not showing in the bibliography, thank you for spotting this.

• P3L65: "downlooking" → "downward-looking"

Changed.

• P3L89–90: "such as a general overestimation of photosynthesis [relative to datadriven models]." We don't know the magnitude of the global photosynthesis with certainty. The number could range from 112 to 169 PgC yr-1 (Ryu et al., 2019, RSE). The MTE GPP data product (Jung et al., 2011, JGR) that was used to evaluate the CMIP models would sit near the lower end of this range.

We have added this as a caveat and added the example of the overestimated leaf area index." such as a general overestimation leaf area index and photosynthesis. However, the magnitude of the global photosynthesis is not well constrained by observations, with estimates ranging between 112 and 169 PgC yr^{-1} (Ryu et al., 2019), with the dataset used by Anav et al. (2013) is on the lower end of this range."

P5L131: Missing Dlugokencky et al., 2018 in the References.

Updated this reference to newer version and solved issue preventing it from showing in bibliography, thank you for spotting this.

• P7L203: "parameters" → "variables"

Changed.

• P7L205: Surface observations sample the air within or closer to the boundary layer, and therefore may have a larger seasonal swing.

The larger seasonal swing and thus higher seasonal cycle amplitude at the surface is discussed in the next paragraph. L205 was referring to the total offset of the mean, as evident most clearly in the Cape Grim and Hegyhatsal stations, comparing the blue (station) and red (model surface) curves.

• P8L241: What is the correlation between the observed GR and the multi-model mean GR?

The correlation between the observed and multi-model mean annual GR is 0.48 in CMIP6 and 0.07 in CMIP5, which is higher than most the models. We have added this to the paragraph.

• P9L256: The increase of GR sensitivity to temperature after including 2015 and 2016 data could have been due to El Niño.

This is true and has been added as a note in this sentence (now in the Appendix), as well as mentioned as a reason for suggesting that the timeseries is not long enough to support trying to reproduce this emergent constraint.

• Table 1: Use whole numbers in the "Altitude" column.

Changed to whole numbers.

• Figure 2: I suggest lightening the gray background to prevent it from interfering with the reading of the curves.

Changed the color of the land areas of the underlaying map plot to a very light grey.

• Figure 3: It seems that after detrending, the seasonal variability in the multimodel mean XCO2 would match quite well with that in the observed XCO2, and better than the seasonal variability in any individual models. I wonder what the correlation coefficients would be.

We have extended this figure with panels showing the calculated monthly growth rate and the detrended seasonal cycle. The correlation between the detrended seasonal cycle of the multi-model mean to the observations is 0.98 in CMIP6 and 0.93 in CMIP5. in CMIP6 this is the best correlation, the closest models have a correlation of 0.96 (MRI-ESM2-0 and GFDL-ESM4). For CMIP6 a few models are close and a bit higher than the multi-model mean with 0.93 for NorESM1-ME and MIROC-ESM, 0.94 for MRI-ESM1 and 0.95 for MPI-ESM-LR. So the multi-model mean in CMIP6 indeed captures the seasonal variability better than any individual model.

• Figure 4: I think ranking the models by their average growth rates, from low to high, would make the figure clearer.

Models are now ranked from low to high in the barplot.

• Figures 6a and 6b: Why not use the same scale? One could reserve the purple region of the colormap for the high SCA values from MPI-ESM-LR. This would not affect other models that have values represented in colors from blue to red.

We have adjusted the scale to be the same for both figures. We have furthermore changed the colormap to a non-diverging one, which was requested by Referee #1 for the top panels in figure 6 (formerly 7) to contrast the bottom panels showing the differences. This colormap has been adapted for Figure 5 (formerly 6) as well for consistency.

References

Anav, A., Friedlingstein, P., Kidston, M., Bopp, L., Ciais, P., Cox, P., Jones, C., Jung, M., Myneni, R., and Zhu, Z.: Evaluating the Land and Ocean Components of the Global Carbon Cycle in the CMIP5 Earth System Models, J Climate, 26, 6801-6843, 10.1175/Jcli-D-12-00417.1, 2013.

Bronselaer, B., Winton, M., Russell, J., Sabine, C. L., and Khatiwala, S.: Agreement of CMIP5 Simulated and Observed Ocean Anthropogenic CO2 Uptake, Geophys Res Lett, 44, 12,298-212,305, 10.1002/2017gl074435, 2017.

Buchwitz, M., Reuter, M., Schneising, O., Noel, S., Gier, B., Bovensmann, H., Burrows, J. P., Boesch, H., Anand, J., Parker, R. J., Somkuti, P., Detmers, R. G., Hasekamp, O. P., Aben, I., Butz, A., Kuze, A., Suto, H., Yoshida, Y., Crisp, D., and O'Dell, C.: Computation and analysis of atmospheric carbon dioxide annual mean growth rates from satellite observations during 2003-2016, Atmos Chem Phys, 18, 1-22, 10.5194/acp-18-17355-2018, 2018.

Hoffman, F. M., Randerson, J. T., Arora, V. K., Bao, Q., Cadule, P., Ji, D., Jones, C. D., Kawamiya, M., Khatiwala, S., Lindsay, K., Obata, A., Shevliakova, E., Six, K. D., Tjiputra, J. F., Volodin, E. M., and Wu, T.: Causes and implications of persistent atmospheric carbon dioxide biases in Earth System Models, J Geophys Res-Biogeo, 119, 141-162, 10.1002/2013jg002381, 2014.

Keeling, C. D., Bacastow, R. B., Carter, A. F., Piper, S. C., Whorf, T. P., Heimann, M., Mook, W. G., and Roeloffzen, H.: A three-dimensional model of atmospheric CO2transport based on observed winds: 1. Analysis of observational data, in: Aspects of Climate Variability in the Pacific and the Western Americas, Geophysical Monograph Series, 165-236, 1989.

Reuter, M., Bösch, H., Bovensmann, H., Bril, A., Buchwitz, M., Butz, A., Burrows, J. P., amp, apos, Dell, C. W., Guerlet, S., Hasekamp, O., Heymann, J., Kikuchi, N., Oshchepkov, S., Parker, R., Pfeifer, S., Schneising, O., Yokota, T., and Yoshida, Y.: A joint effort to deliver satellite retrieved atmospheric CO2 concentrations for surface flux inversions: the ensemble median algorithm EMMA, Atmos Chem Phys, 13, 1771-1780, 10.5194/acp-13-1771-2013, 2013.

Reuter, M., Buchwitz, M., Schneising, O., Noël, S., Bovensmann, H., Burrows, J. P., Boesch, H., Di Noia, A., Anand, J., Parker, R. J., Somkuti, P., Wu, L., Hasekamp, O. P., Aben, I., Kuze, A., Suto, H., Shiomi, K., Yoshida, Y., Morino, I., Crisp, D., O'Dell, C. W., Notholt, J., Petri, C., Warneke, T., Velazco, V. A., Deutscher, N. M., Griffith, D. W. T., Kivi, R., Pollard, D. F., Hase, F., Sussmann, R., Té, Y. V., Strong, K., Roche, S., Sha, M. K., De Mazière, M., Feist, D. G., Iraci, L. T., Roehl, C. M., Retscher, C., and Schepers, D.: Ensemble-based satellite-derived carbon dioxide and methane column-averaged dry-air mole fraction data sets (2003–2018) for carbon and climate applications, Atmos. Meas. Tech., 13, 789-819, 10.5194/amt-13-789-2020, 2020.

Ryu, Y., Berry, J. A., and Baldocchi, D. D.: What is global photosynthesis? History, uncertainties and opportunities, Remote Sens Environ, 223, 95-114, https://doi.org/10.1016/j.rse.2019.01.016, 2019.

Relevant changes to the manuscript

1. Added 3 additional CMIP6 models: CanESM5-CanOE, CNRM-ESM2-1, MIROC-ES2L
   → All figures updated accordingly

Suggested by reviewers:

2. Further figure changes:
   a. updated colormap for SCA panels, matched scale for CMIP5 and CMIP6
   b. sorted histogram by values
   c. included p-value for all figures with regression lines
3. Changed figure 3 to not only show timeseries, but also decomposed time series into growth rate and seasonal cycle.
4. Moved investigation of Cox et al. emergent constraint (Trend of growing season temperature and interannual variability of CO_2 growth rate) to Appendix C
5. Shortened abstract
6. Added paragraph to conclusions about limitations and future directions
7. Added several caveats brought up by reviewers

Spatially resolved evaluation of Earth system models with satellite column averaged CO_2

Bettina K. Gier[1,2], Michael Buchwitz[1], Maximilian Reuter[1], Peter M. Cox[3], and Pierre Friedlingstein[3,4], Veronika Eyring[2,1]

[1]University of Bremen, Institute of Environmentral Physics (IUP), Bremen, Germany
[2]Deutsches Zentrum für Luft- und Raumfahrt (DLR), Institut für Physik der Atmosphäre, Oberpfaffenhofen, Germany
[3]College of Engineering, Mathematics and Physical Sciences, University of Exeter, Exeter, EX4 4QE, United Kingdom
[4]LMD/IPSL, ENS, PSL Université, ~~École~~École Polytechnique, Institut Polytechnique de Paris, ~~Srobonne~~Sorbonne Université, CNRS, Paris, France

Correspondence to: Bettina K. Gier (gier@uni-bremen.de)

Abstract. Earth System Models (ESMs) participating in the Coupled Model Intercomparison Project Phase 5 (CMIP5) showed large uncertainties in simulating atmospheric CO_2 concentrations. ~~By comparing the simulations with satellite observations, in this study we find slight improvements in the ESMs participating in the new Phase 6 (CMIP6) compared to CMIP5.~~ We utilize the Earth System Model Evaluation Tool (ESMValTool) to evaluate emission driven CMIP5 and CMIP6 simulations with satellite data of column-average CO_2 mole fractions (XCO_2). XCO_2 time series show a large spread among the model ensembles both in CMIP5 and CMIP6. Compared to the satellite observations, the models have a bias of +25 to -20 ppmv in CMIP5 and +20 ppmv to -15 ppmv in CMIP6, with the multi-model mean biases at +10 ppmv and +2 ppmv respectively. The derived mean atmospheric XCO_2 growth rate (GR) of 2.0 ppmv yr^{-1} is overestimated by 0.4 ppmv yr^{-1} in CMIP5 and 0.3 ppmv yr^{-1} in CMIP6 for the multi-model mean, with a good reproduction of the interannual variability. All models capture the expected increase of the seasonal cycle amplitude (SCA) with increasing latitude, but most models underestimate the SCA. Any SCA derived from data with missing values can only be considered an "effective" SCA, as the missing values could occur at the peaks or troughs. The satellite data are a combined data product covering the period 2003–2014 based on the SCIAMACHY/ENVISAT (2003–2012) and TANSO-FTS/GOSAT (2009–2014) instruments. ~~In this study the Observations for Model Intercomparisons Project (Obs4MIPs) format data product version 3 (O4Mv3) with a spatial resolution~~ While the combined satellite product shows a strong negative trend of ~~5° x 5° and monthly time resolution has been used. Comparisons of~~ decreasing effective SCA with increasing XCO_2 ~~time series show a large spread among~~ in the ~~model~~northern midlatitudes, both CMIP ensembles ~~both in CMIP5 and CMIP6, with differences~~ instead show a non-significant positive trend in the ~~absolute concentrations of up to approximately 20 ppmv relative to the satellite observations. The~~ multi-model mean ~~has a bias of approximately +10 and +2 ppmv in CMIP5 and CMIP6, respectively. The derived atmospheric XCO_2 growth rate (GR) is typically slightly overestimated in the models, with a slightly better average and lower spread for CMIP6. The interannual variability of the growth rate is well reproduced in the multi-model mean~~. The ~~. All models capture the expected increase of the seasonal cycle amplitude (SCA) with increasing latitude, but most models underestimate the SCA. Most models from both ensembles show a positive trend of the SCA over the period 2003–2014, i.e. an increase of the SCA with XCO_2, similar to in~~

situ ground-based measurements. In contrast, the combined satellite product shows a negative trend over this period. Any SCA derived from sampled data can only be considered an "effective" SCA, as sampling can remove the peaks or troughs. This negative trend can beis reproduced by the models when sampling them as the observations. The average , attributing it to sampling characteristics. Applying a mask of the mean data coverage of each satellite to the models, the effective SCA in the models is higher when usingfor the SCIAMACHY/ENVISAT instead ofmask than when using the TANSO-FTS/GOSAT mean data coverage mask, overall leading to amask. This induces an artificial negative trend when using observational sampling over the full period similar to the combined satellite product. Models with a larger difference in the average effective SCA between the two coverages also show a stronger trend reversal. Therefore, this trend reversal in the satellite data is due to sampling characteristics, more specifically the different data coverage of the two satellites that can be reproduced by the models if sampled the same way., as SCIAMACHY/ENVISAT covers the early period until 2012, with TANSO-FTS/GOSAT measurements starting in 2009. Overall, the CMIP6 ensemble shows better agreement with the satellite data than the CMIP5 ensemble in all considered quantities (XCO_2, GR, SCA and trend in SCA), with the biggest improvement in the mean XCO_2 content of the atmosphere.). This study shows that the availability of column-integral CO_2 from satellite provides a promising new way to evaluate the performance of Earth System Models on a global scale, complementing existing studies that are based on in situ measurements from single ground-based stations.

1 Introduction

The Intergovernmental Panel on Climate Change (IPCC) Fifth Assessment Report (AR5) concluded that since 1950 many of the observed changes in the climate system are unprecedented in the instrument record, confirming an unequivocal warming of the climate system (IPCC, 2013). Increasing emissions of greenhouse gases (GHGs) are the key drivers of anthropogenic climate change. The most important anthropogenic greenhouse gas is carbon dioxide (CO_2), with CO_2 emissions contributing more than half of the total global radiative forcing in 2011 relative to 1750 (IPCC, 2013). It is therefore important to monitor the long-term changes in atmospheric CO_2 concentrations, to understand the sources and sinks of carbon, and to provide reliable projections of future CO_2 concentrations under various scenarios.

Plants absorb CO_2 while performing photosynthesis. This CO_2 is later partially released by autotrophic respiration, or after cycling through plant tissues, litter and soil carbon, is released through heterotrophic respiration by soil microbial decomposition, animals and other processes like forest fires. Photosynthesis is dominant in the growing season, resulting incauses a net uptake of atmospheric CO_2 and thus declining atmospheric CO_2 concentrations in the northern hemispheric growing season. Conversely, atmospheric CO_2 concentrations rise throughout the northern hemispheric dormant season when there is a net release of CO_2 from the land due to decomposition of organic matter in soils. This uptake and release of carbon by the terrestrial biosphere throughout the year causes a seasonal cycle of atmospheric CO_2, with a minimum at the end of the northern hemispheric growing season and a maximum at the end of the northern hemispheric dormant season (Keeling et al., 1989). The seasonal cycle amplitude (SCA) has been increasing over the last 50 years, with higher increases in higher latitudes

(Barnes et al., 2016; Graven et al., 2013; Yin et al., 2018; Keeling et al., 1995; Keeling et al., 1996; Myneni et al., 1997; Piao et al., 2018). A number of studies have explored the effects of CO_2 fertilization, land-use change and climate warming on the SCA (Bastos et al., 2019; Zhao et al., 2016; Fernández-Martínez et al., 2019). Although models do not agree unanimously, the dominant ~~effect seems to be~~effects are a positive trend in SCA due to the CO_2 fertilization combined with a negative trend due to climate warming. Some models however show a large positive trend due to climate warming (Zhao et al., 2016). Land-use is found to be a weaker effect in comparison to CO_2 fertilization and climate warming (Bastos et al., 2019; Fernández-Martínez et al., 2019).

Most long-term measurements of CO_2 are from ground-based stations. In situ ground-based measurements at Mauna Loa (Hawaii, USA) started in 1958, providing the first evidence that fossil fuel combustion leads to a measurable increase in atmospheric CO_2 concentrations (Keeling et al., 1976). Other observatories around the globe now also measure atmospheric CO_2, reporting an increase of about 45% since pre-industrial times (Ciais et al., 2013; Friedlingstein et al., 2019).

Satellite measurements of CO_2, with first near-infrared/short-wave-infrared (NIR/SWIR) nadir (~~downlooking~~downward-looking) based satellite retrievals starting in 2002, can complement the ground-based measurement network and provide regional and spatial distributions of CO_2. The quantity obtained from measurements with NIR/SWIR satellite instruments is the column-average dry-air mole fraction of atmospheric CO_2, denoted as XCO_2. XCO_2 is a dimensionless quantity defined as the vertical column of CO_2 divided by the vertical column of dry air (i.e., all air molecules except water vapor) often given in ppmv (parts per million per volume). An analysis of growth rates (GR) and seasonal cycle amplitude (SCA) from satellite data and their sensitivity to growing season temperature anomaly presented in Schneising et al. (2014) shows a negative correlation between SCA and growing season temperature anomaly for the period 2003–2011, which was confirmed by Yin et al. (2018) for SCA anomaly in this timeframe. Satellite XCO_2 products are often used in combination with atmospheric transport inverse modelling approaches to obtain information on surface fluxes by using a global or regional transport model with free fit parameters (Basu et al., 2013; Houweling et al., 2015; Reuter et al., 2014; Chevallier et al., 2014). The satellite data can also be used to constrain process parameters of a terrestrial biosphere model, e.g., as part of a Carbon Cycle Data Assimilation System (CCDAS, e.g. Kaminski et al. (2013)), and have been used for the evaluation of chemistry-climate models (Hayman et al., 2014; Shindell et al., 2013). In the last few years, satellite data have also been used in direct comparison to output from climate models (e.g. Calle et al., 2019) characterizing rise and fall segments in seasonal cycles from GOSAT and comparing them to model output.

A large ensemble of climate model simulations for different type of experiments under common forcings is provided by the Coupled Model Intercomparison Project (CMIP), with output available for CMIP5 (Taylor et al., 2012) and more recently Phase 6 (CMIP6, Eyring et al. (2016a)). ESMs produce a large range in projected atmospheric CO_2, as a result of uncertainties in the future evolution of natural fluxes (Arora et al., 2013; Friedlingstein et al., 2006). Overall CMIP5 models overestimate the carbon content of the atmosphere (Friedlingstein et al., 2014; Hoffman et al., 2014). The largest uncertainties are associated with the response of the land carbon cycle to changes in climate and atmospheric CO_2 (Friedlingstein et al., 2014; Hajima et al., 2014). The ability of ESMs to simulate the land and ocean contemporary carbon cycle has previously been investigated by

Anav et al. (2013). They showed that most models were able to correctly reproduce the main climatic variables and their seasonal evolution, but found weaknesses in reproducing specific biogeochemical fields, such as a general overestimation ~~of photosynthesis. For CMIP6, Arora et al. (2019) analyzed simulations with a CO_2 increase of 1 % per year to quantify the carbon-climate feedbacks.~~leaf area index and photosynthesis. However, the magnitude of the global photosynthesis is not well constrained by observations, with estimates ranging between 112 and 169 PgC yr^{-1} (Ryu et al., 2019), and the dataset used by Anav et al. (2013) is on the lower end of this range. For CMIP6, (Arora et al., 2020) analyzed simulations with a CO_2 increase of 1 % per year to quantify the carbon-climate feedbacks. They found no significant change in behavior from CMIP5 to CMIP6, but lower absolute values for models which included a nitrogen cycle.

In this paper we focus on evaluating the growth rate and the seasonal cycle amplitude of simulated CO_2, converted to XCO_2, from CMIP ESMs which performed emission driven simulations with satellite observations in CMIP5 and CMIP6. The paper is structured as follows: the data products used in this study are introduced in Section 2. Section 3 describes the methods used, including the calculation of all derived quantities. A comparison between CO_2 flask measurements and XCO_2 measurements at different locations is given in Section 4. The evaluation of CMIP simulations with satellite data is presented in Section 5, divided into sections focusing ~~at~~on the models' ability to simulate XCO_2 time series, growth rate and seasonal cycle amplitude. A summary and conclusion is given in Section 6.

2 Data

2.1 Observational datasets

2.1.1 Satellite XCO_2

We use the Observations for Model Intercomparisons Project (obs4MIPs) version 3 (O4Mv3) XCO_2 satellite data (Buchwitz et al., 2017a; Buchwitz et al., 2018). Obs4MIPs hosts observationally based datasets which have been formatted according to the CMIP model output requirements (e.g. variable definitions, coordinates, frequencies) in order to facilitate an easier comparison between observations and models ~~(Ferraro et al., 2015; Teixeira et al., 2014; Waliser et al., 2019).~~(Ferraro et al., 2015; Teixeira et al., 2014; Waliser et al., 2020). The satellite product used here is a gridded (Level 3) monthly data product with a 5° x 5° spatial resolution following the obs4MIPs format, produced as part of the Copernicus Climate Change Service (C3S). The O4Mv3 product is retrieved from the two satellite instruments SCIAMACHY/ENVISAT (Bovensmann et al., 1999; Burrows et al., 1995) and TANSO-FTS/GOSAT (Kuze et al., 2009).

This monthly mean XCO_2 satellite dataset covers a 14-year timespan (2003–2016). It is obtained by gridding the level 2 product (individual soundings) generated with the Ensemble Median Algorithm (EMMA¸ Reuter et al. (2013)), in this case EMMA version 3.0 (EMMAv3, Reuter et al. (2017)). EMMA combines several different XCO_2 level 2 satellite data products from SCIAMACHY/ENVISAT (2003–2012) and TANSO-FTS/GOSAT (2009–2016~~).~~) and includes a bias correction to all products during overlap phases, resulting in a good agreement during the overlap period. This product was validated against

Total Carbon Column Observing Network (TCCON, Wunch et al. (2011)) ground-based observations of XCO_2, revealing a +0.23 ppmv global bias, a relative accuracy (defined as standard deviation of the station-to-station biases) of 0.3 ppmv, and a very good stability in terms of a linear bias trend (-0.02 ± 0.04 ppmv yr^{-1}) (Buchwitz et al., 2017b). While the dataset ends in 2016, our evaluation only goes up to the year 2014 because the historical simulations for CMIP6 end in 2014 and scenarios from the emission-driven simulations that could be used to extend the runs are not yet available~~.~~ for all considered models. The number of observations depends significantly on the location with most points over locations with low cloud cover, high surface reflectivity and (at least) moderate to high sun elevation. Coverage over ocean is sparse as ocean retrievals are only included from GOSAT sun-glint mode observations - outside of glint conditions the reflectivity of water is very low in the NIR/SWIR spectral region. Figure 1 shows the mean monthly coverage of the dataset for 2003–2014. In Section 5 we will show that taking into account this sampling in the evaluation of ESMs is essential for a proper comparison.

The dataset also contains uncertainty estimates for each grid cell, with a mean value of 0.92 ppmv, accounting for both statistical uncertainties from the individual soundings and uncertainties from potential regional and temporal biases (Buchwitz et al., 2017a). However, the overall uncertainties are small compared to inter-model differences (see Section 3.1), and are therefore neglected in our analysis.

2.1.2 Surface CO_2 measurements

For the comparison of satellite XCO_2 and surface CO_2 data in Section 4 we have obtained surface flask measurements from the NOAA ESRL Carbon Cycle Cooperative Global Air Sampling Network ~~(Dlugokencky et al., 2018). The sites were selected to cover different regions in the world and were chosen to have a maximum time overlap with the considered satellite period from 2003–2014. Furthermore, we excluded sites at locations with no available satellite data, which ruled out the four baseline observatories in Mauna Loa, Samoa, as well as the South Pole and Point Barrow sites.~~(Dlugokencky et al., 2020). Measurement sites at locations with no available satellite data were excluded from the analysis, which ruled out the four baseline observatories in Mauna Loa, Samoa, as well as the South Pole and Point Barrow sites. Furthermore, sites which did not collect data during the period from 2003–2014 were discarded. From the remaining sites, a sample of five sites was chosen which had the best coverage of different latitudes, and when latitudes were similar, different longitudes were selected for increased spatial coverage. The selected sites are listed in Table 1.

2.2 Model simulations

We use monthly mean output data from ten CMIP5 and ~~seven~~ten CMIP6 models which performed emission driven simulations, with three of the CMIP5 and ~~four~~five of the CMIP6 models including a nitrogen cycle. Tables 2 and 3 list all the CMIP5 and CMIP6 models used in this paper along with their atmosphere, land and ocean model component, respectively. Only models with interactive carbon cycle are able to perform the emission driven simulations, in which the emissions rather than the concentrations of the greenhouse gases are prescribed (Taylor et al., 2012; Eyring et al., 2016a). This allows the carbon cycle in the models to react to changes in climate and atmospheric CO_2, by adjusting their carbon fluxes to the new climate conditions

and providing the atmospheric CO_2 concentration as an output (Friedlingstein et al., 2014). In order to facilitate the comparison between the satellite data and the CMIP5 emission driven simulations, the historical simulations (1850–2005) were extended beyond 2005 with simulations from the Representative Concentration Pathway (RCP) 8.5 (2006–2100), for which most ESM simulations are available. Since the period of observations only extends a decade beyond the historical runs, the choice of emissions scenario has a negligible impact on the results that we present below. For CMIP6 only the historical simulations are used, which end in 2014. For CMIP5, only one model had more than one ensemble member performing the emission driven RCP 8.5 simulation and thus only one ensemble member for each model has been used. In CMIP6, several models have three or more ensemble members. We consider all of them in Figure 3 for the timeseries to show the models' intrinsic variability, but then proceed the analysis with only the first ensemble member for each model. The different initial value ensemble members similarly to each other for the analysis presented in this paper, and using an ensemble mean would reduce the interannual variability found in each individual member.

3 Methods

3.1 Sampling of observations and models

For comparison of model and satellite data, first the CO_2 data of the models were converted to XCO_2 data. The model data was interpolated to the grid of the satellite dataset using a bilinear interpolation scheme and grid cells with missing values in the satellite data were also set to missing values in the model fields. Further sampling considerations are discussed in more detail in Section 5.3.2 and in Appendix A.

Most analysis is carried out with regional averages covering several grid cells. Unless specifically stated otherwise, these are calculated by taking the arithmetic averages over all grid cells weighted by their area for each month.

3.2. Calculation of growth rate, seasonal cycle amplitude and growing season temperature anomaly

We compute the growth rate (GR) following the method described in Buchwitz et al. (2018). Monthly resolved annual growth rates are calculated by subtracting the XCO_2 value 6 months in the future from the one 6 months in the past. Then these monthly resolved growth rates are averaged to a yearly GR for a calendar year, and any years with less than 7 months of data are flagged as missing. The addition of the 7–month data availability was introduced to be consistent with the constraint on SCA as explained below.

We define the SCA as the peak-to-trough amplitude in a calendar year of the detrended time series. The time series is detrended with the cumulative sum of monthly growth rates, using the annual mean growth rates as substitution for missing values where necessary. The SCA is calculated by subtracting the minimum from the maximum value for each year with a minimum data availability of 7 months. When investigating the seasonal cycle of observationally sampled simulations at higher latitudes, the maximum value of the time series was generally only accounted for if more than 7 months of data were available. We therefore introduce the cutoff of 7–month data availability to preserve as many peaks as possible without restricting the data too much.

However, as peak preservation cannot be guaranteed when any missing values are present, we can only speak of an effective SCA. The absolute SCA is not as important in our comparison, because we use the same sampling for both the model and observations.

The growing season temperature anomaly ΔT is calculated from the GIStemp (Hansen et al., 2010) temperature anomaly map following Schneising et al. (2014). The data is masked to include only vegetated areas, using the MODIS Land Cover Classification (Friedl et al., 2010; Channan et al., 2014). Surface temperature anomalies are calculated with respect to their monthly climatologies. The data is averaged over the growing season if it covers only one hemisphere (AprilSeptember for the Northern Hemisphere, December to May for the Southern Hemisphere). Additionally, if the data covers both hemispheres, the whole year is taken into account. The growing season averages are taken because the temperature has a large influence on the plant growth and the resulting biospheric CO_2 fluxes, which in turn drive both the SCA and interannual variability of the GR (Schneising et al., 2014).

3.3 Earth System Model Evaluation Tool (ESMValTool)

All figures in this paper were produced with the Earth System Model Evalution Tool (ESMValTool) version 2.0 (v2.0) (Righi et al., 2020; Eyring et al., 2019a; Lauer et al., 2020a; Eyring et al., 2020; Lauer et al., 2020b). Since its first release in 2016 (Eyring et al., 2016b) the ESMValTool has been further advanced facilitating analysis of many different ESM components, providing well-documented source code and scientific background of implemented diagnostics and metrics and allowing for traceability and reproducibility of results (provenance). ESMValTool v2.0 has been developed as a large community effort to specifically target the increased data volume of CMIP6 and the related challenges posed by analysis and evaluation of output from multiple high-resolution and complex ESMs. For this, the core functionalities have been completely rewritten in order to take advantage of state-of-the-art computational libraries and methods to allow for efficient and user-friendly data processing (Righi et al., 2020). Common operations on the input data such as regridding or computation of multi-model statistics are now centralized in a highly optimized preprocessor written in Python. The ESMValTool v2.0 includes an extended set of large-scale diagnostics for quasi-operational and comprehensive evaluation of ESMs (Eyring et al., 2020), new diagnostics for extreme events, regional model and impact evaluation and analysis of ESMs (Weigel et al., 2020, submitted), as well as diagnostics for emergent constraints and analysis of future projections from ESMs (Lauer et al., 2020a, b). For the study here, a new ESMValTool recipe has been developed that can be used to reproduce all plots of this paper.

4. Comparison of XCO_2 and surface CO_2

Until recent years, most model-observation comparisons have been carried-out using in situ surface CO_2 data (e.g. Wenzel et al., 2016). As such, it is interesting to compare the differences between XCO_2 and surface CO_2 at different locations. Figure 2 shows a comparison of time series between both kinds of observations and the multi-model mean for both XCO_2 and surface CO_2 for CMIP6 (top) and CMIP5 (bottom) models. The multi-model mean for both XCO_2 and surface CO_2~~The multi-model~~

~~mean and satellite data are averaged between all grid cells covering a 5° x 5° radius around the stations, which results in a maximum of four grid cells to be considered. The multi-model mean~~ is offset to have the same mean value as the satellite data, and this offset is noted above each time series panel. It is interesting to note that the offset appears to be larger at higher latitudes thus showing a different ~~spatial~~latitudinal gradient between the models and the satellite data, indicating potential issues with surface fluxes or transport in the models. The multi-model mean and satellite data are averaged between all grid cells covering a 5° x 5° radius around the stations, which results in a maximum of four grid cells to be considered. The mean and growth rate of XCO_2 and surface CO_2 are in very good agreement, while the multi-model mean overestimates both ~~parameters~~variables at all sites, with the overestimated mean XCO_2 arising from the effect of higher growth rates over time. Furthermore, the offset from the modelled surface CO_2 is higher than that of XCO_2, while this difference is smaller for CMIP5. This might be due to the fact that the CMIP5 offset for multi-model mean XCO_2 was larger overall with approximately 10 ppmv compared to the CMIP6 offset of approximately 2 ppmv.

SCA is higher at higher latitudes, and also generally higher at the surface compared to the column average. This is to be expected as the processes dominating the seasonal cycle, respiration and photosynthesis, take place at the surface~~.~~ leading to the higher SCA for station data and surface CO_2 from models compared to the XCO_2 values. Mixing of air coming from lower latitudes with lower SCA dampens the SCA in the column compared to surface SCA. This is evident in the increasing SCA difference between XCO_2 and surface CO_2 going from low latitude to high latitude stations, with no discernible seasonal cycle in the southern hemisphere due to the lack of land and vegetation. The multi-model mean follows this trend in the observations, although it underestimates the higher latitude SCA, with a larger underestimation at the surface while capturing the XCO_2 SCA relatively well. As this study aims at evaluating model simulations with satellite data, further analysis is restricted to XCO_2.

5. Evaluation of CMIP simulations with satellite data

5.1. XCO_2 time series

The globally averaged time series of XCO_2 is shown in Figure 3 on the top panel, with CMIP6 (~~top~~a) and CMIP5 (~~bottom~~b) models sampled as the satellite observations (see Section 3.1). The observational uncertainty is too small to be seen in this plot and is therefore neglected. The middle panel shows the monthly resolved annual growth rate and the bottom panel the detrended seasonal cycle. All available ensemble members for CMIP6 models are used to show their internal variability. All ensemble members perform similar to one another. The multi-model mean is computed using the first ensemble member, which is also used in the further analysis. As in Figure 2, an increase of XCO_2 with time and a pronounced seasonal cycle for all models can be seen. The focus here is on the absolute values, as the trend (GR) and SCA are discussed in dedicated sections below. The ~~CMIP5~~CMIP6 models display a large range of absolute XCO_2 values, ranging from an underestimation by 15 ppmv (MRI-ESM2.0 and MIROC-ES2L) to an overestimation by 20 ppmv (GFDL-ESM4). The models closest to the observations ~~are~~is CNRM-ESM2-1 which reproduces the mean value well, with the next closest models being NorESM2-LM and MPI-ESM1.2-

LR both overestimating XCO_2 by about 5 ppmv. The multi-model mean shows an overestimation by approximately 2 ppmv or equivalently a time-shift of 1 year. While the spread in the models has not decreased much since CMIP5, the overestimation of the multi-model mean has decreased from 10 ppmv to 2 ppmv. Furthermore, CMIP6 models which have predecessors in CMIP5 show similar biases as their predecessors~~. The MPI model has~~, besides the ~~closest fit~~MIROC models, which overestimated the mean by 15ppmv in ~~both ensembles, while both~~CMIP5 and underestimates it by that much in CMIP6. Both MRI models underestimate XCO_2 significantly, while GFDL-ESM4 overestimates the atmospheric content even more. The MRI-ESM1 model was the only model in CMIP5 to underestimate XCO_2 with respect to the observations, and this by about 20 ppmv. This model underestimates the historical warming, causing plant and soil respiration to be too low, which leads to a larger land sink and a reduced atmospheric CO_2 concentration (Adachi et al., 2013). This underestimation has been reduced by about 5 ppmv in CMIP6. The GFDL models show an overestimation of about 15 ppmv in both ensembles, and both CanESM models are 10 ppmv too high. A minor improvement can be seen for NorESM-LM over NorESM1-ME, with a decrease of the overestimation from 15 to 10 ppmv.

5.2 Growth Rate

The middle panel of Figure 3 shows that while models capture the interannual variability of the growth rate quite well, they overestimate the mean growth rate compared to the observations. The correlation coefficient for the multi-model mean is at 0.48 in CMIP6 and 0.07 in CMIP5 which shows a large improvement in this area. The pronounced feature in 2009 is due to the introduction of the GOSAT data which changed the shape of the seasonal cycle and thus due to its calculation the monthly resolved annual growth rate. Fortunately, this feature gets averaged out when computing the annual growth rate and does not tangibly affect our conclusions. Figure 4 shows the global mean GR of XCO_2 for 2003–2014 and its standard deviation over all years depicted as error bars, with the observations shown in black and the multi-model mean in red. The annual mean GR of the satellite data is 1.9 ± 0.4 ppmv yr^{-1}, while the CMIP5 models (right) range from 1.5 ± 0.4 ppmv yr^{-1} (MRI-ESM1) to 3.0 ± 0.9 ppmv yr^{-1} (CanESM2) with a multi-model mean of 2.4 ± 0.4 ppmv yr^{-1}. In CMIP6 (left), the multi-model mean is slightly lower at 2.3 ± 0.3 ppmv yr^{-1} and the spread has ~~decrased~~decreased by 0.6 ppmv yr^{-1}, with a range from 1.7 ± 0.4 ppmv yr^{-1} (MRI-ESM2.0) to 2.6 ± 0.7 ppmv yr^{-1} (GFDL-ESM4). As expected from Figure 3, the models - with the exception of MRI-ESM1~~ and,~~ MRI-ESM2.0 and MIROC-ES2L - overestimate the growth rate, leading to an increased XCO_2 level in the present-day atmosphere compared to observations. The interannual variability of the growth rate for the models is generally higher than that of the observations, but well reproduced in the multi-model mean.

Emergent Constraints are relationships defined using an ensemble of models, between a measurable aspect of current or past climate and an aspect of Earth system feedback in the future, which can be constrained using observational data (Eyring et al., 2019b). In Appendix C we have tried to reproduce the trend in interannual variability (IAV) of CO_2 growth rate to IAV of tropical temperature used by Cox et al. (2013) to develop an emergent constraint on the sensitivity of tropical land carbon to climate change, but were unable to find a significant trend for this much shorter satellite-derived time series.

The spatial variability of the GR is small, as CO_2 is long-lived and well mixed in the atmosphere with a ~~1~~one year mean interhemispheric crossing time. Thus there should be no significant regional changes on an annual level. Buchwitz et al. (2018) found the growth rate of the satellite dataset to be in agreement with those quoted by NOAA ESRLs global and Mauna Loa time series, as well as robust over several latitude bands. Our own analysis also shows only very small regional differences in the growth rate (not shown). No significant changes to the annual growth rates due to the satellite spatial coverage were found. ~~Emergent Constraints are relationships defined using an ensemble of models, between a measurable aspect of current or past climate and an aspect of Earth system feedback in the future, which can be constrained using observational data (Eyring et al., 2019b). Cox et al. (2013) developed an emergent constraint on the sensitivity of tropical land carbon to climate change using the sensitivity of the interannual variability (IAV) of CO_2 growth rate to the IAV of tropical temperature, which was later adapted by Wenzel et al. (2014) to CMIP5 models. Figure 5 shows the sensitivity of the IAV of XCO_2 growth rate to the tropical growing season temperature IAV for CMIP6 (left) and CMIP5 (right) models, both compared with observations. The observational temperature is taken from the GISTEMP v4 dataset (Lenssen et al., 2019) and the models use their own modeled temperature. We find an observational value of 0.23 ± 0.70 ppmv yr^{-1} K^{-1} for the 2003–2014 period. However, when using the full span of the satellite data until 2016, the slope increases to 0.75 ± 0.6 ppmv yr^{-1} K^{-1} (not shown), as the additional years show both a high growing season temperature and GR IAV. This shows that the time period 2003–2014 is not sufficient to reproduce the emergent constraint, but it might be feasible once CMIP6 emission driven future simulations are available for a longer time overlap between models and observations. CMIP5 model values for the timeframe 2003–2014 range from 0.53 ± 0.51 ppmv yr^{-1} K^{-1} (NorESM1-ME) to 3.14 ± 0.63 ppmv yr^{-1} K^{-1} (MRI-ESM1), with only CESM1-BGC showing a negative trend of -0.64 ± 0.55 ppmv yr^{-1} K^{-1}. The multi-model mean has a value of 0.23 ± 0.70 ppmv yr^{-1} K^{-1}. In CMIP6 the range is significantly decreased with a minimum of 1.14 ± 0.56 ppmv yr^{-1} K^{-1} (ACCESS-ESM1.5) to a maximum of 2.07 ± 0.33 ppmv yr^{-1} K^{-1} (CanESM5), with the multi-model mean at 1.36 ± 0.32 ppmv yr^{-1} K^{-1}.~~

5.3 Seasonal Cycle Amplitude

This section about the seasonal cycle amplitude (SCA) is divided into two subsections, with the first one taking a closer look at inter-model differences, while the second subsection is devoted to the impact of observational sampling.

5.3.1 Model differences

~~Figure 6~~The lower panel in Figure 3 shows the detrended global seasonal cycle for all models. Models in CMIP6 (a) show a strong improvement in their ability to capture both the seasonal cycle amplitude, as well as its phase compared to CMIP5 (b), but still underestimate the SCA. The correlation coefficient to the observed seasonal cycle is 0.93 in CMIP5 and 0.98 in CMIP6 for the multi-model mean. The only model in CMIP6 to significantly underestimate the seasonal cycle amplitude is CNRM-ESM2-1. Two errors have been identified causing this dampened seasonal cycle: Ocean carbon fluxes are lagged in time, and in the emission driven simulations, CO_2 is considered as an active tracer and coupled with atmospheric chemistry. These chemical fields are restored to global mean climatological concentrations at the model surface, acting as a damping component

to the CO_2 concentrations (Séférian et al., 2019). Figure 5 shows maps of the climatological mean SCA (2003–2014) for all models, with the global mean given in the top right. and the zonal averages shown in the panel attached to the right of the maps. All CMIP6 models (Figure 6a5a) underestimate the SCA compared to satellite observations (Figure 76 middle) in the global mean, with the closest mean SCA being CanESM5MIROC-ES2L. This underestimation was already present in CMIP5 (Figure 6b5b), with several studies revealingdiscussing it for surface CO_2 SCA (Wenzel et al., 2016; Graven et al., 2013). In CMIP6 the multi-model mean has a globally averaged mean SCA of 3.4525 ppmv, compared to 2.92 ppmv for CMIP5, while the observations show an effective SCA of 5.89 ppmv (Figure 76).

Both models and observations show the well-known increasing SCA with increasing latitude, due to the more pronounced seasonal cycle of the climate at higher latitudes. Most models show a decreased growth from 0-30°N, with higher SCA increases in the lower tropics and northern midlatitudes. Overall the zonal distribution is quite similar throughout the models, with UK-ESM1-0-LL showing increased SCA at 30-90°S. Tropical land regions in northern South America, Africa and south east Asia show increased SCA values compared to the ocean SCA at this latitude for the same model. While in the GFDL CMIP5 models this was so pronounced that these regions showed a higher SCA than the higher latitudes (Dunne et al., 2013), this is no longer the case for GFDL-ESM4 in CMIP6. Dunne et al. (2013) attributed the GFDL problem in CMIP5 to the seasonality of respiration in the northern latitudes and an Amazonian low-precipitation bias which reversed the seasonal cycle synchronizing it with the African and Oceanian rain forests. The improvement in CMIP6 is due to a reduced ocean-atmosphere CO_2 flux in the Southern Hemisphere, as well as the reduction of the high tropical land-atmosphere fluxes expressed over the ocean (Dunne et al., 2020).

The SCA in the CMIP5 MPI-ESM-LR model is on average twice as large as the observed one. The high SCA has been discussed in Giorgetta et al. (2013) where it was attributed to a combination of an overestimation of net primary productivity in ocean and land biology and uncertainties in atmospheric tracer transport. A particularly severe overestimation was seen in the Southern Hemisphere when comparing to station data. As shown in Figure 6, we additionally find a large overestimation in XCO_2 SCA in the Northern Hemisphere, in particular in the extra-tropics. For the CMIP6 successor model, MPI-ESM1.2-LR, the SCA is still the highest of the model ensemble, but is no longer twice as high as the other models. However, it now shows a more pronounced SCA over the tropical land regions mentioned above, which was not as dominant in CMIP5.

It is known that nitrogen limitations tend to suppress CO_2 fertilization (Reich et al., 2006). Of the four models with the lowest overall SCA in CMIP5 (CESM1-BGC, FIO-ESM, NorESM1-ME and BNU-ESM), three of them – BNU-ESM, CESM1-BGC, NorESM1-ME - include a nitrogen cycle. The SCA of NorESM1-ME and CESM1-BGC are very similar, which can be attributed to sharing the same land model (CLM4). FIO-ESM uses the predecessor CLM3.5 and is also comparable to the other two models. In CMIP6, ACCESS-ESM1.5, MPI-ESM1.2-LRIt was found that CLM4 had an unrealistically strong nitrogen limitation, which has been reduced in CLM5 (Wieder et al., 2019). In CMIP6, ACCESS-ESM1.5, MPI-ESM1.2-LR, MIROC-ES2L, NorESM2-LM and UKESM1.0-LL include a nitrogen model but none of them share the same land model. While ACCESS-ESM1.5 has the second lowest overall SCA, MPI-ESM1.2-LR hasand MIROC-ES2L have the highest, and thus the observation from CMIP5 models that N-cycle models feature a lower SCA no longer stands for CMIP6.

5.3.2 Influence of Sampling

There are a number of ways to compare model SCA to observational SCA, beginning with a grid box comparison. Figure ~~7~~6 shows a comparison of the multi-model mean of CMIP6 (Figure ~~7a~~6a) and CMIP5 (Figure ~~7b~~6b) to observations. The top right shows the unsampled SCA. The top left panel shows the effective SCA when using observational sampling and the middle panel the satellite data's effective SCA. All numbers are given in ppmv. For an easier comparison the bottom panels show the absolute difference plots, with the left panel depicting the difference between sampled model and observations, and the right panel the difference between the sampled and unsampled model. Observational sampling slightly lowers the SCA, which is to be expected, as it could lead to masking out the peaks or troughs. While this effect was minimized by imposing the restriction of only computing the SCA of a year when at least 7 months of data are available, it is still a possibility. We therefore classify this SCA as an "effective SCA". However, the SCA does not seem to decrease significantly through sampling and the difference does not follow a trend in latitude, so a grid box comparison seems feasible. This paves the way for more comprehensive spatial investigations, which previously relied on data from ground-based stations with sparse spatial coverage. While the stations provide data in higher latitudes that the satellite dataset does not cover, in the tropics and mid-latitudes the spatial coverage of the satellite is superior to the ground-based stations. A downside with this approach is the sparsity of the data when using observational sampling. Furthermore, this becomes a computationally expensive operation, as the SCA will need to be calculated for each grid box.

Another approach often used in model analysis is area averaging, e.g. over different latitude bands like the tropics or the northern mid-latitudes. Using surface flask measurements Wenzel et al. (2016) found an increased SCA with rising CO_2 concentration for CMIP5 using model data from the full historical simulation 1850 to 2005 – CO_2 fertilization -, and used this to establish an emergent constraint on the fertilization of terrestrial gross primary productivity (GPP). Figure ~~8~~7 shows the SCA trend of CMIP6 models versus XCO_2 for 2003–2014 in the northern mid-latitudes (30–60° N), including a linear regression including slope, mean SCA ~~and~~, Pearson correlation coefficient and p-value. The left panel shows the trend in the unsampled models, while the right one shows the trend when following the sampling of the satellite data. The SCA was computed after a weighted area-average on the XCO_2 time series. While some of the unsampled models show an increasing SCA trend with increasing XCO_2, which is in agreement with the findings from Wenzel et al. (2016), others don't show a statistically significant trend and the multi-model mean shows an insignificant positive trend. The sampled model data ~~instead shows~~ (right) show a significant negative trend. Calculating the average with a zonal average before summing up the latitude bands does not change this result.

To investigate this ~~reversal~~change in trend due to observational sampling, Figure ~~9~~8 shows the data coverage for different time periods, 2003–2008 for SCIAMACHY only measurements (top), the overlap between the two satellites in 2009–2012 (middle), and 2013–2014 for the GOSAT satellite only (bottom), with the pattern marking areas with a coverage of 50 % or above. Above 50° N SCIAMACHY measurements include more areas with 50 % or more coverage compared to GOSAT measurements. With a larger SCA in higher latitudes, it implies that SCIAMACHY would have a larger average SCA over

this region compared to GOSAT, hence artificially generating a decreasing trend in the observed SCA, when moving from SCIAMACHY to GOSAT. Figure ~~10~~9 shows the CMIP6 effective SCA trend with XCO_2 using SCIAMACHY and GOSAT masks obtained from masking out points with less than 50 % coverage. While the slopes remain largely the same, the mean effective SCA is higher in the models using the SCIAMACHY mask than when using the GOSAT mask. This mean SCA difference is larger than the total SCA difference within a model using the same sampling for the whole time period. Thus when considering the observational time series and its full sampling, the ~~positive~~ trend intrinsic to the model is dominated by the negative SCA difference going from the SCIAMACHY to the GOSAT data coverage and thus ~~reversed~~changed to the negative trend seen in the observations. We can therefore attribute ~~this trend reversal~~at least part of the negative trend in the satellite data to the ~~influence of the~~ different data coverage of the two satellites ~~and~~. We are able to reproduce ~~it~~this negative trend with the models, when these are sampled consistently with the satellite data. This study on sampling also holds true for CMIP5 models, with the equivalent figures shown in Appendix B (Figures B1 and B2).

Further impacts on CO_2 concentrations could come through temporal sampling, such as the fact that the satellites data only includes measurements with low cloud cover and is limited to 13:00 local time. While cloud cover can impact photosynthesis, the response can be fundamentally different for various ecosystems (Still et al., 2009), we expect a larger effect from the diurnal cycle in CO_2 which is included in the model means but not the satellite data. Due to a lack of CO_2 data from models with a higher temporal resolution, this effect cannot be estimated in this study.

6. Summary and Conclusion

In this paper we have evaluated the performance of CMIP5 and CMIP6 ESMs with interactive carbon cycle (Tables 2 and 3) against column integral CO_2 (XCO_2) data from satellite retrievals. Our analysis has compared ESM simulations to the 2003-2014 Obs4MIPs XCO_2 satellite dataset O4Mv3 retrieved from radiance spectra measured by the SCIAMACHY/ENVISAT (20032012) and TANSO-FTS/GOSAT (2009–2014) satellite instruments. The O4Mv3 data product has a spatial resolution of 5°x5° and monthly time resolution. For CMIP5, the historical simulations covering the period 2003–2005 were combined with simulations from the RCP 8.5 scenario (2006–2014) and for CMIP6 the historical ~~simulation was~~simulations were used (2003–2014).

The evaluation of the CMIP models with the satellite data focused on the time series, the growth-rate (GR) and the seasonal cycle amplitude (SCA) ~~of column integral CO_2 (XCO_2).~~ All SCAs computed with a masked time series are considered to be "effective" SCAs due to the possibility of masking out peaks and troughs.

The XCO_2 time series comparison shows that most models overestimate the carbon content of the atmosphere relative to the satellite observations in both model ensembles, with a lower overestimation for the CMIP6 models of 2 ppmv for the multi-model mean and a wide range of individual model differences of -15 ppmv to +20 ppmv. The CMIP5 models overestimate by 5 to 25 ppmv with the exception of the MRI-ESM1 model, which underestimates by 20 ppmv. The CMIP5 multi-model mean overestimates by 10 ppmv compared to the observations, which has also previously been found for surface comparisons

(Friedlingstein et al., 2014;Hoffman et al., 2014). Overall, CMIP6 models follow the same trends as their CMIP5 counterparts, but with reduced systematic biases.

The XCO_2 annual mean growth rate is typically slightly overestimated compared to the observational value of 1.9 ± 0.4 ppmv yr^{-1}. CMIP6 models range from 1.7 ± 0.4 ppmv yr^{-1} (MRI-ESM2.0) to 2.6 ± 0.7 ppmv yr^{-1} (GFDL-ESM4) with a multi-model mean of 2.3 ± 0.3 ppmv yr^{-1}. CMIP5 models have a slightly higher multi-model mean growth rate of 2.4 ± 0.4 ppmv yr^{-1}, and a larger spread, with the CMIP5 lowest model being MRI-ESM1 at 1.5 ± 0.4 ppmv yr^{-1} and the highest CMIP5 growth rate shown by CanESM2 at 3.0 ± 0.9 ppmv yr^{-1}. ~~We were able to reproduce the trend of increasing GR with increasing temperature anomaly in the tropics used by Cox et al. (2013) for the models, but the satellite observations showed a high variance in the considered timespan. No discernible sampling effect on GR or mean carbon content of the atmosphere was found, consistent with expectations.~~

All models capture the expected increase of the SCA with increasing latitudes, but most models underestimate the SCA to differing degrees in different regions. This result is in line with previous studies (Wenzel et al., 2016;Graven et al., 2013). Models with similar model components show similar behavior, with models including a nitrogen cycle generally showing a lower SCA in CMIP5, but this influence is not clear in CMIP6. Finally, the connection between SCA and XCO_2 was investigated in the northern midlatitudes. Most models from both ensembles show a positive trend, i.e., an increase of the SCA with XCO_2, consistent with findings for surface CO_2 (Wenzel et al., 2016). However, the satellite product shows a strong negative trend in contrast to the models and surface based observations. We have attributed this trend reversal to the sampling characteristics of the satellite products. The average effective SCA is higher for models sampled according to the SCIAMACHY/ENVISAT as opposed to the TANSO-FTS/GOSAT mean data coverage. As the early time series is based solely on the SCIAMACHY/ENVISAT data and the last years only use data from TANSO-FTS/GOSAT, this introduces an artificial negative trend which dominates the positive trend shown by the unsampled models. This demonstrates the importance of equal sampling of models and observations in model evaluation studies.

There are several ways to improve on this analysis in the future. With more available future scenario simulations, the analysis can be extended to a longer time series, making use of longer observational timeseries, such as the one introduced in Reuter et al. (2020). Higher temporal resolution of the models would enable studies on the effect of the diurnal cycle of CO_2 on the monthly mean and also allow for the construction of a co-located time series with the Level 2 satellite data. This could help highlight some of the causes of model biases by being able to pinpoint time and space where they occur more precisely. Model biases may also result from the CMIP experimental design, such as requiring the climate state to be in equilibrium in 1850 while the real world may not have been (Bronselaer et al., 2017), or the parametrizations of biological and physical processes not allowing the system to change rapidly enough (Hoffman et al., 2014). Along with a longer time series, newer satellites, such as OCO-2 or the planned Sentinel 7 bring higher resolutions and more data, potentially helping to fill the gaps and reduce the impact of the sampling we discussed in Section 5.3.2.

Overall, the CMIP6 ensemble shows an improved agreement with the satellite data in all considered quantities (mean XCO_2, growth rate, SCA and trend in SCA), with the biggest improvement shown in the mean XCO_2 content of the atmosphere. The

paper demonstrates the great potential of satellite data for climate model evaluation as it allows to go beyond regional means or single point observations from in situ data, and also enables the investigation of regional effects on SCA, such as the increase in SCA at higher latitudes.

Appendix A. Calculation of XCO_2

Here we documents the general procedure used to compute model XCO_2 for comparison with the satellite-based obs4MIPs product following the description in (Buchwitz and Reuter, 2016).

$$XCO_2 = \frac{\sum n_d \cdot c_{CO_2}}{\sum n_d} \quad (A1)$$

Here, c_{CO_2} represents the modeled CO_2 dry air mole fraction on model layers (i.e., layer centers or full levels) and n_d the number of dry air particles (air molecules excluding water vapor) within these levels. The summations are performed over all model layers. The number of dry air particles can be computed as follows:

$$n_d = \frac{N_a \cdot \Delta p \cdot (1 - q)}{m_d \cdot g} \quad (A2)$$

N_a is the Avogadro constant ($6.022140857 \cdot 10^{23} mol^{-1}$) and m_d the molar mass of dry air ($28.9644 \cdot 10^{-3} kg\ mol^{-1}$). Δp is the pressure difference (in hPa) computed from the model's pressure levels (i.e., layer boundaries or half levels) surrounding the model layers, q is the modeled specific humidity (in kg/kg), and g the gravitational accelaration approximated by:

$$g = \sqrt{g_0^2 - 2 \cdot f \cdot \phi} \quad (A3)$$

This includes the model's geopotential ϕ (in $m^2 s^{-2}$) on layers, the free air correction constant $f = 3.0825959 \cdot 10^{-6} s^{-2}$, and the gravitational acceleration g_0 on the geoid approximated by the international gravity formula depending only on the latitude φ:

$$g_0 = 9.780327 \cdot [1 + 0.0053024 \cdot \sin^2(\varphi) - 0.0000058 \cdot \sin^2(2\varphi)] \quad (A4)$$

Appendix B. Satellite data mean coverage impact on CMIP5 SCA trend

The analysis from Section 5.3.2. on the influence of the satellite data mean coverage on the trend of the SCA was also performed for CMIP5. Figures B1 and B2 are the CMIP5 equivalent of Figures 8 and 10. The CMIP5 models support the analysis of the CMIP6 models and show that the different satellite data coverage results in a different mean effective SCA, with a higher mean effective SCA for SCIAMACHY (2003–2012) than GOSAT (2009–2014) mean data coverage, which overshadows the positive trend and causes it to flip to a negative one in most models.

Appendix C. Trend of growing season temperature and interannual variability of CO_2 growth rate

Cox et al. (2013) developed an emergent constraint on the sensitivity of tropical land carbon to climate change using the sensitivity of the interannual variability (IAV) of CO_2 growth rate to the IAV of tropical temperature, which was later adapted

by Wenzel et al. (2014) to CMIP5 models. Figure C1 shows the sensitivity of the IAV of XCO_2 growth rate to the tropical growing season temperature IAV for CMIP6 (left) and CMIP5 (right) models, both compared with observations. The observational temperature is taken from the GISTEMP v4 dataset (Lenssen et al., 2019) and the models use their own modeled temperature. We find an observational value of -0.23 ± 0.70 ppmv yr^{-1} K^{-1} for the 2003-2014 period. However, when using the full span of the satellite data until 2016, the slope increases to 0.75 ± 0.6 ppmv yr^{-1} K^{-1} (not shown), as the additional years show both a high growing season temperature and GR IAV, coinciding with a strong El Nino. This shows that the time period 2003–2014 is not sufficiently long to reproduce the emergent constraint, although this may become feasible once CMIP6 emission driven future simulations are available for a longer time overlap between models and observations. CMIP5 model values for the timeframe 2003–2014 range from 0.53 ± 0.51 ppmv yr^{-1} K^{-1} (NorESM1-ME) to 3.14 ± 0.63 ppmv yr^{-1} K^{-1} (MRI-ESM1), with only CESM1-BGC showing a negative trend of -0.64 ± 0.55 ppmv yr^{-1} K^{-1}. The multi-model mean has a value of 1.79 ± 0.80 ppmv yr^{-1} K^{-1}. In CMIP6 the range is significantly decreased with a minimum of 1.14 ± 0.56 ppmv yr^{-1} K^{-1} (ACCESS-ESM1.5) to a maximum of 3.37 ± 0.71 ppmv yr^{-1} K^{-1} (CanESM5-CanOE), and a multi-model mean of 1.14 ± 0.37 ppmv yr^{-1} K^{-1}.

7. Data and Code Availability

The O4Mv3 XCO_2 data product is available via the Copernicus Climate Change Service (C3S, https://climate.copernicus.eu/) Climate Data Store (CDS) (https://cds.climate.copernicus.eu/), accessed Aug 2018. The surface flasks measurements were obtained online (ftp://aftp.cmdl.noaa.gov/data/trace_gases/co2/flask/surface/) from Dlugokencky et al. (2018), accessed Aug-2018. Surface temperature anomalies were obtained from the GISTEMP Team, 2020: *GISS Surface Temperature Analysis (GISTEMP), version 4*. NASA Goddard Institute for Space Studies. Dataset accessed 2020~~-0213~~-02-13 at data.giss.nasa.gov/gistemp/. The MODIS IGBP Land Cover Type Classification was obtained from http://glcf.umd.edu/data/lc/ (accessed: 2018-01-31). ~~CMIP5~~CMIP data is available on various ESGF nodes (e.g. https://esgf-data.dkrz.de/search/cmip5-dkrz/) (Williams et al., 2009)~~.~~, with CMIP6 data DOIs given in Table 3.

~~The corresponding recipe that can be used to reproduce the figures of this paper will be included in the ESMValTool v2.0 (Righi et al., 2020; Eyring et al., 2019a) as soon as the paper is published. The ESMValTool is released under the Apache License, VERSION 2.0. The ESMValTool code is available from the ESMValTool webpage at https://www.esmvaltool.org/ and from github (https://github.com/ESMValGroup/ESMValTool).~~

ESMValTool v2.0 (Eyring et al., 2020; Lauer et al., 2020b; Righi et al., 2020) is released under the Apache License, VERSION 2.0. The latest release of ESMValTool v2 is publicly available on Zenodo at https://doi.org/10.5281/zenodo.3401363. The source code of the ESMValCore package, which is installed as a dependency of the ESMValTool v2, is also publicly available on Zenodo at https://doi.org/10.5281/zenodo.3387139. ESMValTool and ESMValCore are developed on the GitHub repositories available at https://github.com/ESMValGroup. The corresponding recipe that can be used to reproduce the figures of this paper will be included in ESMValTool v2 at the time of publication of the paper.

8 Author contributions

BG led the writing and analysis of the paper. MB and MR provided the satellite dataset. VE, PC and PF contributed to the evaluation of the CMIP simulations. All authors contributed to the writing of the manuscript.

9 Competing interests

The authors declare that they have no conflict of interest.

10 Acknowledgements

This work has been supported by ESA Climate Change Initiative (CCI) Climate Modelling User Group (CMUG) project, the Horizon 2020 project Climate-Carbon Interactions in the Current Century (4C) funded by the EU (Grant agreement ID 821003) and the EVal4CMIP project funded by the Helmholtz Society. The generation of the satellite XCO_2 data product has received funding from ESA (GHG-CCI) and the EU (Copernicus Climate Change Service – C3S, led by ECMWF). We acknowledge the World Climate Research Programme (WCRP), which, through its Working Group on Coupled Modelling, coordinated and promoted CMIP6. We thank the climate modeling groups (listed in Tables 2 and 3 of this paper) for producing and making available their model output, the Earth System Grid Federation (ESGF) for archiving the data and providing access, and the multiple funding agencies who support CMIP and ESGF.

We also thank both anonymous reviewers for their helpful comments on this paper and the handling editor Trevor Keenan for taking on this paper.

References

Adachi, Y., Yukimoto, S., Deushi, M., Obata, A., Nakano, H., Tanaka, T. Y., Hosaka, M., Sakami, T., Yoshimura, H., Hirabara, M., Shindo, E., Tsujino, H., Mizuta, R., Yabu, S., Koshiro, T., Ose, T., and Kitoh, A.: Basic performance of a new earth system model of the Meteorological Research Institute (MRI-ESM1), Papers in Meteorology and Geophysics, 64, 1-19, 10.2467/mripapers.64.1, 2013.

Anav, A., Friedlingstein, P., Kidston, M., Bopp, L., Ciais, P., Cox, P., Jones, C., Jung, M., Myneni, R., and Zhu, Z.: Evaluating the Land and Ocean Components of the Global Carbon Cycle in the CMIP5 Earth System Models, J Climate, 26, 6801-6843, 10.1175/Jcli-D-12-00417.1, 2013.

Arora, V. K., Scinocca, J. F., Boer, G. J., Christian, J. R., Denman, K. L., Flato, G. M., Kharin, V. V., Lee, W. G., and Merryfield, W. J.: Carbon emission limits required to satisfy future representative concentration pathways of greenhouse gases, Geophys Res Lett, 38, n/a-n/a, Artn L05805
10.1029/2010gl046270, 2011.

Arora, V. K., Boer, G. J., Friedlingstein, P., Eby, M., Jones, C. D., Christian, J. R., Bonan, G., Bopp, L., Brovkin, V., Cadule, P., Hajima, T., Ilyina, T., Lindsay, K., Tjiputra, J. F., and Wu, T.: Carbon-Concentration and Carbon-Climate Feedbacks in CMIP5 Earth System Models, J Climate, 26, 5289-5314, 10.1175/Jcli-D-12-00494.1, 2013.

Arora, V. K., Katavouta, A., Williams, R. G., Jones, C. D., Brovkin, V., Friedlingstein, P., Schwinger, J., Bopp, L., Boucher, O., Cadule, P., Chamberlain, M. A., Christian, J. R., Delire, C., Fisher, R. A., Hajima, T., Ilyina, T., Joetzjer, E., Kawamiya, M., Koven, C., Krasting, J., Law, R. M., Lawrence, D. M., Lenton, A., Lindsay, K., Pongratz, J., Raddatz, T., Séférian, R., Tachiiri, K., Tjiputra, J. F., Wiltshire, A., Wu, T., and Ziehn, T.: Carbon-concentration and carbon-climate feedbacks in CMIP6 models, and their comparison to CMIP5 models, Biogeosciences Discuss., 2019, 1-124, 10.5194/bg-2019-473, 2019.

Arora, V. K., Katavouta, A., Williams, R. G., Jones, C. D., Brovkin, V., Friedlingstein, P., Schwinger, J., Bopp, L., Boucher, O., Cadule, P., Chamberlain, M. A., Christian, J. R., Delire, C., Fisher, R. A., Hajima, T., Ilyina, T., Joetzjer, E., Kawamiya, M., Koven, C. D., Krasting, J. P., Law, R. M., Lawrence, D. M., Lenton, A., Lindsay, K., Pongratz, J., Raddatz, T., Séférian, R., Tachiiri, K., Tjiputra, J. F., Wiltshire, A., Wu, T., and Ziehn, T.: Carbon–concentration and carbon–climate feedbacks in CMIP6 models and their comparison to CMIP5 models, Biogeosciences, 17, 4173-4222, 10.5194/bg-17-4173-2020, 2020.

Bao, Y., Qiao, F.-L., and Song, Z.: The historical global carbon cycle simulation of FIO-ESM, 6834, 2012.

Barnes, E. A., Parazoo, N., Orbe, C., and Denning, A. S.: Isentropic transport and the seasonal cycle amplitude of CO2, J Geophys Res-Atmos, 121, 8106-8124, 10.1002/2016jd025109, 2016.

Bastos, A., Ciais, P., Chevallier, F., Rodenbeck, C., Ballantyne, A. P., Maignan, F., Yin, Y., Fernandez-Martinez, M., Friedlingstein, P., Penuelas, J., Piao, S. L., Sitch, S., Smith, W. K., Wang, X. H., Zhu, Z. C., Haverd, V., Kato, E., Jain, A. K., Lienert, S., Lombardozzi, D., Nabel, J. E. M. S., Peylin, P., Poulter, B., and Zhu, D.: Contrasting effects of CO2 fertilization, land-use change and warming on seasonal amplitude of Northern Hemisphere CO2 exchange, Atmos Chem Phys, 19, 12361-12375, 10.5194/acp-19-12361-2019, 2019.

Basu, S., Guerlet, S., Butz, A., Houweling, S., Hasekamp, O., Aben, I., Krummel, P., Steele, P., Langenfelds, R., Torn, M., Biraud, S., Stephens, B., Andrews, A., and Worthy, D.: Global CO2 fluxes estimated from GOSAT retrievals of total column CO2, Atmos Chem Phys, 13, 8695-8717, 10.5194/acp-13-8695-2013, 2013.

Bovensmann, H., Burrows, J. P., Buchwitz, M., Frerick, J., Noel, S., Rozanov, V. V., Chance, K. V., and Goede, A. P. H.: SCIAMACHY: Mission objectives and measurement modes, J Atmos Sci, 56, 127-150, Doi 10.1175/1520-0469(1999)056<0127:Smoamm>2.0.Co;2, 1999.

Bronselaer, B., Winton, M., Russell, J., Sabine, C. L., and Khatiwala, S.: Agreement of CMIP5 Simulated and Observed Ocean Anthropogenic CO2 Uptake, Geophys Res Lett, 44, 12,298-212,305, 10.1002/2017gl074435, 2017.

Buchwitz, M., and Reuter, M.: Merged SCIAMACHY/ENVISAT and TANSO-FTS/GOSAT atmospheric column-average dry-air mole fraction of CO2 (XCO2) (XCO2_CRDP3_001) - Technical Document, 2016.

Buchwitz, M., Reuter, M., Schneising-Weigel, O., Aben, I., Detmers, R. G., Hasekamp, O. P., Boesch, H., Anand, J., Crevoisier, C., and Armante, R.: Product User Guide and Specification (PUGS) – Main document, Technical Report Copernicus Climate Change Service (C3S), 1-91, 2017a.

Buchwitz, M., Reuter, M., Schneising-Weigel, O., Aben, I., Detmers, R. G., Hasekamp, O. P., Boesch, H., Anand, J., Crevoisier, C., and Armante, R.: Product Quality Assessment Report (PQAR) – Main document, Technical Report Copernicus Climate Change Service (C3S), 1-103, 2017b.

Buchwitz, M., Reuter, M., Schneising, O., Noel, S., Gier, B., Bovensmann, H., Burrows, J. P., Boesch, H., Anand, J., Parker, R. J., Somkuti, P., Detmers, R. G., Hasekamp, O. P., Aben, I., Butz, A., Kuze, A., Suto, H., Yoshida, Y., Crisp, D., and O'Dell, C.: Computation and analysis of atmospheric carbon dioxide annual mean growth rates from satellite observations during 2003-2016, Atmos Chem Phys, 18, 1-22, 10.5194/acp-18-17355-2018, 2018.

Burrows, J. P., Holzle, E., Goede, A. P. H., Visser, H., and Fricke, W.: Sciamachy - Scanning Imaging Absorption Spectrometer for Atmospheric Chartography, Acta Astronaut, 35, 445-451, Doi 10.1016/0094-5765(94)00278-T, 1995.

Calle, L., Poulter, B., and Patra, P. K.: A segmentation algorithm for characterizing rise and fall segments in seasonal cycles: an application to XCO2 to estimate benchmarks and assess model bias, Atmos. Meas. Tech., 12, 2611-2629, 10.5194/amt-12-2611-2019, 2019.

Channan, S., Collins, K., and Emanuel, W. R.: Global mosaics of the standard MODIS Vegetation Continuous Fields data, University of Maryland and the Pacific Northwest National Laboratory, College Park, Maryland, USA., 2014.

Cheng, S. J., Steiner, A. L., Hollinger, D. Y., Bohrer, G., and Nadelhoffer, K. J.: Using satellite-derived optical thickness to assess the influence of clouds on terrestrial carbon uptake, Journal of Geophysical Research: Biogeosciences, 121, 1747-1761, 10.1002/2016jg003365, 2016.

Chevallier, F., Palmer, P. I., Feng, L., Boesch, H., O'Dell, C. W., and Bousquet, P.: Toward robust and consistent regional CO2 flux estimates from in situ and spaceborne measurements of atmospheric CO2, Geophys Res Lett, 41, 1065-1070, 10.1002/2013gl058772, 2014.

Ciais, P., Sabine, C., Bala, G., Bopp, L., Brovkin, V., Canadell, J., Chhabra, A., DeFries, R., Galloway, J., Heimann, M., Jones, C., Le Quéré, C., Myneni, R. B., Piao, S., and Thornton, P.: Carbon and Other Biogeochemical Cycles, Climate Change 2013: The Physical Science Basis. Contribution of Working Group I to the Fifth Assessment Report of the Intergovernmental Panel on Climate Change, 465-570, 10.1017/CBO9781107415324.015, 2013.

Cox, P. M., Pearson, D., Booth, B. B., Friedlingstein, P., Huntingford, C., Jones, C. D., and Luke, C. M.: Sensitivity of tropical carbon to climate change constrained by carbon dioxide variability, Nature, 494, 341-344, 10.1038/nature11882, 2013.

Dlugokencky, E. J., Lang, P. M., Mund, J. W., Crotwell, A. M., Crotwell, M. J., and Thoning, K. W.: Atmospheric Carbon Dioxide Dry Air Mole Fractions from the NOAA ESRL Carbon Cycle Cooperative Global Air Sampling Network, 2018-07-31, ftp://aftp.cmdl.noaa.gov/data/trace_gases/co2/flask/surface/, 2018.

Dlugokencky, E. J., Mund, J. W., Crotwell, A. M., Crotwell, M. J., and Thoning, K. W.: Atmospheric Carbon Dioxide Dry Air Mole Fractions from the NOAA GML Carbon Cycle Cooperative Global Air Sampling Network, 1968-2019, https://doi.org/10.15138/wkgj-f215, 2020.

Dunne, J. P., John, J. G., Adcroft, A. J., Griffies, S. M., Hallberg, R. W., Shevliakova, E., Stouffer, R. J., Cooke, W., Dunne, K. A., Harrison, M. J., Krasting, J. P., Malyshev, S. L., Milly, P. C. D., Phillipps, P. J., Sentman, L. T., Samuels, B. L., Spelman, M. J., Winton, M., Wittenberg, A. T., and Zadeh, N.: GFDL's ESM2 Global Coupled Climate-Carbon Earth System Models. Part I: Physical Formulation and Baseline Simulation Characteristics, J Climate, 25, 6646-6665, 10.1175/Jcli-D-11-00560.1, 2012.

Dunne, J. P., John, J. G., Shevliakova, E., Stouffer, R. J., Krasting, J. P., Malyshev, S. L., Milly, P. C. D., Sentman, L. T., Adcroft, A. J., Cooke, W., Dunne, K. A., Griffies, S. M., Hallberg, R. W., Harrison, M. J., Levy, H., Wittenberg, A. T., Phillips, P. J., and Zadeh, N.: GFDL's ESM2 Global Coupled Climate-Carbon Earth System Models. Part II: Carbon System Formulation and Baseline Simulation Characteristics, J Climate, 26, 2247-2267, 10.1175/Jcli-D-12-00150.1, 2013.

Dunne, J. P., Horowitz, L. W., Adcroft, A. J., Ginoux, P., Held, I. M., John, J. G., Krasting, J. P., Malyshev, S., Naik, V., Paulot, F., Shevliakova, E., Stock, C. A., Zadeh, N., Balaji, V., Blanton, C., Dunne, K. A., Dupuis, C., Durachta, J., Dussin, R., Gauthier, P. P. G., Griffies, S. M., Guo, H., Hallberg, R. W., Harrison, M., He, J., Hurlin, W., McHugh, C., Menzel, R., Milly, P. C. D., Nikonov, S., Paynter, D. J., Ploshay, J., Radhakrishnan, A., Rand, K., Reichl, B. G., Robinson, T., Schwarzkopf, D. M., Sentman, L. T., Underwood, S., Vahlenkamp, H., Winton, M., Wittenberg, A. T., Wyman, B., Zeng, Y., and Zhao, M.: The GFDL Earth System Model version 4.1 (GFDL-ESM 4.1): Overall coupled model description and simulation characteristics, J Adv Model Earth Sy, n/a, e2019MS002015, 10.1029/2019ms002015, 2020.

Eyring, V., Bony, S., Meehl, G. A., Senior, C. A., Stevens, B., Stouffer, R. J., and Taylor, K. E.: Overview of the Coupled Model Intercomparison Project Phase 6 (CMIP6) experimental design and organization, Geosci Model Dev, 9, 1937-1958, 10.5194/gmd-9-1937-2016, 2016a.

Eyring, V., Righi, M., Lauer, A., Evaldsson, M., Wenzel, S., Jones, C., Anav, A., Andrews, O., Cionni, I., Davin, E. L., Deser, C., Ehbrecht, C., Friedlingstein, P., Gleckler, P., Gottschaldt, K. D., Hagemann, S., Juckes, M., Kindermann, S., Krasting, J., Kunert, D., Levine, R., Loew, A., Makela, J., Martin, G., Mason, E., Phillips, A. S., Read, S., Rio, C., Roehrig, R., Senftleben, D., Sterl, A., van Ulft, L. H., Walton, J., Wang, S. Y., and Williams, K. D.: ESMValTool (v1.0) - a community diagnostic and performance metrics tool for routine evaluation of Earth system models in CMIP, Geosci Model Dev, 9, 1747-1802, 10.5194/gmd-9-1747-2016, 2016b.

Eyring, V., Bock, L., Lauer, A., Righi, M., Schlund, M., Andela, B., Arnone, E., Bellprat, O., Brötz, B., Caron, L. P., Carvalhais, N., Cionni, I., Cortesi, N., Crezee, B., Davin, E., Davini, P., Debeire, K., de Mora, L., Deser, C., Docquier, D., Earnshaw, P., Ehbrecht, C., Gier, B. K., Gonzalez-Reviriego, N., Goodman, P., Hagemann, S., Hardiman, S., Hassler, B., Hunter, A., Kadow, C., Kindermann, S., Koirala, S., Koldunov, N. V., Lejeune, Q., Lembo, V., Lovato, T., Lucarini, V., Massonnet, F., Müller, B., Pandde, A., Pérez-Zanón, N., Phillips, A., Predoi, V., Russell, J., Sellar, A., Serva, F., Stacke, T., Swaminathan, R., Torralba, V., Vegas-Regidor, J., von Hardenberg, J., Weigel, K., and Zimmermann, K.: ESMValTool v2.0 - Extended set of large-scale diagnostics for quasi-operational and comprehensive evaluation of Earth system models in CMIP, Geosci. Model Dev. Discuss., 2019, 1-81, 10.5194/gmd-2019-291, 2019a.

Eyring, V., Cox, P. M., Flato, G. M., Gleckler, P. J., Abramowitz, G., Caldwell, P., Collins, W. D., Gier, B. K., Hall, A. D., Hoffman, F. M., Hurtt, G. C., Jahn, A., Jones, C. D., Klein, S. A., Krasting, J. P., Kwiatkowski, L., Lorenz, R., Maloney, E., Meehl, G. A., Pendergrass, A. G., Pincus, R., Ruane, A. C., Russell, J. L., Sanderson, B. M., Santer, B. D., Sherwood, S. C., Simpson, I. R., Stouffer, R. J., and Williamson, M. S.: Taking climate model evaluation to the next level, Nature Climate Change, 9, 102-110, 10.1038/s41558-018-0355-y, 2019b.

Eyring, V., Bock, L., Lauer, A., Righi, M., Schlund, M., Andela, B., Arnone, E., Bellprat, O., Brötz, B., Caron, L. P., Carvalhais, N., Cionni, I., Cortesi, N., Crezee, B., Davin, E. L., Davini, P., Debeire, K., de Mora, L., Deser, C., Docquier, D., Earnshaw, P., Ehbrecht, C., Gier, B. K., Gonzalez-Reviriego, N., Goodman, P., Hagemann, S., Hardiman, S., Hassler, B., Hunter, A., Kadow, C., Kindermann, S., Koirala, S., Koldunov, N., Lejeune, Q., Lembo, V., Lovato, T., Lucarini, V., Massonnet, F., Müller, B., Pandde, A., Pérez-Zanón, N., Phillips, A., Predoi, V., Russell, J., Sellar, A., Serva, F., Stacke, T., Swaminathan, R., Torralba, V., Vegas-Regidor, J., von Hardenberg, J., Weigel, K., and Zimmermann, K.: Earth System Model Evaluation Tool (ESMValTool) v2.0 – an extended set of large-scale diagnostics for quasi-operational and comprehensive evaluation of Earth system models in CMIP, Geosci. Model Dev., 13, 3383-3438, 10.5194/gmd-13-3383-2020, 2020.

Fernández-Martínez, M., Sardans, J., Chevallier, F., Ciais, P., Obersteiner, M., Vicca, S., Canadell, J. G., Bastos, A., Friedlingstein, P., Sitch, S., Piao, S. L., Janssens, I. A., and Peñuelas, J.: Global trends in carbon sinks and their relationships with CO2 and temperature, Nature Climate Change, 9, 73-79, 10.1038/s41558-018-0367-7, 2019.

Ferraro, R., Waliser, D. E., Gleckler, P., Taylor, K. E., and Eyring, V.: Evolving Obs4MIPs to Support Phase 6 of the Coupled Model Intercomparison Project (CMIP6), Bulletin of the American Meteorological Society, 96, ES131-ES133, 10.1175/bams-d-14-00216.1, 2015.

Friedl, M. A., Sulla-Menashe, D., Tan, B., Schneider, A., Ramankutty, N., Sibley, A., and Huang, X. M.: MODIS Collection 5 global land cover: Algorithm refinements and characterization of new datasets, Remote Sens Environ, 114, 168-182, 10.1016/j.rse.2009.08.016, 2010.

Friedlingstein, P., Cox, P., Betts, R., Bopp, L., von Bloh, W., Brovkin, V., Cadule, P., Doney, S., Eby, M., Fung, I., Bala, G., John, J., Jones, C., Joos, F., Kato, T., Kawamiya, M., Knorr, W., Lindsay, K., Matthews, H. D., Raddatz, T., Rayner, P., Reick, C., Roeckner, E., Schnitzler, K. G., Schnur, R., Strassmann, K., Weaver, A. J., Yoshikawa, C., and Zeng, N.: Climate–Carbon Cycle Feedback Analysis: Results from the C4MIP Model Intercomparison, J Climate, 19, 3337-3353, 10.1175/jcli3800.1, 2006.

Friedlingstein, P., Meinshausen, M., Arora, V. K., Jones, C. D., Anav, A., Liddicoat, S. K., and Knutti, R.: Uncertainties in CMIP5 Climate Projections due to Carbon Cycle Feedbacks, J Climate, 27, 511-526, 10.1175/Jcli-D-12-00579.1, 2014.

Friedlingstein, P., Jones, M. W., O'Sullivan, M., Andrew, R. M., Hauck, J., Peters, G. P., Peters, W., Pongratz, J., Sitch, S., Le Quéré, C., Bakker, D. C. E., Canadell, J. G., Ciais, P., Jackson, R. B., Anthoni, P., Barbero, L., Bastos, A., Bastrikov, V., Becker, M., Bopp, L., Buitenhuis, E., Chandra, N., Chevallier, F., Chini, L. P., Currie, K. I., Feely, R. A., Gehlen, M., Gilfillan, D., Gkritzalis, T., Goll, D. S., Gruber, N., Gutekunst, S., Harris, I., Haverd, V., Houghton, R. A., Hurtt, G., Ilyina, T., Jain, A. K., Joetzjer, E., Kaplan, J. O., Kato, E., Klein Goldewijk, K., Korsbakken, J. I., Landschützer, P., Lauvset, S. K., Lefèvre, N., Lenton, A., Lienert, S., Lombardozzi, D., Marland, G., McGuire, P. C., Melton, J. R., Metzl, N., Munro, D. R., Nabel, J. E. M. S., Nakaoka, S. I., Neill, C., Omar, A. M., Ono, T., Peregon, A., Pierrot, D., Poulter, B., Rehder, G., Resplandy, L., Robertson, E., Rödenbeck, C., Séférian, R., Schwinger, J., Smith, N., Tans, P. P., Tian, H., Tilbrook, B., Tubiello, F. N., van der Werf, G. R., Wiltshire, A. J., and Zaehle, S.: Global Carbon Budget 2019, Earth Syst. Sci. Data, 11, 1783-1838, 10.5194/essd-11-1783-2019, 2019.

Gent, P. R., Danabasoglu, G., Donner, L. J., Holland, M. M., Hunke, E. C., Jayne, S. R., Lawrence, D. M., Neale, R. B., Rasch, P. J., Vertenstein, M., Worley, P. H., Yang, Z. L., and Zhang, M. H.: The Community Climate System Model Version 4, J Climate, 24, 4973-4991, 10.1175/2011jcli4083.1, 2011.

Giorgetta, M. A., Jungclaus, J., Reick, C. H., Legutke, S., Bader, J., Bottinger, M., Brovkin, V., Crueger, T., Esch, M., Fieg, K., Glushak, K., Gayler, V., Haak, H., Hollweg, H. D., Ilyina, T., Kinne, S., Kornblueh, L., Matei, D., Mauritsen, T., Mikolajewicz, U., Mueller, W., Notz, D., Pithan, F., Raddatz, T., Rast, S., Redler, R., Roeckner, E., Schmidt, H., Schnur, R., Segschneider, J., Six, K. D., Stockhause, M., Timmreck, C., Wegner, J., Widmann, H., Wieners, K. H., Claussen, M., Marotzke, J., and Stevens, B.: Climate and carbon cycle changes from 1850 to 2100 in MPI-ESM simulations for the Coupled Model Intercomparison Project phase 5, J Adv Model Earth Sy, 5, 572-597, 10.1002/jame.20038, 2013.

Graven, H. D., Keeling, R. F., Piper, S. C., Patra, P. K., Stephens, B. B., Wofsy, S. C., Welp, L. R., Sweeney, C., Tans, P. P., Kelley, J. J., Daube, B. C., Kort, E. A., Santoni, G. W., and Bent, J. D.: Enhanced seasonal exchange of CO2 by northern ecosystems since 1960, Science, 341, 1085-1089, 10.1126/science.1239207, 2013.

Hajima, T., Tachiiri, K., Ito, A., and Kawamiya, M.: Uncertainty of Concentration-Terrestrial Carbon Feedback in Earth System Models, J Climate, 27, 3425-3445, 10.1175/Jcli-D-13-00177.1, 2014.

Hajima, T., Abe, M., Arakawa, O., Suzuki, T., Komuro, Y., Ogochi, K., Watanabe, M., Yamamoto, A., Tatebe, H., Noguchi, M. A., Ohgaito, R., Ito, A., Yamazaki, D., Ito, A., Takata, K., Watanabe, S., Kawamiya, M., and Tachiiri, K.: MIROC MIROC-ES2L model output prepared for CMIP6 CMIP esm-hist v20200318, Earth System Grid Federation, 10.22033/ESGF/CMIP6.5496, 2020a.

Hajima, T., Watanabe, M., Yamamoto, A., Tatebe, H., Noguchi, M. A., Abe, M., Ohgaito, R., Ito, A., Yamazaki, D., Okajima, H., Ito, A., Takata, K., Ogochi, K., Watanabe, S., and Kawamiya, M.: Development of the MIROC-ES2L Earth system model

and the evaluation of biogeochemical processes and feedbacks, Geosci. Model Dev., 13, 2197-2244, 10.5194/gmd-13-2197-2020, 2020b.

Hansen, J., Ruedy, R., Sato, M., and Lo, K.: Global Surface Temperature Change, Rev Geophys, 48, Artn Rg4004 10.1029/2010rg000345, 2010.

Hayman, G. D., O'Connor, F. M., Dalvi, M., Clark, D. B., Gedney, N., Huntingford, C., Prigent, C., Buchwitz, M., Schneising, O., Burrows, J. P., Wilson, C., Richards, N., and Chipperfield, M.: Comparison of the HadGEM2 climate-chemistry model against in situ and SCIAMACHY atmospheric methane data, Atmos Chem Phys, 14, 13257-13280, 10.5194/acp-14-13257-2014, 2014.

Hoffman, F. M., Randerson, J. T., Arora, V. K., Bao, Q., Cadule, P., Ji, D., Jones, C. D., Kawamiya, M., Khatiwala, S., Lindsay, K., Obata, A., Shevliakova, E., Six, K. D., Tjiputra, J. F., Volodin, E. M., and Wu, T.: Causes and implications of persistent atmospheric carbon dioxide biases in Earth System Models, J Geophys Res-Biogeo, 119, 141-162, 10.1002/2013jg002381, 2014.

Houweling, S., Baker, D., Basu, S., Boesch, H., Butz, A., Chevallier, F., Deng, F., Dlugokencky, E. J., Feng, L., Ganshin, A., Hasekamp, O., Jones, D., Maksyutov, S., Marshall, J., Oda, T., O'Dell, C. W., Oshchepkov, S., Palmer, P. I., Peylin, P., Poussi, Z., Reum, F., Takagi, H., Yoshida, Y., and Zhuravlev, R.: An intercomparison of inverse models for estimating sources and sinks of CO2using GOSAT measurements, Journal of Geophysical Research: Atmospheres, 120, 5253-5266, 10.1002/2014jd022962, 2015.

IPCC: Climate Change 2013: The Physical Science Basis. Contribution of Working Group I to the Fifth Assessment Report of the Intergovernmental Panel on Climate Change, Cambridge University Press, 1535, 10.1017/CBO9781107415324, 2013.

Ji, D., Wang, L., Feng, J., Wu, Q., Cheng, H., Zhang, Q., Yang, J., Dong, W., Dai, Y., Gong, D., Zhang, R. H., Wang, X., Liu, J., Moore, J. C., Chen, D., and Zhou, M.: Description and basic evaluation of Beijing Normal University Earth System Model (BNU-ESM) version 1, Geosci Model Dev, 7, 2039-2064, 10.5194/gmd-7-2039-2014, 2014.

Kaminski, T., Knorr, W., Schurmann, G., Scholze, M., Rayner, P. J., Zaehle, S., Blessing, S., Dorigo, W., Gayler, V., Giering, R., Gobron, N., Grant, J. P., Heimann, M., Hooker-Stroud, A., Houweling, S., Kato, T., Kattge, J., Kelley, D., Kemp, S., Koffi, E. N., Kostler, C., Mathieu, P. P., Pinty, B., Reick, C. H., Rodenbeck, C., Schnur, R., Scipal, K., Sebald, C., Stacke, T., van Scheltinga, A. T., Vossbeck, M., Widmann, H., and Ziehn, T.: The BETHY/JSBACH Carbon Cycle Data Assimilation System: experiences and challenges, J Geophys Res-Biogeo, 118, 1414-1426, 10.1002/jgrg.20118, 2013.

Keeling, C. D., Bacastow, R. B., Bainbridge, A. E., Ekdahl, C. A., Guenther, P. R., Waterman, L. S., and Chin, J. F. S.: Atmospheric Carbon-Dioxide Variations at Mauna-Loa Observatory, Hawaii, Tellus, 28, 538-551, 10.1111/j.2153-3490.1976.tb00701.x, 1976.

Keeling, C. D., Bacastow, R. B., Carter, A. F., Piper, S. C., Whorf, T. P., Heimann, M., Mook, W. G., and Roeloffzen, H.: A three-dimensional model of atmospheric CO2transport based on observed winds: 1. Analysis of observational data, in: Aspects of Climate Variability in the Pacific and the Western Americas, Geophysical Monograph Series, 165-236, 1989.

Keeling, C. D., Whorf, T. P., Wahlen, M., and Vanderplicht, J.: Interannual Extremes in the Rate of Rise of Atmospheric Carbon-Dioxide since 1980, Nature, 375, 666-670, DOI 10.1038/375666a0, 1995.

Keeling, C. D., Chin, J. F. S., and Whorf, T. P.: Increased activity of northern vegetation inferred from atmospheric CO2 measurements, Nature, 382, 146-149, 10.1038/382146a0, 1996.

Krasting, J. P., John, J. G., Blanton, C., McHugh, C., Nikonov, S., Radhakrishnan, A., Rand, K., Zadeh, N. T., Balaji, V., Durachta, J., Dupuis, C., Menzel, R., Robinson, T., Underwood, S., Vahlenkamp, H., Dunne, K. A., Gauthier, P. P. G., Ginoux, P., Griffies, S. M., Hallberg, R., Harrison, M., Hurlin, W., Malyshev, S., Naik, V., Paulot, F., Paynter, D. J., Ploshay, J., Schwarzkopf, D. M., Seman, C. J., Silvers, L., Wyman, B., Zeng, Y., Adcroft, A., Dunne, J. P., Dussin, R., Guo, H., He, J., Held, I. M., Horowitz, L. W., Lin, P., Milly, P. C. D., Shevliakova, E., Stock, C., Winton, M., Xie, Y., and Zhao, M.: NOAA-GFDL GFDL-ESM4 model output prepared for CMIP6 CMIP esm-hist v20190829, Earth System Grid Federation, 10.22033/ESGF/CMIP6.8522, 2018.

Kuze, A., Suto, H., Nakajima, M., and Hamazaki, T.: Thermal and near infrared sensor for carbon observation Fourier-transform spectrometer on the Greenhouse Gases Observing Satellite for greenhouse gases monitoring, Appl Opt, 48, 6716-6733, 10.1364/AO.48.006716, 2009.

Lauer, A., Eyring, V., Bellprat, O., Bock, L., Gier, B. K., Hunter, A., Lorenz, R., Pérez-Zanón, N., Righi, M., Schlund, M., Senftleben, D., Weigel, K., and Zechlau, S.: Earth System Model Evaluation Tool (ESMValTool) v2.0 – diagnostics for emergent constraints and future projections from Earth system models in CMIP, Geosci. Model Dev. Discuss., 2020, 1-47, 10.5194/gmd-2020-60, 2020a.

Lauer, A., Eyring, V., Bellprat, O., Bock, L., Gier, B. K., Hunter, A., Lorenz, R., Pérez-Zanón, N., Righi, M., Schlund, M., Senftleben, D., Weigel, K., and Zechlau, S.: Earth System Model Evaluation Tool (ESMValTool) v2.0 – diagnostics for emergent constraints and future projections from Earth system models in CMIP, Geosci. Model Dev., 13, 4205-4228, 10.5194/gmd-13-4205-2020, 2020b.

Law, R. M., Ziehn, T., Matear, R. J., Lenton, A., Chamberlain, M. A., Stevens, L. E., Wang, Y. P., Srbinovsky, J., Bi, D., Yan, H., and Vohralik, P. F.: The carbon cycle in the Australian Community Climate and Earth System Simulator (ACCESS-ESM1) – Part 1: Model description and pre-industrial simulation, Geosci. Model Dev., 10, 2567-2590, 10.5194/gmd-10-2567-2017, 2017.

Lenssen, N. J. L., Schmidt, G. A., Hansen, J. E., Menne, M. J., Persin, A., Ruedy, R., and Zyss, D.: Improvements in the GISTEMP Uncertainty Model, Journal of Geophysical Research: Atmospheres, 124, 6307-6326, 10.1029/2018jd029522, 2019.

Lindsay, K., Bonan, G. B., Doney, S. C., Hoffman, F. M., Lawrence, D. M., Long, M. C., Mahowald, N. M., Moore, J. K., Randerson, J. T., and Thornton, P. E.: Preindustrial-Control and Twentieth-Century Carbon Cycle Experiments with the Earth System Model CESM1(BGC), J Climate, 27, 8981-9005, 10.1175/Jcli-D-12-00565.1, 2014.

Mauritsen, T., Bader, J., Becker, T., Behrens, J., Bittner, M., Brokopf, R., Brovkin, V., Claussen, M., Crueger, T., Esch, M., Fast, I., Fiedler, S., Fläschner, D., Gayler, V., Giorgetta, M., Goll, D. S., Haak, H., Hagemann, S., Hedemann, C., Hohenegger, C., Ilyina, T., Jahns, T., Jimenéz-de-la-Cuesta, D., Jungclaus, J., Kleinen, T., Kloster, S., Kracher, D., Kinne, S., Kleberg, D., Lasslop, G., Kornblueh, L., Marotzke, J., Matei, D., Meraner, K., Mikolajewicz, U., Modali, K., Möbis, B., Müller, W. A., Nabel, J. E. M. S., Nam, C. C. W., Notz, D., Nyawira, S.-S., Paulsen, H., Peters, K., Pincus, R., Pohlmann, H., Pongratz, J., Popp, M., Raddatz, T. J., Rast, S., Redler, R., Reick, C. H., Rohrschneider, T., Schemann, V., Schmidt, H., Schnur, R., Schulzweida, U., Six, K. D., Stein, L., Stemmler, I., Stevens, B., von Storch, J.-S., Tian, F., Voigt, A., Vrese, P., Wieners, K.-H., Wilkenskjeld, S., Winkler, A., and Roeckner, E.: Developments in the MPI-M Earth System Model version 1.2 (MPI-ESM1.2) and Its Response to Increasing CO2, J Adv Model Earth Sy, 11, 998-1038, 10.1029/2018ms001400, 2019.

Myneni, R. B., Keeling, C. D., Tucker, C. J., Asrar, G., and Nemani, R. R.: Increased plant growth in the northern high latitudes from 1981 to 1991, Nature, 386, 698-702, 10.1038/386698a0, 1997.

Piao, S., Liu, Z., Wang, Y., Ciais, P., Yao, Y., Peng, S., Chevallier, F., Friedlingstein, P., Janssens, I. A., Peñuelas, J., Sitch, S., and Wang, T.: On the causes of trends in the seasonal amplitude of atmospheric CO2, Global Change Biology, 24, 608-616, 10.1111/gcb.13909, 2018.

Qiao, F. L., Song, Z. Y., Bao, Y., Song, Y. J., Shu, Q., Huang, C. J., and Zhao, W.: Development and evaluation of an Earth System Model with surface gravity waves, J Geophys Res-Oceans, 118, 4514-4524, 10.1002/jgrc.20327, 2013.

Reich, P. B., Hobbie, S. E., Lee, T., Ellsworth, D. S., West, J. B., Tilman, D., Knops, J. M. H., Naeem, S., and Trost, J.: Nitrogen limitation constrains sustainability of ecosystem response to CO2, Nature, 440, 922-925, 10.1038/nature04486, 2006.

Reuter, M., Bösch, H., Bovensmann, H., Bril, A., Buchwitz, M., Butz, A., Burrows, J. P., amp, apos, Dell, C. W., Guerlet, S., Hasekamp, O., Heymann, J., Kikuchi, N., Oshchepkov, S., Parker, R., Pfeifer, S., Schneising, O., Yokota, T., and Yoshida, Y.: A joint effort to deliver satellite retrieved atmospheric CO2 concentrations for surface flux inversions: the ensemble median algorithm EMMA, Atmos Chem Phys, 13, 1771-1780, 10.5194/acp-13-1771-2013, 2013.

Reuter, M., Buchwitz, M., Hilker, M., Heymann, J., Schneising, O., Pillai, D., Bovensmann, H., Burrows, J. P., Bosch, H., Parker, R., Butz, A., Hasekamp, O., O'Dell, C. W., Yoshida, Y., Gerbig, C., Nehrkorn, T., Deutscher, N. M., Warneke, T., Notholt, J., Hase, F., Kivi, R., Sussmann, R., Machida, T., Matsueda, H., and Sawa, Y.: Satellite-inferred European carbon sink larger than expected, Atmos Chem Phys, 14, 13739-13753, 10.5194/acp-14-13739-2014, 2014.

Reuter, M., Buchwitz, M., and Schneising-Weigel, O.: Product User Guide and Specification (PUGS) – ANNEX D for products XCO2_EMMA and XCH4_EMMA, 1-19, 2017.

Reuter, M., Buchwitz, M., Schneising, O., Noël, S., Bovensmann, H., Burrows, J. P., Boesch, H., Di Noia, A., Anand, J., Parker, R. J., Somkuti, P., Wu, L., Hasekamp, O. P., Aben, I., Kuze, A., Suto, H., Shiomi, K., Yoshida, Y., Morino, I., Crisp, D., O'Dell, C. W., Notholt, J., Petri, C., Warneke, T., Velazco, V. A., Deutscher, N. M., Griffith, D. W. T., Kivi, R., Pollard, D. F., Hase, F., Sussmann, R., Té, Y. V., Strong, K., Roche, S., Sha, M. K., De Mazière, M., Feist, D. G., Iraci, L. T., Roehl, C. M., Retscher, C., and Schepers, D.: Ensemble-based satellite-derived carbon dioxide and methane column-averaged dry-air mole fraction data sets (2003–2018) for carbon and climate applications, Atmos. Meas. Tech., 13, 789-819, 10.5194/amt-13-789-2020, 2020.

Righi, M., Andela, B., Eyring, V., Lauer, A., Predoi, V., Schlund, M., Vegas-Regidor, J., Bock, L., Brötz, B., de Mora, L., Diblen, F., Dreyer, L., Drost, N., Earnshaw, P., Hassler, B., Koldunov, N., Little, B., Loosveldt Tomas, S., and Zimmermann, K.: Earth System Model Evaluation Tool (ESMValTool) v2.0 – technical overview, Geosci. Model Dev., 13, 1179-1199, 10.5194/gmd-13-1179-2020, 2020.

Ryu, Y., Berry, J. A., and Baldocchi, D. D.: What is global photosynthesis? History, uncertainties and opportunities, Remote Sens Environ, 223, 95-114, https://doi.org/10.1016/j.rse.2019.01.016, 2019.

Schneising, O., Reuter, M., Buchwitz, M., Heymann, J., Bovensmann, H., and Burrows, J. P.: Terrestrial carbon sink observed from space: variation of growth rates and seasonal cycle amplitudes in response to interannual surface temperature variability, Atmos Chem Phys, 14, 133-141, 10.5194/acp-14-133-2014, 2014.

Seferian, R.: CNRM-CERFACS CNRM-ESM2-1 model output prepared for CMIP6 CMIP esm-hist v20200715, Earth System Grid Federation, 10.22033/ESGF/CMIP6.4003, 2019.

Séférian, R., Nabat, P., Michou, M., Saint-Martin, D., Voldoire, A., Colin, J., Decharme, B., Delire, C., Berthet, S., Chevallier, M., Sénési, S., Franchisteguy, L., Vial, J., Mallet, M., Joetzjer, E., Geoffroy, O., Guérémy, J.-F., Moine, M.-P., Msadek, R., Ribes, A., Rocher, M., Roehrig, R., Salas-y-Mélia, D., Sanchez, E., Terray, L., Valcke, S., Waldman, R., Aumont, O., Bopp,

L., Deshayes, J., Éthé, C., and Madec, G.: Evaluation of CNRM Earth System Model, CNRM-ESM2-1: Role of Earth System Processes in Present-Day and Future Climate, J Adv Model Earth Sy, 11, 4182-4227, 10.1029/2019ms001791, 2019.

Seland, Ø., Bentsen, M., Oliviè, D. J. L., Toniazzo, T., Gjermundsen, A., Graff, L. S., Debernard, J. B., Gupta, A. K., He, Y., Kirkevåg, A., Schwinger, J., Tjiputra, J., Aas, K. S., Bethke, I., Fan, Y., Griesfeller, J., Grini, A., Guo, C., Ilicak, M., Karset, I. H. H., Landgren, O. A., Liakka, J., Moseid, K. O., Nummelin, A., Spensberger, C., Tang, H., Zhang, Z., Heinze, C., Iversen, T., and Schulz, M.: NCC NorESM2-LM model output prepared for CMIP6 CMIP esm-hist v20190920, Earth System Grid Federation, 10.22033/ESGF/CMIP6.7924, 2019.

Seland, Ø., Bentsen, M., Seland Graff, L., Olivié, D., Toniazzo, T., Gjermundsen, A., Debernard, J. B., Gupta, A. K., He, Y., Kirkevåg, A., Schwinger, J., Tjiputra, J., Schancke Aas, K., Bethke, I., Fan, Y., Griesfeller, J., Grini, A., Guo, C., Ilicak, M., Hafsahl Karset, I. H., Landgren, O., Liakka, J., Onsum Moseid, K., Nummelin, A., Spensberger, C., Tang, H., Zhang, Z., Heinze, C., Iverson, T., and Schulz, M.: The Norwegian Earth System Model, NorESM2 - Evaluation of theCMIP6 DECK and historical simulations, Geosci. Model Dev. Discuss., 2020, 1-68, 10.5194/gmd-2019-378, 2020.

Sellar, A. A., Jones, C. G., Mulcahy, J. P., Tang, Y., Yool, A., Wiltshire, A., O'Connor, F. M., Stringer, M., Hill, R., Palmieri, J., Woodward, S., de Mora, L., Kuhlbrodt, T., Rumbold, S. T., Kelley, D. I., Ellis, R., Johnson, C. E., Walton, J., Abraham, N. L., Andrews, M. B., Andrews, T., Archibald, A. T., Berthou, S., Burke, E., Blockley, E., Carslaw, K., Dalvi, M., Edwards, J., Folberth, G. A., Gedney, N., Griffiths, P. T., Harper, A. B., Hendry, M. A., Hewitt, A. J., Johnson, B., Jones, A., Jones, C. D., Keeble, J., Liddicoat, S., Morgenstern, O., Parker, R. J., Predoi, V., Robertson, E., Siahaan, A., Smith, R. S., Swaminathan, R., Woodhouse, M. T., Zeng, G., and Zerroukat, M.: UKESM1: Description and Evaluation of the U.K. Earth System Model, J Adv Model Earth Sy, 11, 4513-4558, 10.1029/2019MS001739, 2019.

Shindell, D. T., Lamarque, J. F., Schulz, M., Flanner, M., Jiao, C., Chin, M., Young, P. J., Lee, Y. H., Rotstayn, L., Mahowald, N., Milly, G., Faluvegi, G., Balkanski, Y., Collins, W. J., Conley, A. J., Dalsoren, S., Easter, R., Ghan, S., Horowitz, L., Liu, X., Myhre, G., Nagashima, T., Naik, V., Rumbold, S. T., Skeie, R., Sudo, K., Szopa, S., Takemura, T., Voulgarakis, A., Yoon, J. H., and Lo, F.: Radiative forcing in the ACCMIP historical and future climate simulations, Atmos Chem Phys, 13, 2939-2974, 10.5194/acp-13-2939-2013, 2013.

Still, C. J., Riley, W. J., Biraud, S. C., Noone, D. C., Buenning, N. H., Randerson, J. T., Torn, M. S., Welker, J., White, J. W. C., Vachon, R., Farquhar, G. D., and Berry, J. A.: Influence of clouds and diffuse radiation on ecosystem-atmosphere CO2 and CO18O exchanges, Journal of Geophysical Research: Biogeosciences, 114, 10.1029/2007jg000675, 2009.

Swart, N. C., Cole, J. N. S., Kharin, V. V., Lazare, M., Scinocca, J. F., Gillett, N. P., Anstey, J., Arora, V., Christian, J. R., Hanna, S., Jiao, Y., Lee, W. G., Majaess, F., Saenko, O. A., Seiler, C., Seinen, C., Shao, A., Sigmond, M., Solheim, L., von Salzen, K., Yang, D., and Winter, B.: The Canadian Earth System Model version 5 (CanESM5.0.3), Geosci. Model Dev., 12, 4823-4873, 10.5194/gmd-12-4823-2019, 2019a.

Swart, N. C., Cole, J. N. S., Kharin, V. V., Lazare, M., Scinocca, J. F., Gillett, N. P., Anstey, J., Arora, V., Christian, J. R., Jiao, Y., Lee, W. G., Majaess, F., Saenko, O. A., Seiler, C., Seinen, C., Shao, A., Solheim, L., von Salzen, K., Yang, D., Winter, B., and Sigmond, M.: CCCma CanESM5 model output prepared for CMIP6 CMIP esm-hist v20190429, Earth System Grid Federation, 10.22033/ESGF/CMIP6.3583, 2019b.

Swart, N. C., Cole, J. N. S., Kharin, V. V., Lazare, M., Scinocca, J. F., Gillett, N. P., Anstey, J., Arora, V., Christian, J. R., Jiao, Y., Lee, W. G., Majaess, F., Saenko, O. A., Seiler, C., Seinen, C., Shao, A., Solheim, L., von Salzen, K., Yang, D., Winter, B., and Sigmond, M.: CCCma CanESM5-CanOE model output prepared for CMIP6 CMIP esm-hist v20190429, Earth System Grid Federation, 10.22033/ESGF/CMIP6.10232, 2019c.

Tang, Y., Rumbold, S., Ellis, R., Kelley, D., Mulcahy, J., Sellar, A., Walton, J., and Jones, C.: MOHC UKESM1.0-LL model output prepared for CMIP6 CMIP esm-hist v20190723, Earth System Grid Federation, 10.22033/ESGF/CMIP6.5929, 2019.

Taylor, K. E., Stouffer, R. J., and Meehl, G. A.: An Overview of CMIP5 and the Experiment Design, Bulletin of the American Meteorological Society, 93, 485-498, 10.1175/bams-d-11-00094.1, 2012.

Teixeira, J., Waliser, D., Ferraro, R., Gleckler, P., Lee, T., and Potter, G.: Satellite Observations for CMIP5: The Genesis of Obs4MIPs, Bulletin of the American Meteorological Society, 95, 1329-1334, 10.1175/bams-d-12-00204.1, 2014.

Tjiputra, J. F., Roelandt, C., Bentsen, M., Lawrence, D. M., Lorentzen, T., Schwinger, J., Seland, O., and Heinze, C.: Evaluation of the carbon cycle components in the Norwegian Earth System Model (NorESM), Geosci Model Dev, 6, 301-325, 10.5194/gmd-6-301-2013, 2013.

Waliser, D., Gleckler, P. J., Ferraro, R., Taylor, K. E., Ames, S., Biard, J., Bosilovich, M. G., Brown, O., Chepfer, H., Cinquini, L., Durack, P., Eyring, V., Mathieu, P. P., Lee, T., Pinnock, S., Potter, G. L., Rixen, M., Saunders, R., Shulz, J., Thepaut, J. N., and Tuma, M.: Observations for Model Intercomparison Project (Obs4MIPs): Status for CMIP6, Geosci. Model Dev. Discuss., 2019, 1-30, 10.5194/gmd-2019-268, 2019.

Waliser, D., Gleckler, P. J., Ferraro, R., Taylor, K. E., Ames, S., Biard, J., Bosilovich, M. G., Brown, O., Chepfer, H., Cinquini, L., Durack, P. J., Eyring, V., Mathieu, P. P., Lee, T., Pinnock, S., Potter, G. L., Rixen, M., Saunders, R., Schulz, J., Thépaut, J. N., and Tuma, M.: Observations for Model Intercomparison Project (Obs4MIPs): status for CMIP6, Geosci. Model Dev., 13, 2945-2958, 10.5194/gmd-13-2945-2020, 2020.

Watanabe, S., Hajima, T., Sudo, K., Nagashima, T., Takemura, T., Okajima, H., Nozawa, T., Kawase, H., Abe, M., Yokohata, T., Ise, T., Sato, H., Kato, E., Takata, K., Emori, S., and Kawamiya, M.: MIROC-ESM 2010: model description and basic results of CMIP5-20c3m experiments, Geosci Model Dev, 4, 845-872, 10.5194/gmd-4-845-2011, 2011.

Weigel, K., Eyring, V., Gier, B. K., Lauer, A., Righi, M., Schlund, M., Adeniyi, K., Arnone, E., Berg, P., Bock, L., Corti, S., Caron, L. P., Cionni, I., Drost, N., Hunter, A., Liedô, L., Mohr, C.-M., Pérez-Zanón, N., Predoi, V., Sandstad, M., Sillmann, J., Sterl, A., Vegas-Regidor, J., and von Hardenberg, J.: Earth System Model Evaluation Tool (ESMValTool) v2.0 - diagnostics for extreme events, regional and impact evaluation and analysis of Earth system models in CMIP, Geosci. Model Dev., 2020, submitted.

Wenzel, S., Cox, P. M., Eyring, V., and Friedlingstein, P.: Emergent constraints on climate-carbon cycle feedbacks in the CMIP5 Earth system models, J Geophys Res-Biogeo, 119, 794-807, 10.1002/2013jg002591, 2014.

Wenzel, S., Cox, P. M., Eyring, V., and Friedlingstein, P.: Projected land photosynthesis constrained by changes in the seasonal cycle of atmospheric CO2, Nature, 538, 499-501, 10.1038/nature19772, 2016.

Wieder, W. R., Lawrence, D. M., Fisher, R. A., Bonan, G. B., Cheng, S. J., Goodale, C. L., Grandy, A. S., Koven, C. D., Lombardozzi, D. L., Oleson, K. W., and Thomas, R. Q.: Beyond Static Benchmarking: Using Experimental Manipulations to Evaluate Land Model Assumptions, Global Biogeochemical Cycles, 33, 1289-1309, 10.1029/2018gb006141, 2019.

Wieners, K.-H., Giorgetta, M., Jungclaus, J., Reick, C., Esch, M., Bittner, M., Legutke, S., Schupfner, M., Wachsmann, F., Gayler, V., Haak, H., de Vrese, P., Raddatz, T., Mauritsen, T., von Storch, J.-S., Behrens, J., Brovkin, V., Claussen, M., Crueger, T., Fast, I., Fiedler, S., Hagemann, S., Hohenegger, C., Jahns, T., Kloster, S., Kinne, S., Lasslop, G., Kornblueh, L., Marotzke, J., Matei, D., Meraner, K., Mikolajewicz, U., Modali, K., Müller, W., Nabel, J., Notz, D., Peters, K., Pincus, R., Pohlmann, H., Pongratz, J., Rast, S., Schmidt, H., Schnur, R., Schulzweida, U., Six, K., Stevens, B., Voigt, A., and Roeckner, E.: MPI-M MPI-ESM1.2-LR model output prepared for CMIP6 CMIP esm-hist v20190710, Earth System Grid Federation, 10.22033/ESGF/CMIP6.6545, 2019.

Williams, D. N., Ananthakrishnan, R., Bernholdt, D. E., Bharathi, S., Brown, D., Chen, M., Chervenak, A. L., Cinquini, L., Drach, R., Foster, I. T., Fox, P., Fraser, D., Garcia, J., Hankin, S., Jones, P., Middleton, D. E., Schwidder, J., Schweitzer, R.,

Schuler, R., Shoshani, A., Siebenlist, F., Sim, A., Strand, W. G., Su, M., and Wilhelmi, N.: The Earth System Grid: Enabling Access to Multimodel Climate Simulation Data, Bulletin of the American Meteorological Society, 90, 195-206, 10.1175/2008bams2459.1, 2009.

Wunch, D., Toon, G. C., Blavier, J. F., Washenfelder, R. A., Notholt, J., Connor, B. J., Griffith, D. W., Sherlock, V., and Wennberg, P. O.: The total carbon column observing network, Philos Trans A Math Phys Eng Sci, 369, 2087-2112, 10.1098/rsta.2010.0240, 2011.

Yin, Y., Ciais, P., Chevallier, F., Li, W., Bastos, A., Piao, S. L., Wang, T., and Liu, H. Y.: Changes in the Response of the Northern Hemisphere Carbon Uptake to Temperature Over the Last Three Decades, Geophys Res Lett, 45, 4371-4380, 10.1029/2018gl077316, 2018.

Yukimoto, S., Yoshimura, H., Hosaka, M., Sakami, T., Tsujino, H., Hirabara, M., Tanaka, T. Y., Deushi, M., Obata, A., Nakano, H., Adachi, Y., Shindo, E., Yabu, S., Ose, T., and Kitoh, A.: Meteorological Research Institute-Earth System Model Version 1 (MRI-ESM1), Technical Reports, 64, 88, 10.11483/mritechrepo.64, 2011.

Yukimoto, S., Adachi, Y., Hosaka, M., Sakami, T., Yoshimura, H., Hirabara, M., Tanaka, T. Y., Shindo, E., Tsujino, H., Deushi, M., Mizuta, R., Yabu, S., Obata, A., Nakano, H., Koshiro, T., Ose, T., and Kitoh, A.: A New Global Climate Model of the Meteorological Research Institute: MRI-CGCM3 - Model Description and Basic Performance -, Journal of the Meteorological Society of Japan, 90A, 23-64, 10.2151/jmsj.2012-A02, 2012.

Yukimoto, S., Kawai, H., Koshiro, T., Oshima, N., Yoshida, K., Urakawa, S., Tsujino, H., Deushi, M., Tanaka, T., Hosaka, M., Yabu, S., Yoshimura, H., Shindo, E., Mizuta, R., Obata, A., Adachi, Y., and Ishii, M.: The Meteorological Research Institute Earth System Model Version 2.0, MRI-ESM2.0: Description and Basic Evaluation of the Physical Component, Journal of the Meteorological Society of Japan. Ser. II, 97, 931-965, 10.2151/jmsj.2019-051, 2019a.

Yukimoto, S., Koshiro, T., Kawai, H., Oshima, N., Yoshida, K., Urakawa, S., Tsujino, H., Deushi, M., Tanaka, T., Hosaka, M., Yoshimura, H., Shindo, E., Mizuta, R., Ishii, M., Obata, A., and Adachi, Y.: MRI MRI-ESM2.0 model output prepared for CMIP6 CMIP esm-hist v20191205, Earth System Grid Federation, 10.22033/ESGF/CMIP6.6807, 2019b.

Zhao, F., Zeng, N., Asrar, G., Friedlingstein, P., Ito, A., Jain, A., Kalnay, E., Kato, E., Koven, C. D., Poulter, B., Rafique, R., Sitch, S., Shu, S. J., Stocker, B., Viovy, N., Wiltshire, A., and Zaehle, S.: Role of CO2, climate and land use in regulating the seasonal amplitude increase of carbon fluxes in terrestrial ecosystems: a multimodel analysis, Biogeosciences, 13, 5121-5137, 10.5194/bg-13-5121-2016, 2016.

Ziehn, T., Lenton, A., Law, R. M., Matear, R. J., and Chamberlain, M. A.: The carbon cycle in the Australian Community Climate and Earth System Simulator (ACCESS-ESM1) – Part 2: Historical simulations, Geosci. Model Dev., 10, 2591-2614, 10.5194/gmd-10-2591-2017, 2017.

Ziehn, T., Chamberlain, M., Lenton, A., Law, R., Bodman, R., Dix, M., Wang, Y., Dobrohotoff, P., Srbinovsky, J., Stevens, L., Vohralik, P., Mackallah, C., Sullivan, A., O'Farrell, S., and Druken, K.: CSIRO ACCESS-ESM1.5 model output prepared for CMIP6 CMIP esm-hist v20191203, Earth System Grid Federation, 10.22033/ESGF/CMIP6.4242, 2019.

Tables

Table 1: List of active NOAA surface flask measurement sites used in this study.

Code	Location	Latitude [°]	Longitude [°]	Altitude [m]	Start Year
ASK	Assekrem, Algeria	23.2625	5.6322	2710~~.00~~	1995
CGO	Cape Grim, Australia	-40.6800	144.6800	94~~.00~~	1984
LEF	Park Falls, United States	45-945	269.7300	868~~.00~~	1994
HUN	Hegyhatsal, Hungary	46.950	16.650	248~~.00~~	1993
WIS	Ketura, Israel	30.8595	34.7809	482~~.00~~	1995

Table 2: CMIP5 models analysed in this study. Under Comments, D stands for models including dynamic vegetation, and N for models including Nitrogen cycles.

Model	Institute	Atmosphere Model	Land Model	Ocean Model	Comment	Main Reference
BNU-ESM	College of Global Change and Earth System Science,	CAM3.5	CoLM + BNU-DGVM	MOM4p1 + IBGC	N, D	Ji et al. (2014)
CanESM2	Canadian Center for Climate Modeling and Analysis, BC, Canada	CanAM4	CLASS2.7 + CTEM1	CMOC		Arora et al. (2011)
CESM1-BGC	National Center for Atmospheric Research Boulder, CO, USA	CAM4	CLM4	POP2 + BEC	N	Gent et al. (2011); Lindsay et al. (2014)
FIO-ESM	The First Institute of Oceanography, SOA, China	CAM3.0	CLM3.5 + CASA	POP2.0 + OCMIP-2		Bao et al. (2012); Qiao et al. (2013)
GFDL-ESM2G	Geophysical Fluid Dynamics Laboratory, United States	AM2	LM3.0	GOLD + TOPAZ2	D	Dunne et al. (2012); Dunne et al. (2013)
GFDL-ESM2M	Geophysical Fluid Dynamics Laboratory, United States	AM2	LM3.0	MOM4.1 + TOPAZ2	D	Dunne et al. (2012); Dunne et al. (2013)
MIROC-ESM	Japan Agency for Marine-Earth Science and Technology, Japan; Atmosphere and Ocean Research Institute, Japan	MIROC-AGCM + SPRINTARS	MATSIRO + SEIB-DGVM	COCO3.4 + NPZD	D	Watanabe et al. (2011)
MPI-ESM-LR	Max Planck Institute for Meteorology, Hamburg, Germany	ECHAM6	JSBACH + BETHY	MPIOM + HAMOCC5	D	Giorgetta et al. (2013)

MRI-ESM1	Meteorological Research Institute, Japan	MRI-AGCM3.3 + MASINGAR mk-2 + MRI-CCM2	HAL	MRI.COM3	D	Adachi et al. (2013); Yukimoto et al. (2012); Yukimoto et al. (2011)
NorESM1-ME	Norwegian Climate Center, Norway	CAM4-Oslo	CLM4	HAMOCC5	N	Tjiputra et al. (2013)

Table 3: CMIP6 models analysed in this study. Under Comments, D stands for models including dynamic vegetation, and N for models including Nitrogen cycles.

Model	Institute	Atmosphere Model	Land Model	Ocean Model	Comment	Main Reference & Data DOI
ACCESS-ESM1-5	Commonwealth Scientific and Industrial Research Organisation, Australia	UM7.3	CABLE2.4 with CASA-CNP	MOM5 + WOMBAT	N	Law et al. (2017); Ziehn et al. (2017) Data: Ziehn et al. (2019)
CanESM5	Canadian Center for Climate Modeling and Analysis, BC, Canada	CanAM5	CLASS-CTEM	NEMO 3.4.1. + CMOC		Swart et al. (2019a) Data: Swart et al. (2019b)
CanESM5-CanOE	Canadian Center for Climate Modeling and Analysis, BC, Canada	CanAM5	CLASS-CTEM	NEMO 3.4.1. + CanOE		Swart et al. (2019a) Data: Swart et al. (2019c)
CNRM-ESM2-1	CNRM-CERFACS, France	ARPEGE-Climat v6.3 + SURFEX v8.0	ISBA + CTRIP	NEMO v3.6 + GELATO + PISCESv2		Séférian et al. (2019) Data: Seferian (2019)
GFDL-ESM4	Geophysical Fluid Dynamics Laboratory, United States	AM4.1	LM4.1	OM4 MOM6 + COBALTv2	D	Dunne et al. (2020) ~~(submitted)~~ Data: Krasting et al. (2018)
MIROC-ES2L	MIROC, Japan	MIROC-AGCM + SPRINTARS	VISIT-e & MATSIRO6	COCO + OECO v2	N	Hajima et al. (2020b) Data: Hajima et al. (2020a)
MPI-ESM1-2-LR	Max Planck Institute for Meteorology, Hamburg, Germany	ECHAM6.3	JSBACH3.2	MPIOM1.6 + HAMOCC6	N, D	Mauritsen et al. (2019) Data: Wieners et al. (2019)
MRI-ESM2-0	Meteorological Research Institute, Japan	MRI-AGCM3.5 + MASINGAR	HAL	MRI.COMv4		Yukimoto et al. (2019a) Data: Yukimoto et al. (2019b)

		mk-2r4c + MRI-CCM2.1				
NorESM2-LM	Norwegian Climate Center, Norway	Modified CAM6	CLM5	HAMOCC	N	Seland et al. (2020) Data: Seland et al. (2019)
UKESM1-0-LL	Met Office Hadley Centre, United Kingdom	Unified Model	JULES-ES-1.0	NEMO + MEDUSA-2	N, D	Sellar et al. (2019) Data: Tang et al. (2019)

Figures

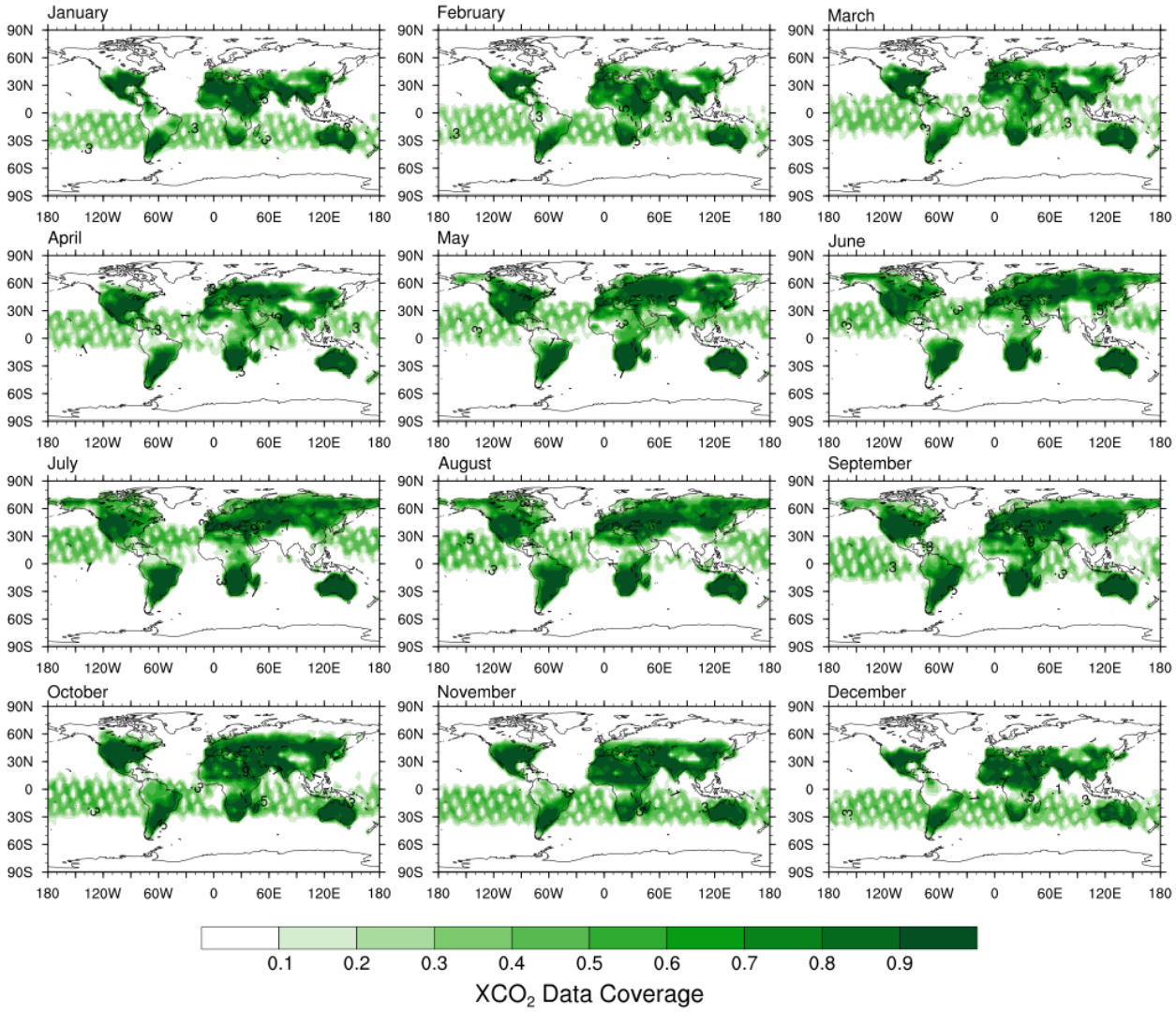

Figure 1: Mean fractional coverage of monthly satellite data for 2003–2014. A value of 0 (white) signifies no available data, while a value of 1 (dark green) means that this gridcell contains data for all years of this month.

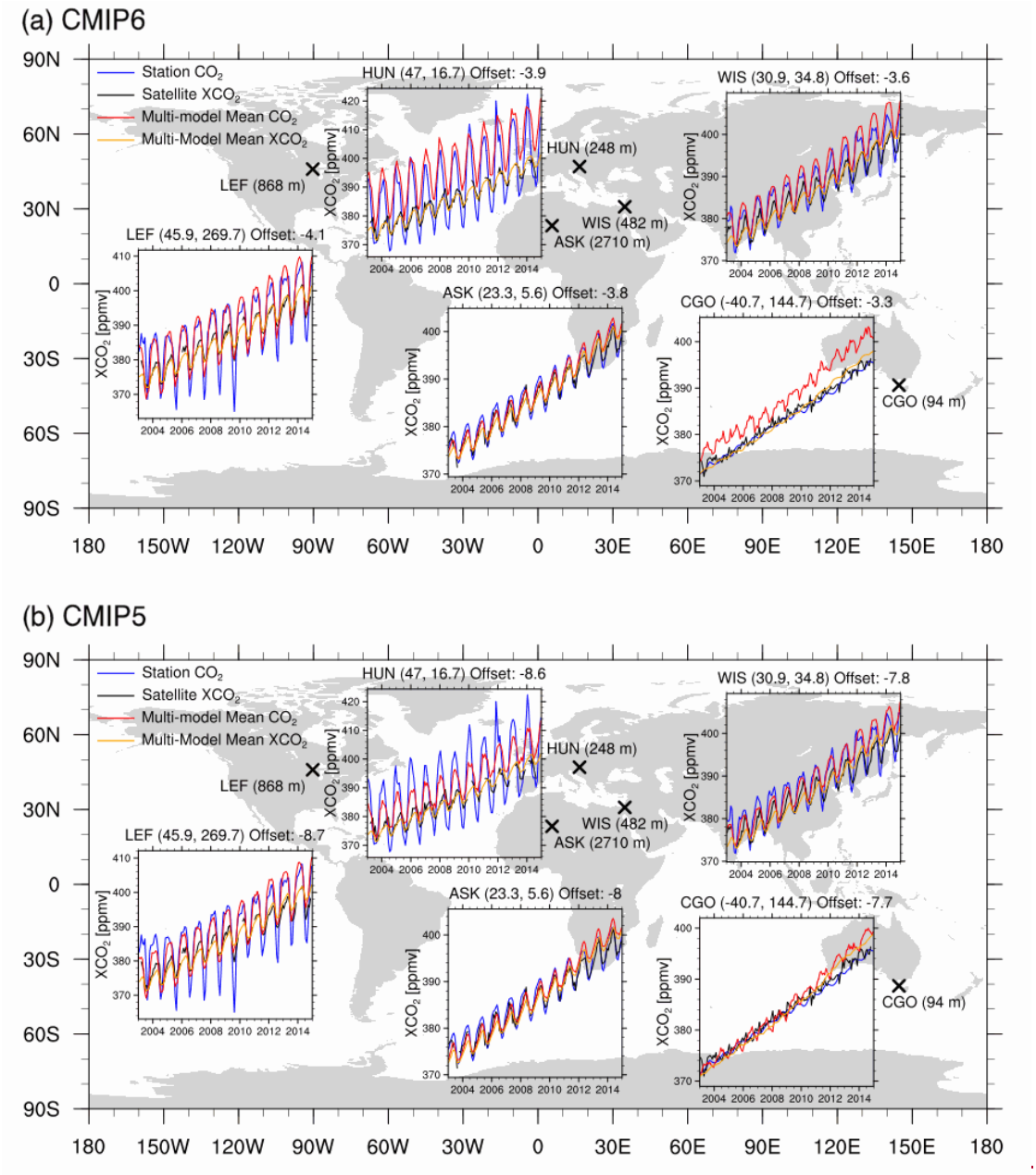
(a) CMIP6
Station CO_2
Satellite XCO_2
Multi-model Mean CO_2
Multi-Model Mean XCO_2
HUN (47, 16.7) Offset: -3.9
HUN (248 m)
LEF (868 m)
WIS (482 m)
ASK (2710 m)
WIS (30.9, 34.8) Offset: -3.6
LEF (45.9, 269.7) Offset: -4.1
ASK (23.3, 5.6) Offset: -3.8
CGO (-40.7, 144.7) Offset: -3.3
CGO (94 m)
XCO_2 [ppmv]
90N
60N
30N
0
30S
60S
90S
180
150W
120W
90W
60W
30W
0
30E
60E
90E
120E
150E
180
2004 2006 2008 2010 2012 2014
(b) CMIP5
Station CO_2
Satellite XCO_2
Multi-model Mean CO_2
Multi-Model Mean XCO_2
HUN (47, 16.7) Offset: -8.6
HUN (248 m)
LEF (868 m)
WIS (482 m)
ASK (2710 m)
WIS (30.9, 34.8) Offset: -7.8
LEF (45.9, 269.7) Offset: -8.7
ASK (23.3, 5.6) Offset: -8
CGO (-40.7, 144.7) Offset: -7.7
CGO (94 m)
XCO_2 [ppmv]
90N
60N
30N
0
30S
60S
90S
180
150W
120W
90W
60W
30W
0
30E
60E
90E
120E
150E
180
2004 2006 2008 2010 2012 2014

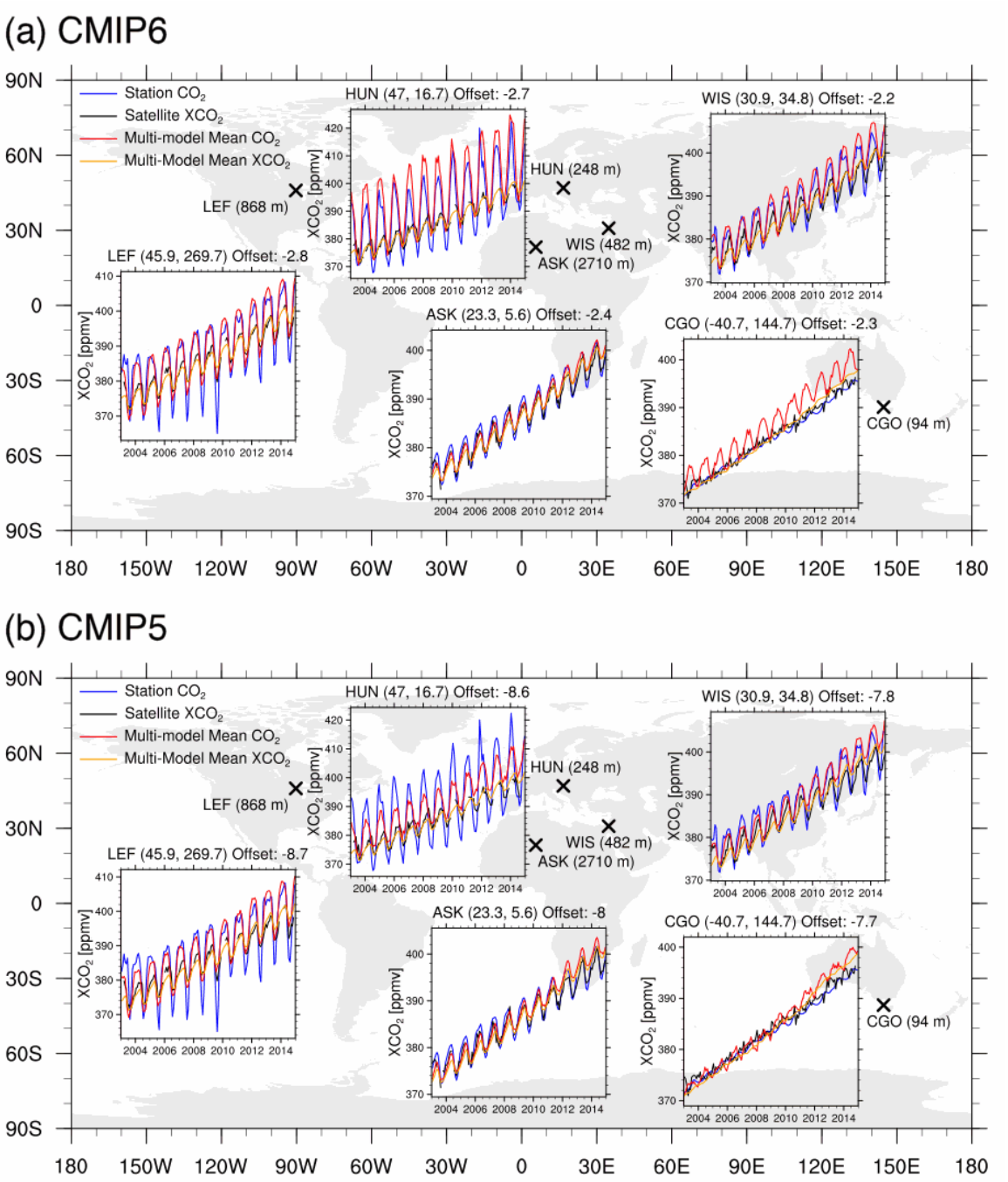

Figure 2: Comparison of time series from satellite XCO_2 (black), multi-model mean XCO_2 (orange) and surface CO_2 (red), and NOAA surface CO_2 station data (blue) at selected sites, with the coordinates noted in brackets above the time series and the altitudes shown in the map plot (see table 1). The multi-model mean for both XCO_2 and surface CO_2 was offset to have the same average value as the satellite XCO_2 for better comparison, and this offset is noted above each time series. CMIP6 and CMIP5 multi-model mean are shown on the top (a) and bottom (b) panels respectively.

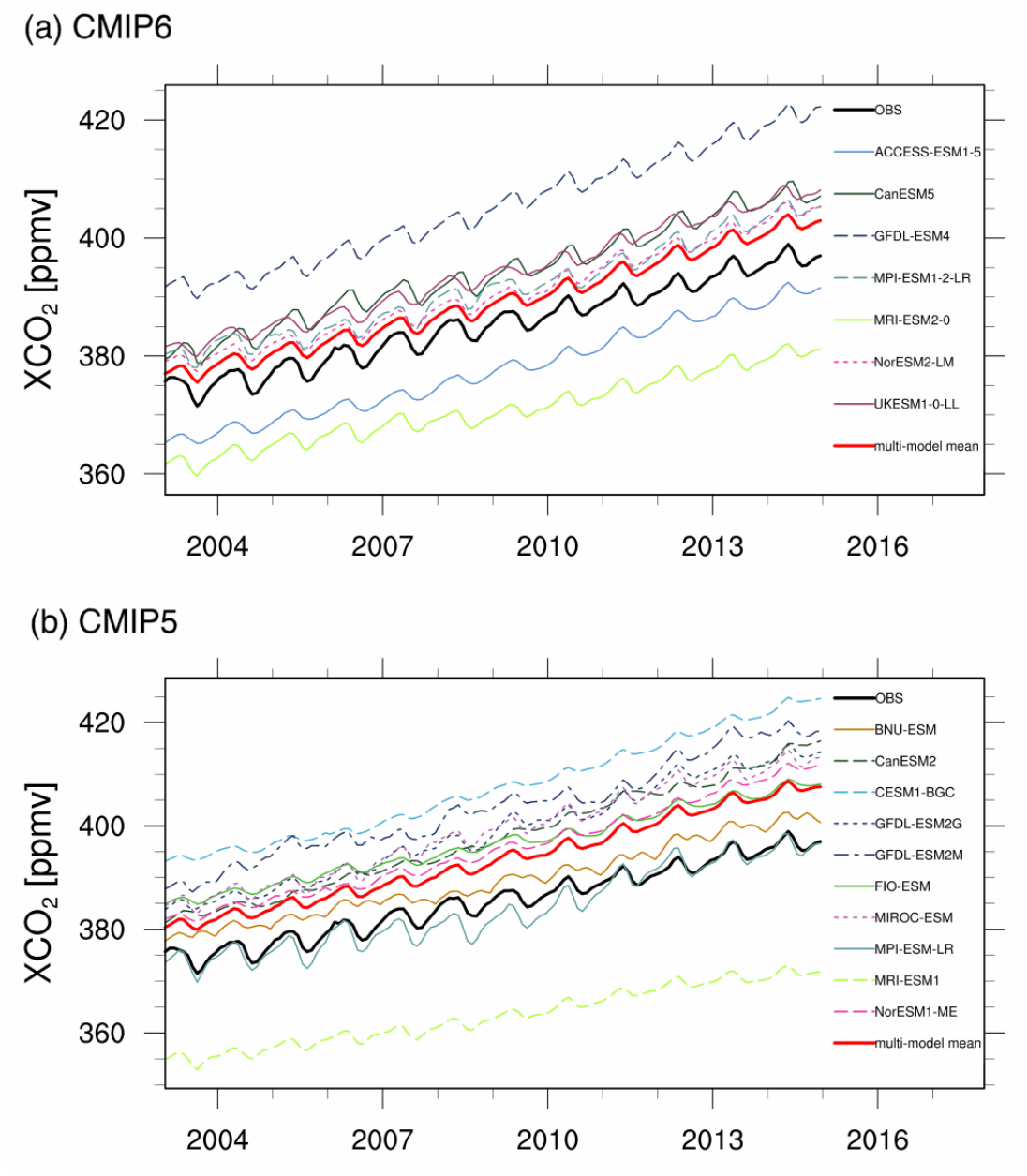
(a) CMIP6
420
400
380
360
XCO2 [ppmv]
2004
2007
2010
2013
2016
OBS
ACCESS-ESM1-5
CanESM5
GFDL-ESM4
MPI-ESM1-2-LR
MRI-ESM2-0
NorESM2-LM
UKESM1-0-LL
multi-model mean
(b) CMIP5
420
400
380
360
XCO2 [ppmv]
2004
2007
2010
2013
2016
OBS
BNU-ESM
CanESM2
CESM1-BGC
GFDL-ESM2G
GFDL-ESM2M
FIO-ESM
MIROC-ESM
MPI-ESM-LR
MRI-ESM1
NorESM1-ME
multi-model mean

1335

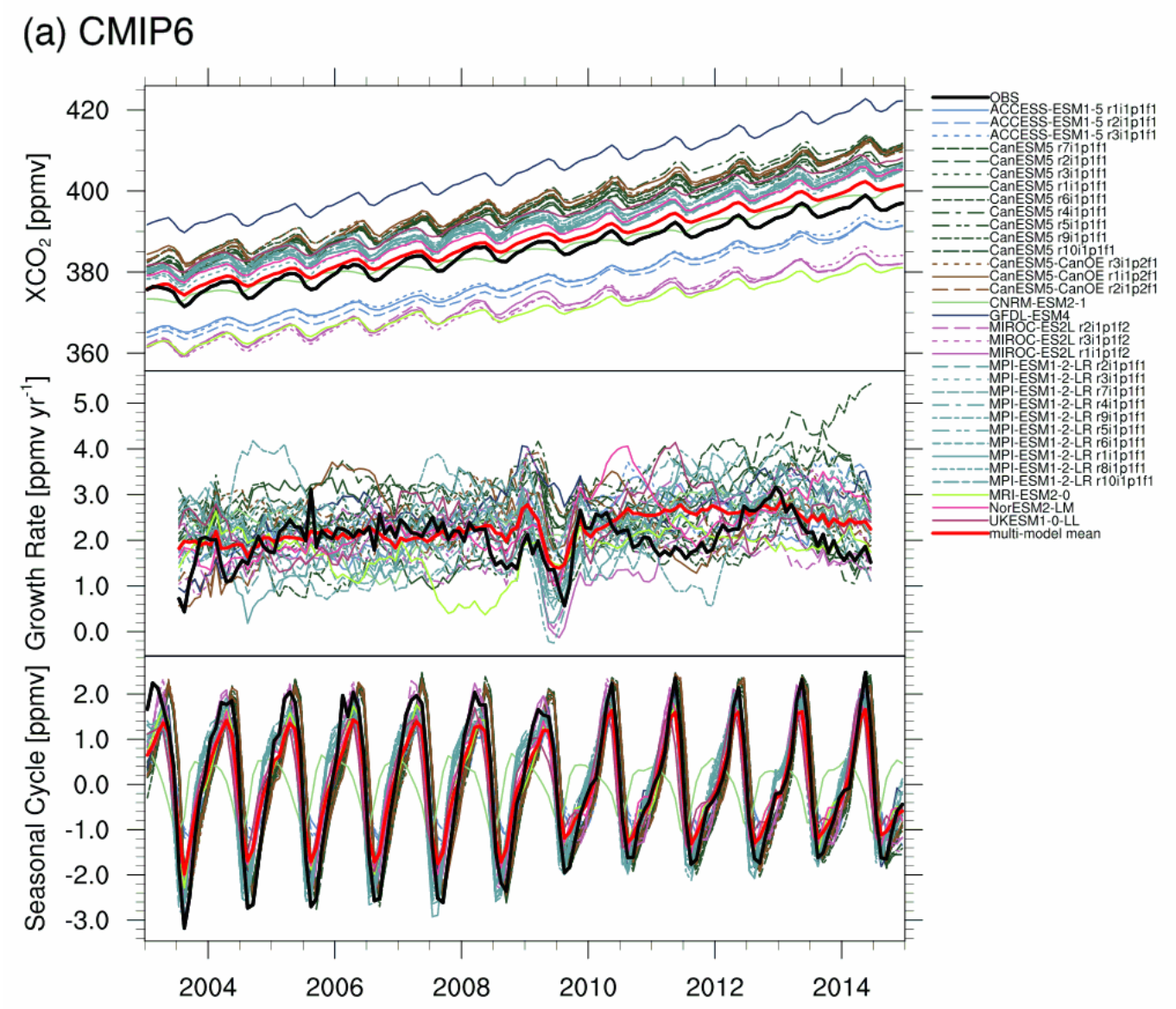

Figure ~~33~~3a: Global time series of monthly mean column averaged carbon dioxide (XCO_2) from 2003 to 2014, for the emission driven CMIP6 ~~(a) and CMIP5 (b)~~ model simulations in comparison to satellite XCO_2 data (bold black line). ~~The model output is sampled as the satellite data~~The model output is sampled as the satellite data. The top panels show the time series, while the middle panels show the computed monthly growth rate, which has been used to detrend the data to obtain the seasonal cycle shown in the bottom panel. All available ensemble members for each model are shown to show the intrinsic variability of the models.

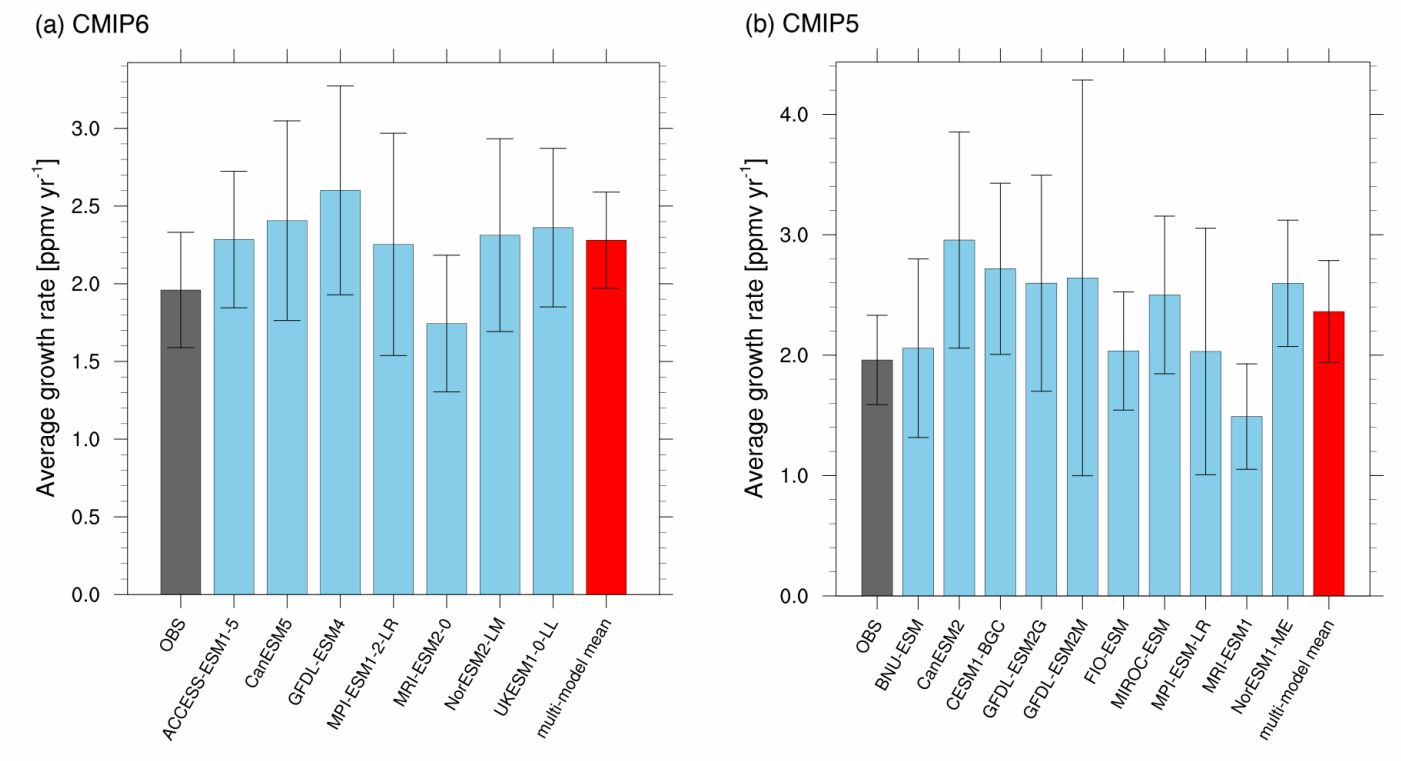
(a) CMIP6
Average growth rate [ppmv yr-1]
0.0
0.5
1.0
1.5
2.0
2.5
3.0
OBS
ACCESS-ESM1-5
CanESM5
GFDL-ESM4
MPI-ESM1-2-LR
MRI-ESM2-0
NorESM2-LM
UKESM1-0-LL
multi-model mean
(b) CMIP5
Average growth rate [ppmv yr-1]
0.0
1.0
2.0
3.0
4.0
OBS
BNU-ESM
CanESM2
CESM1-BGC
GFDL-ESM2G
GFDL-ESM2M
FIO-ESM
MIROC-ESM
MPI-ESM-LR
MRI-ESM1
NorESM1-ME
multi-model mean

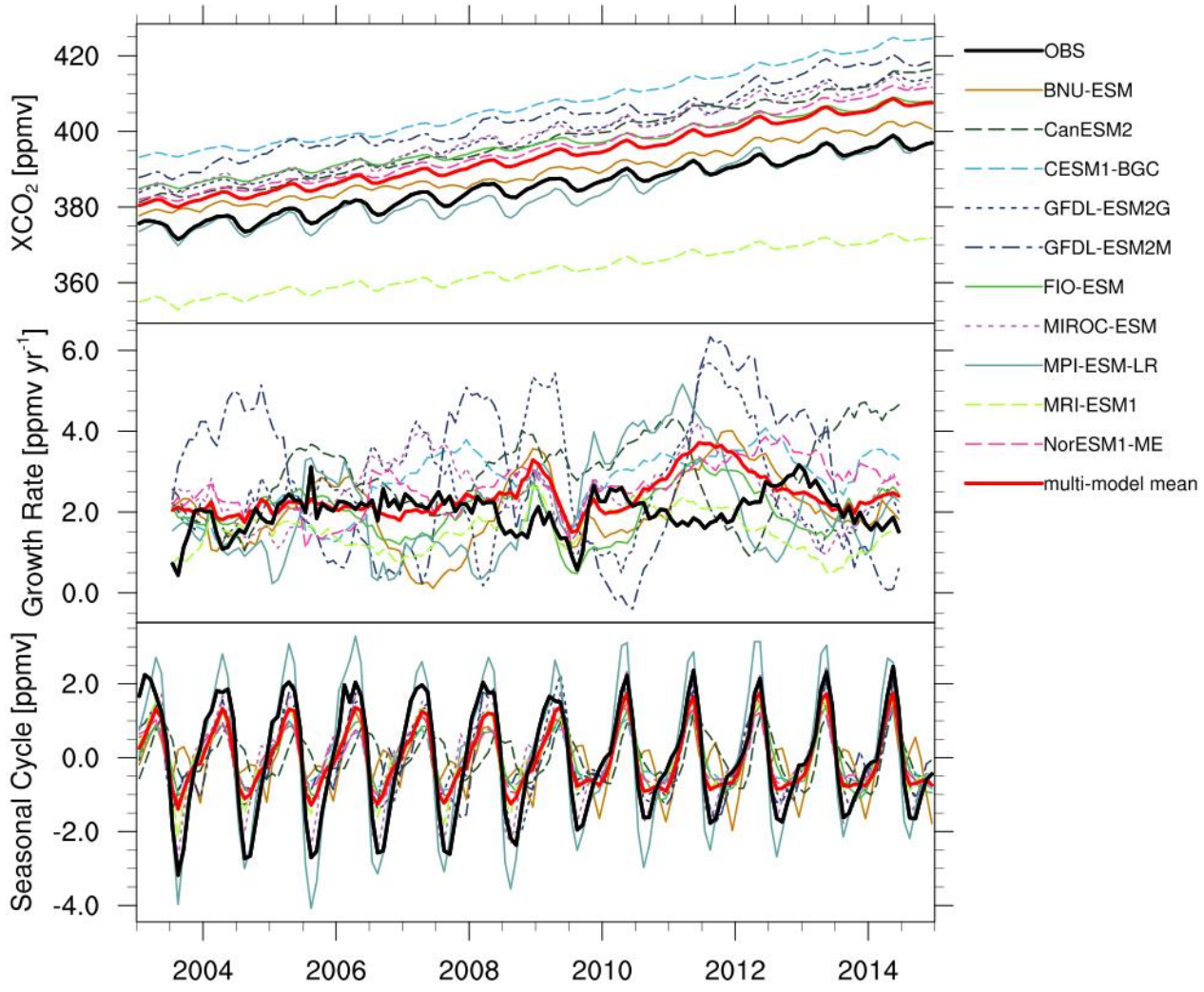

Figure 3b: Same as Figure 3a but for CMIP5. Only one ensemble member is shown.

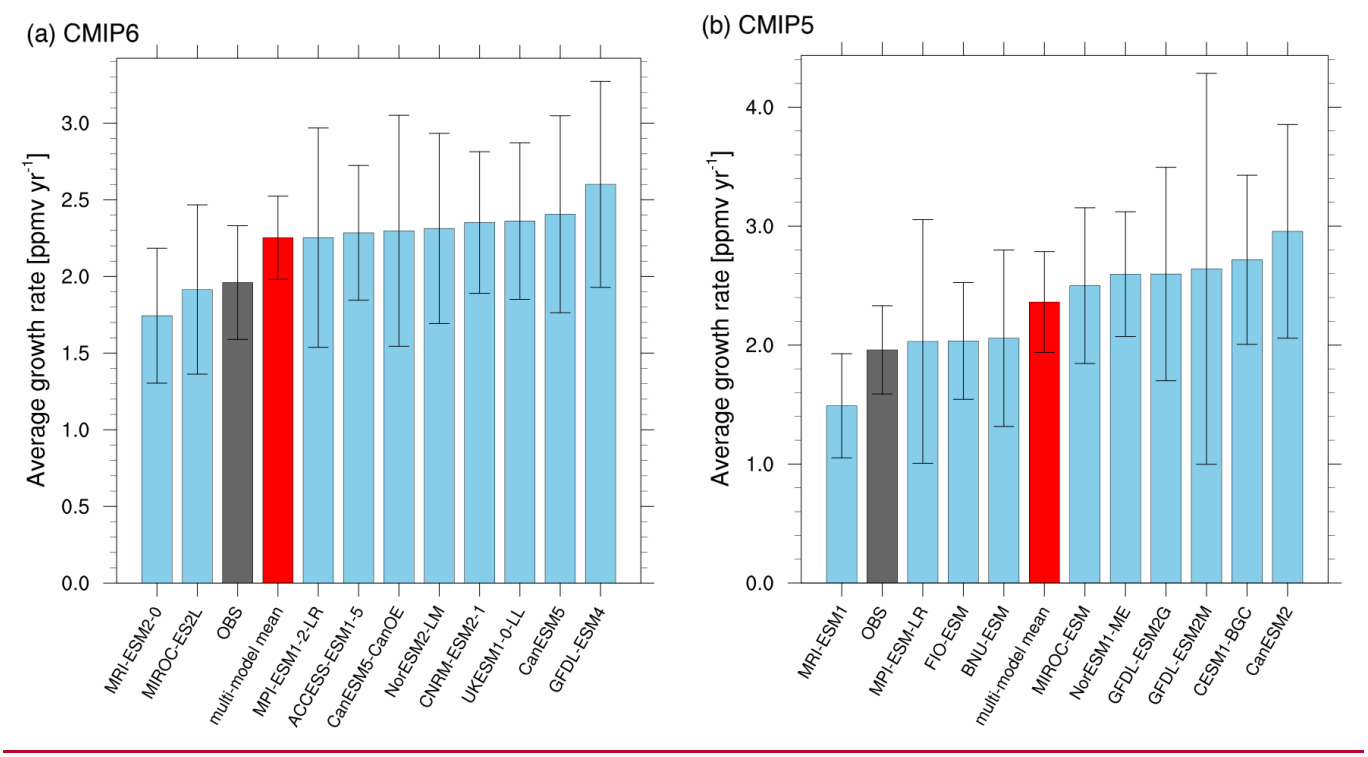

Figure 4. Global mean and standard deviation over all years of annual growth rate of XCO_2 during 2003–2014, for CMIP6 models (a) and CMIP5 models (b). The ~~leftmost~~black bar ~~(black)~~ represents the satellite observations, while the ~~rightmost~~red bar ~~(red)~~ depicts the multi-model mean.

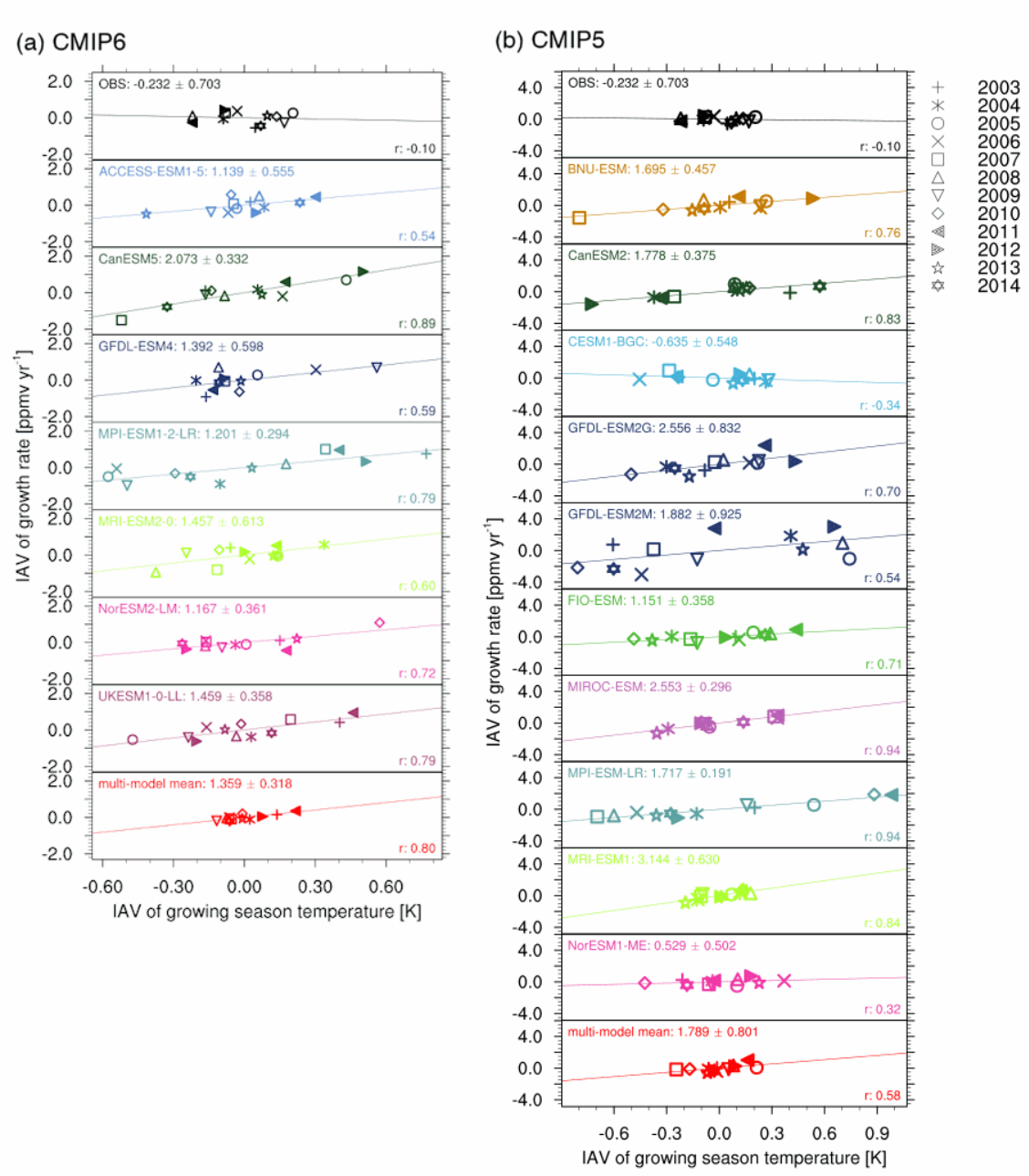

~~**Figure 5: Sensitivity of the interannual variability of the XCO_2 growth rate in the tropics (30° S–30° N) to the interannual variability of tropical growing season temperature for CMIP6 models (a) and CMIP5 models (b). The observational temperature taken from the GISTemp temperature anomaly map, while the models use their own simulated temperature. A linear regression is performed on the data for each dataset. Model colors are the same as in Figure 3, and symbols denote the years. In the top left of each panel the regression coefficient and its uncertainty is shown, while the bottom right states the correlation coefficient.**~~

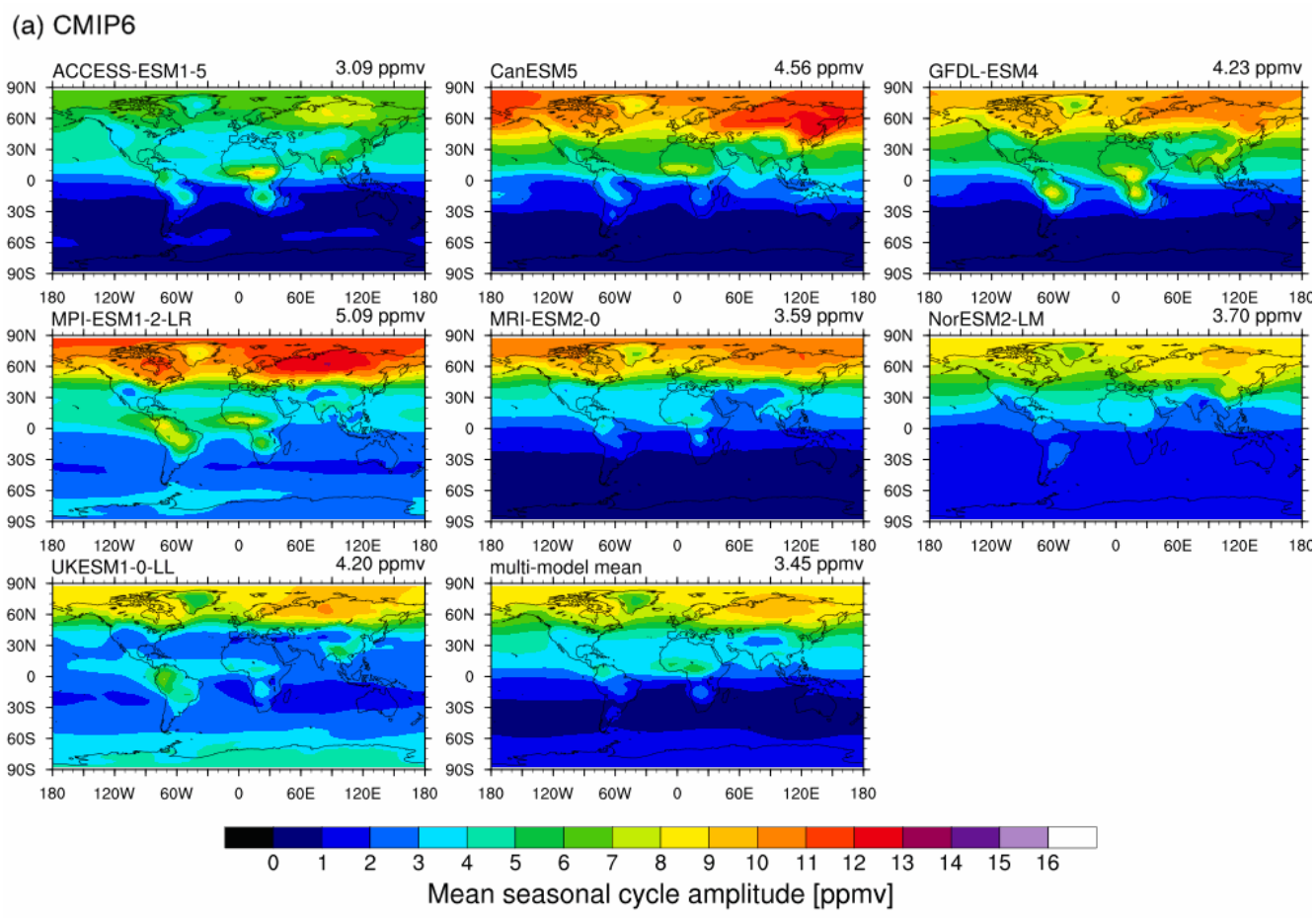
(a) CMIP6
ACCESS-ESM1-5
3.09 ppmv
CanESM5
4.56 ppmv
GFDL-ESM4
4.23 ppmv
MPI-ESM1-2-LR
5.09 ppmv
MRI-ESM2-0
3.59 ppmv
NorESM2-LM
3.70 ppmv
UKESM1-0-LL
4.20 ppmv
multi-model mean
3.45 ppmv
90N
60N
30N
0
30S
60S
90S
180
120W
60W
0
60E
120E
180
0 1 2 3 4 5 6 7 8 9 10 11 12 13 14 15 16
Mean seasonal cycle amplitude [ppmv]

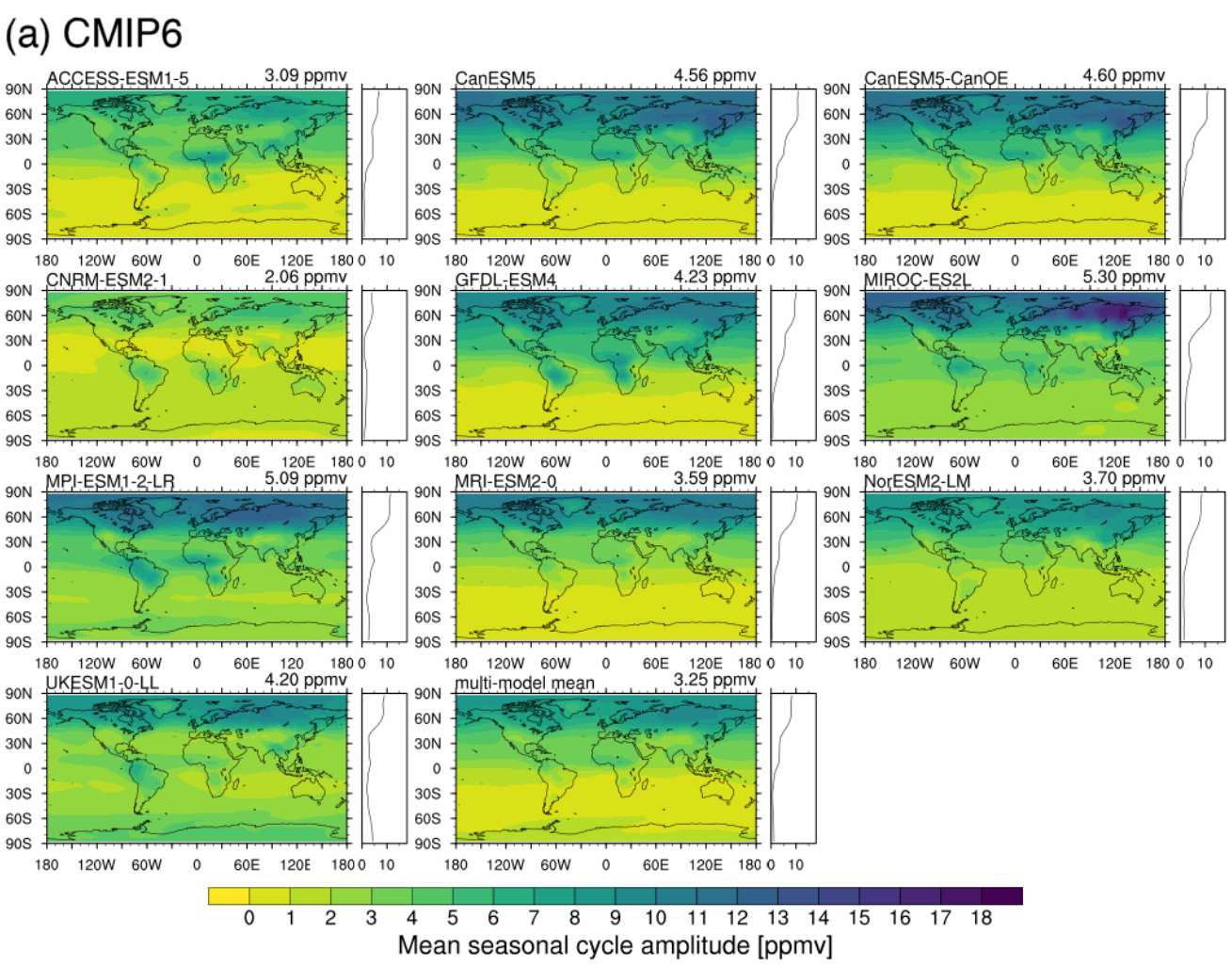

Figure ~~6a~~5a: Maps of mean annual seasonal cycle amplitude for 2003–2014 for CMIP6 models. The model name is given at the top left of each panel, while the top right shows the global average of the mean annual seasonal cycle. The panel to the right of the maps shows the zonal mean SCA.

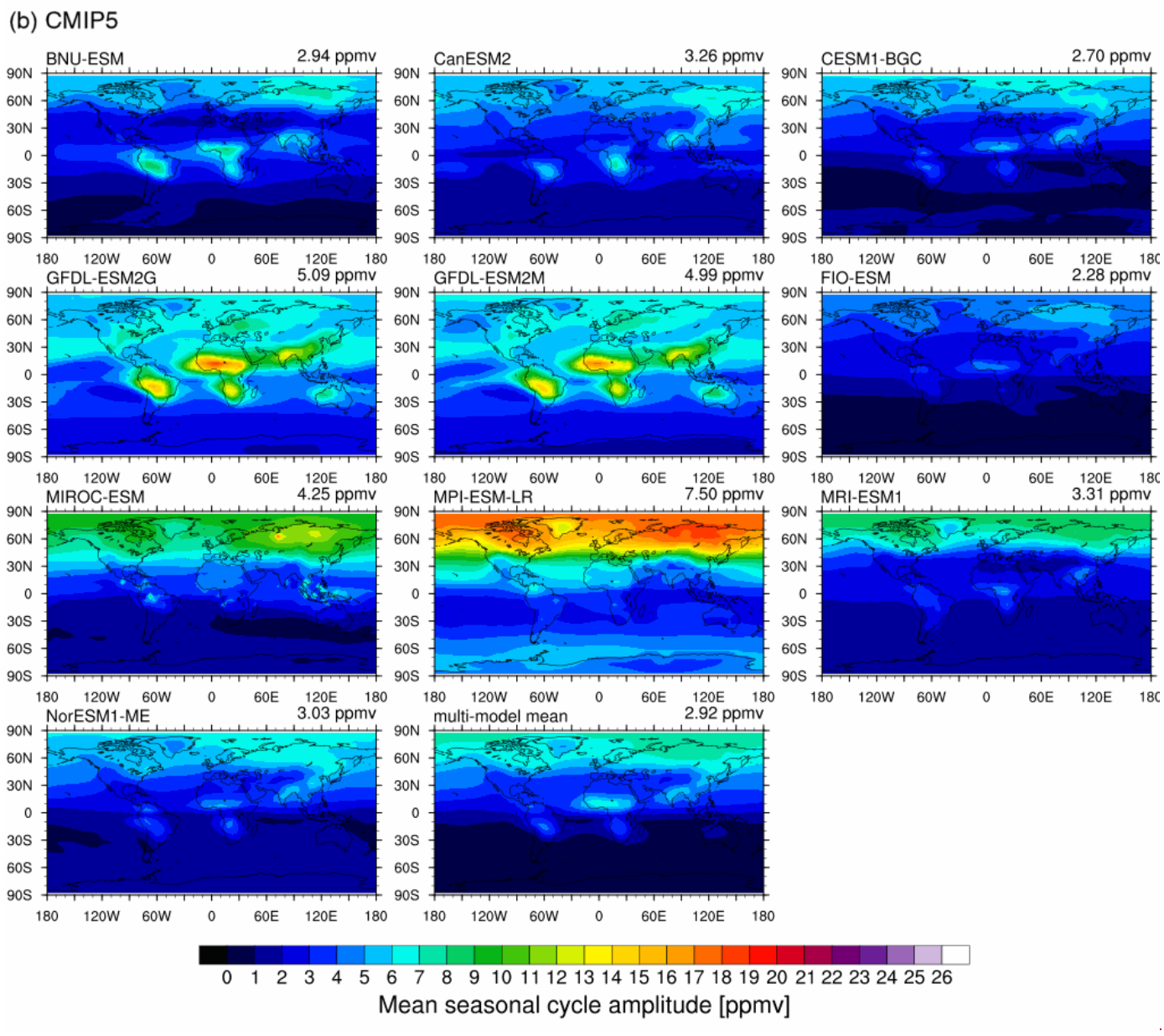
(b) CMIP5
BNU-ESM
2.94 ppmv
CanESM2
3.26 ppmv
CESM1-BGC
2.70 ppmv
GFDL-ESM2G
5.09 ppmv
GFDL-ESM2M
4.99 ppmv
FIO-ESM
2.28 ppmv
MIROC-ESM
4.25 ppmv
MPI-ESM-LR
7.50 ppmv
MRI-ESM1
3.31 ppmv
NorESM1-ME
3.03 ppmv
multi-model mean
2.92 ppmv
90N
60N
30N
0
30S
60S
90S
180
120W
60W
0
60E
120E
180
0 1 2 3 4 5 6 7 8 9 10 11 12 13 14 15 16 17 18 19 20 21 22 23 24 25 26
Mean seasonal cycle amplitude [ppmv]

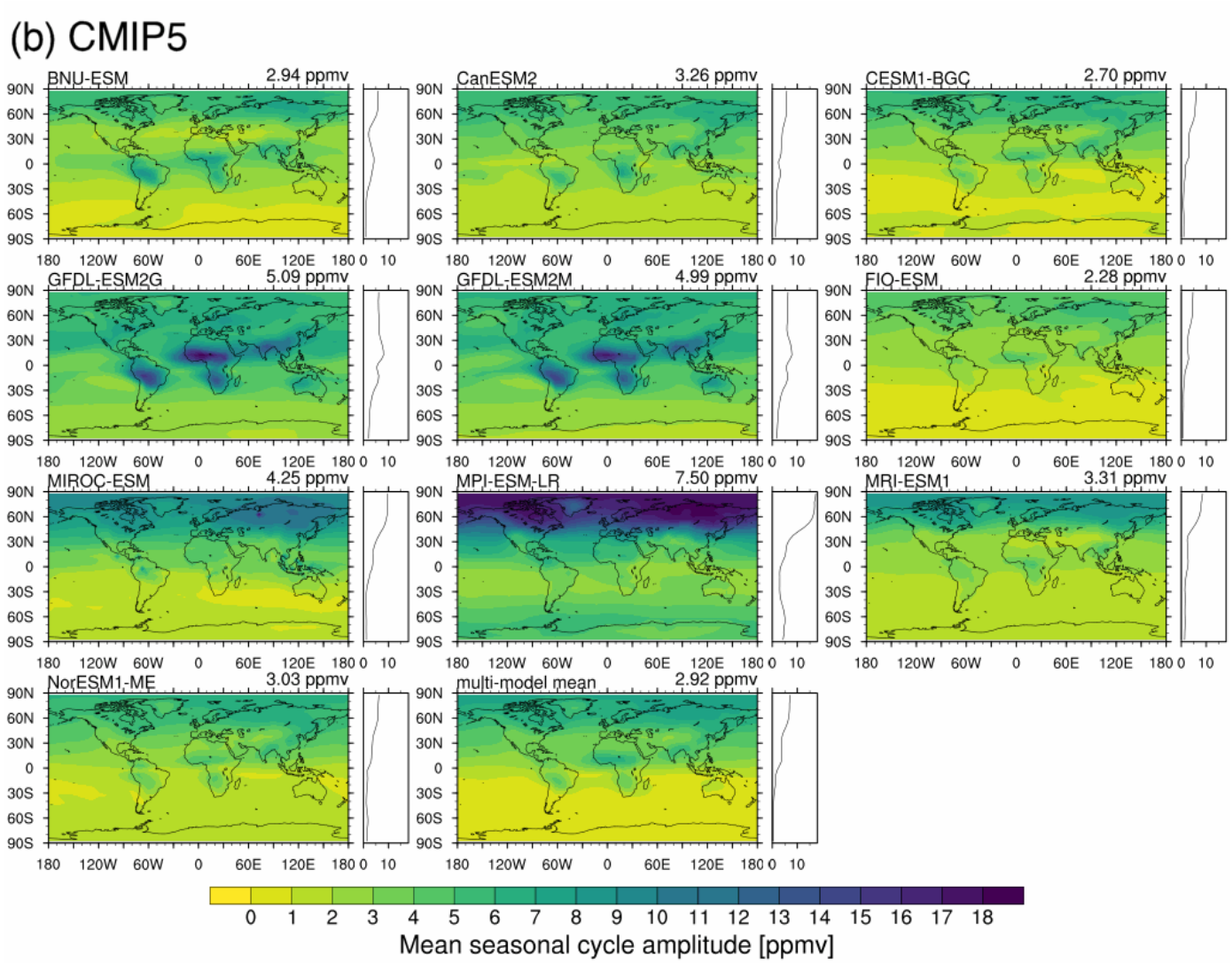

Figure ~~6b~~5b: Same as Figure ~~6a~~5a but for CMIP5 models. ~~**Note the different scale for the CMIP5 models to fit the increased SCA of the MPI-ESM-LR model.**~~

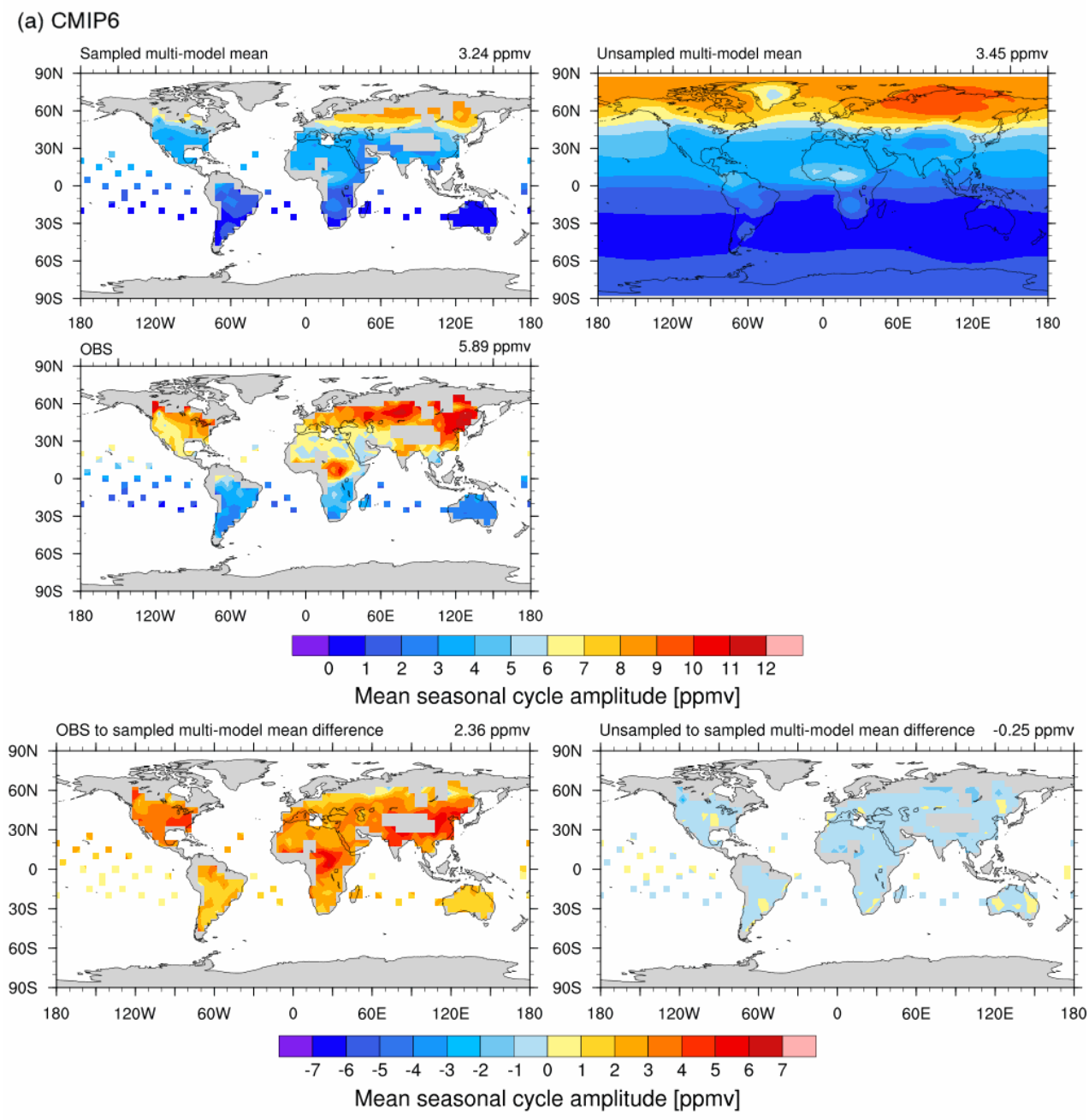
(a) CMIP6
Sampled multi-model mean
3.24 ppmv
Unsampled multi-model mean
3.45 ppmv
OBS
5.89 ppmv
90N
60N
30N
0
30S
60S
90S
180
120W
60W
0
60E
120E
180
0 1 2 3 4 5 6 7 8 9 10 11 12
Mean seasonal cycle amplitude [ppmv]
OBS to sampled multi-model mean difference
2.36 ppmv
Unsampled to sampled multi-model mean difference
-0.25 ppmv
-7 -6 -5 -4 -3 -2 -1 0 1 2 3 4 5 6 7
Mean seasonal cycle amplitude [ppmv]

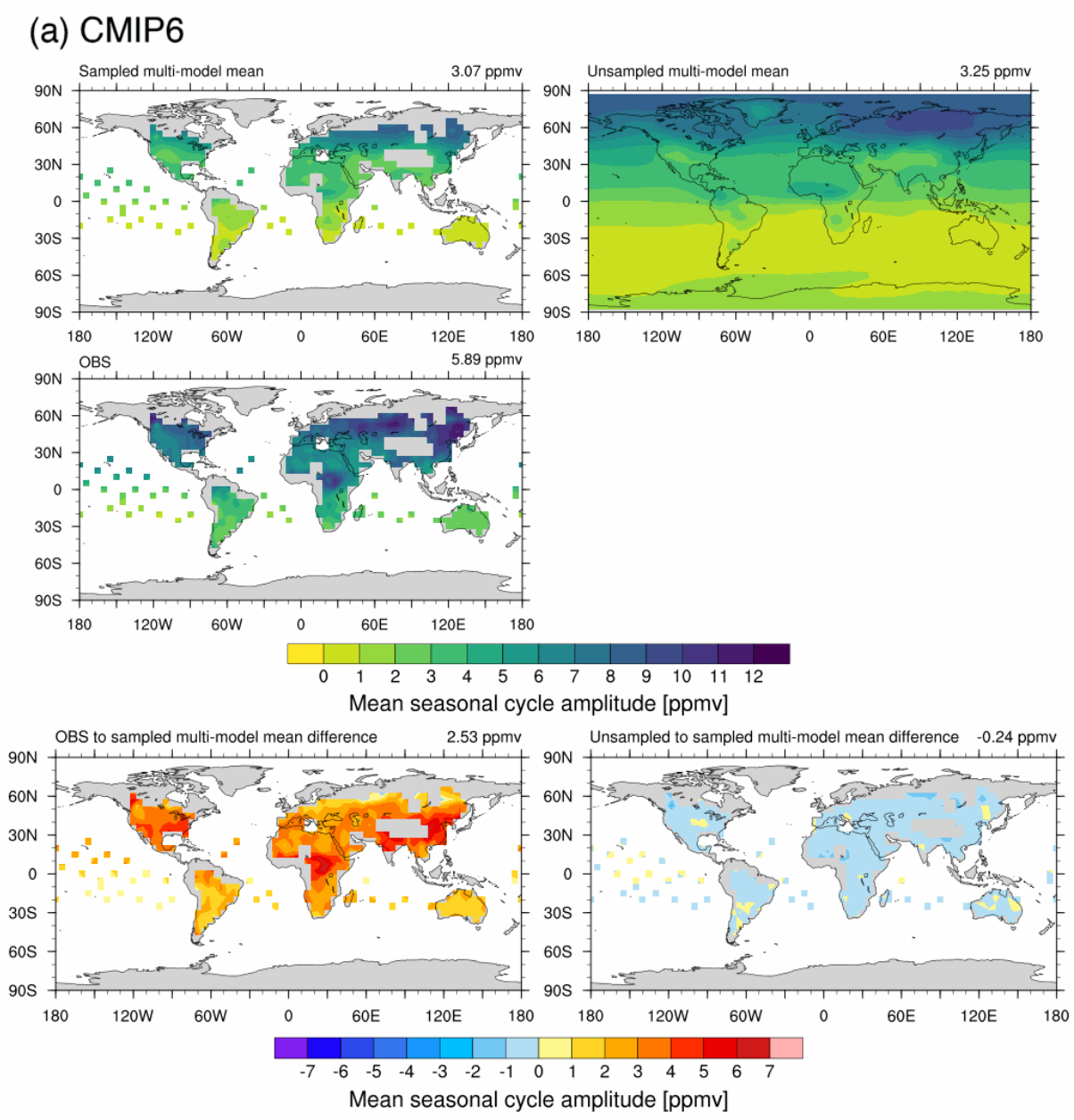

Figure ~~7a~~6a: Maps of mean SCA of the CMIP6 multi-model mean for 2003–2014. Top: SCA of multi-model mean with observational sampling (left) and without sampling (right). Middle: SCA of the satellite observations. Bottom: Difference between observations and sampled model data (left) and sampled and unsampled model (right).

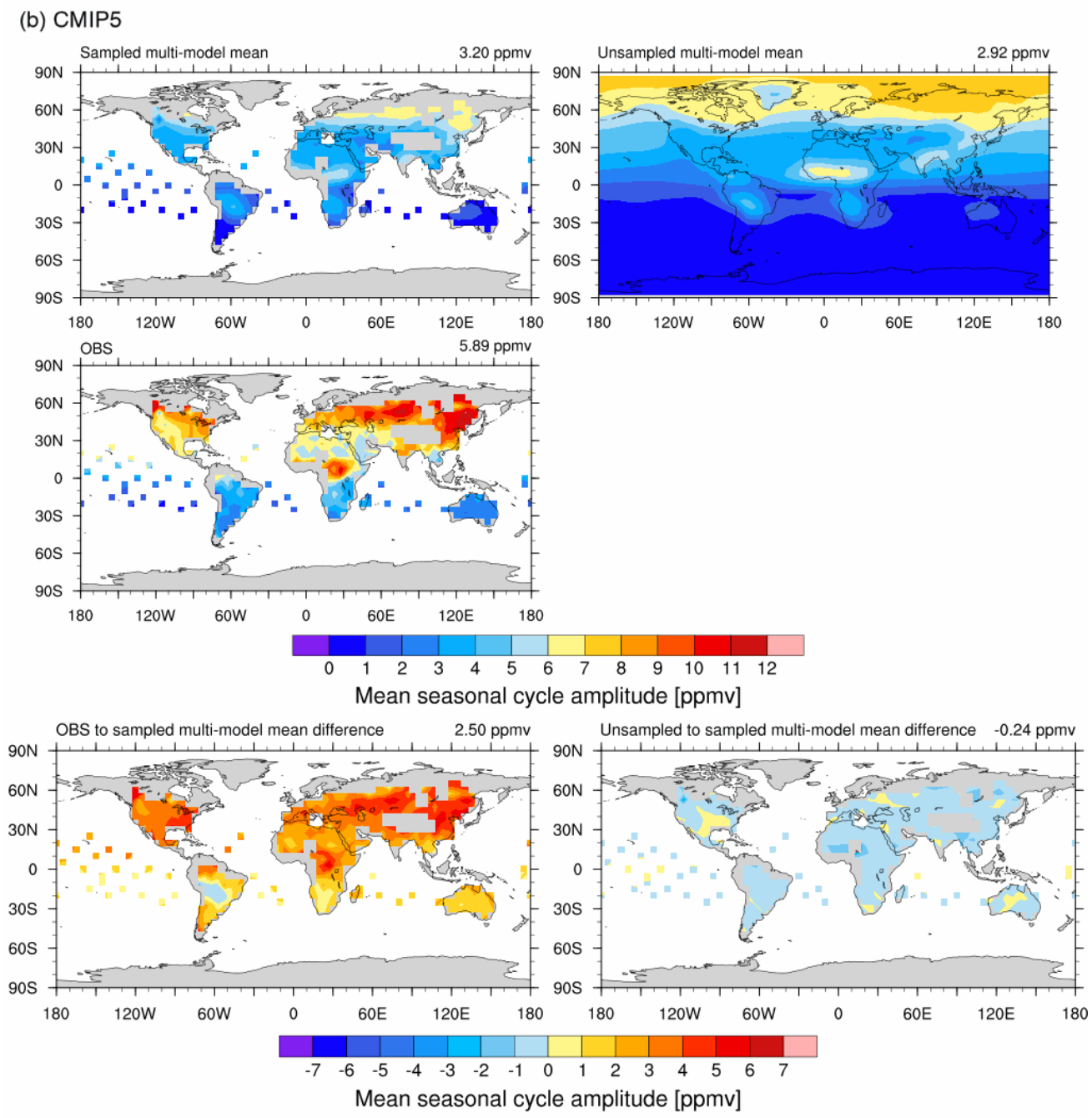
(b) CMIP5
Sampled multi-model mean
3.20 ppmv
Unsampled multi-model mean
2.92 ppmv
OBS
5.89 ppmv
90N
60N
30N
0
30S
60S
90S
180
120W
60W
0
60E
120E
180
0 1 2 3 4 5 6 7 8 9 10 11 12
Mean seasonal cycle amplitude [ppmv]
OBS to sampled multi-model mean difference
2.50 ppmv
Unsampled to sampled multi-model mean difference
-0.24 ppmv
-7 -6 -5 -4 -3 -2 -1 0 1 2 3 4 5 6 7
Mean seasonal cycle amplitude [ppmv]

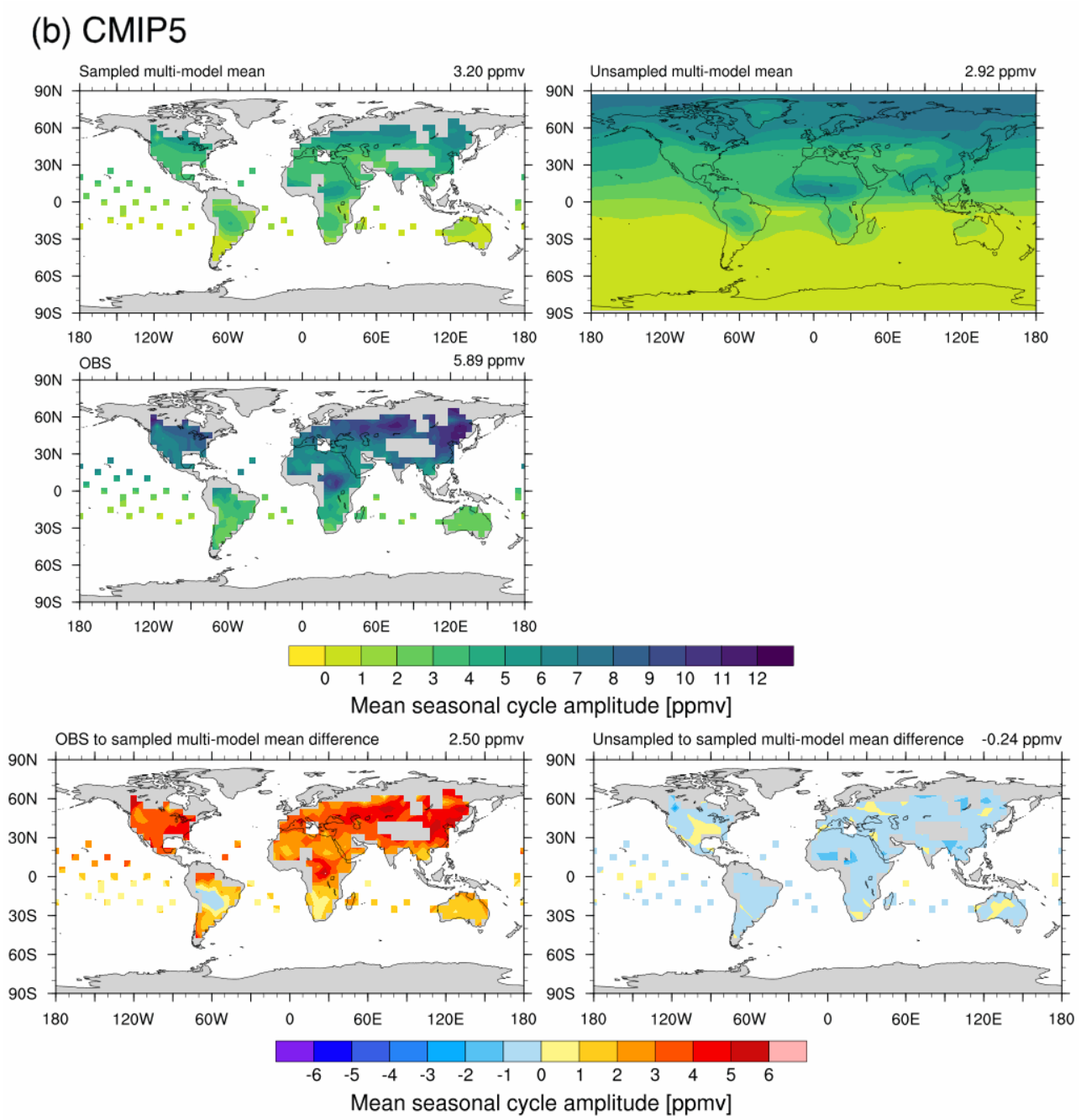

Figure ~~7b~~6b: Same as Figure ~~7a~~6a but for the CMIP5 multi-model mean.

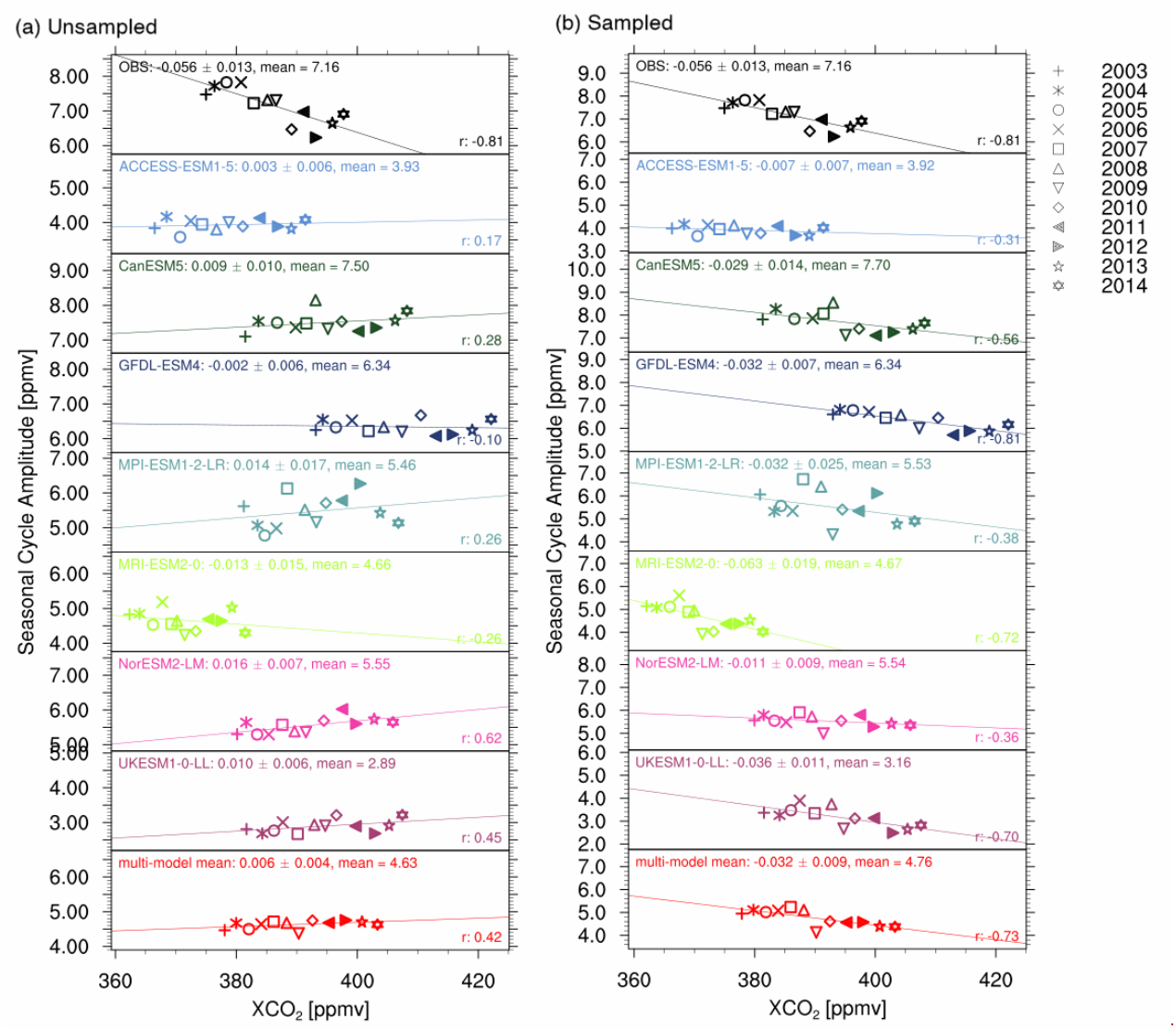
(a) Unsampled
(b) Sampled
OBS: -0.056 ± 0.013, mean = 7.16
r: -0.81
ACCESS-ESM1-5: 0.003 ± 0.006, mean = 3.93
r: 0.17
CanESM5: 0.009 ± 0.010, mean = 7.50
r: 0.28
GFDL-ESM4: -0.002 ± 0.006, mean = 6.34
r: -0.10
MPI-ESM1-2-LR: 0.014 ± 0.017, mean = 5.46
r: 0.26
MRI-ESM2-0: -0.013 ± 0.015, mean = 4.66
r: -0.26
NorESM2-LM: 0.016 ± 0.007, mean = 5.55
r: 0.62
UKESM1-0-LL: 0.010 ± 0.006, mean = 2.89
r: 0.45
multi-model mean: 0.006 ± 0.004, mean = 4.63
r: 0.42
ACCESS-ESM1-5: -0.007 ± 0.007, mean = 3.92
r: -0.31
CanESM5: -0.029 ± 0.014, mean = 7.70
r: -0.56
GFDL-ESM4: -0.032 ± 0.007, mean = 6.34
r: -0.81
MPI-ESM1-2-LR: -0.032 ± 0.025, mean = 5.53
r: -0.38
MRI-ESM2-0: -0.063 ± 0.019, mean = 4.67
r: -0.72
NorESM2-LM: -0.011 ± 0.009, mean = 5.54
r: -0.36
UKESM1-0-LL: -0.036 ± 0.011, mean = 3.16
r: -0.70
multi-model mean: -0.032 ± 0.009, mean = 4.76
r: -0.73
Seasonal Cycle Amplitude [ppmv]
XCO2 [ppmv]
2003
2004
2005
2006
2007
2008
2009
2010
2011
2012
2013
2014

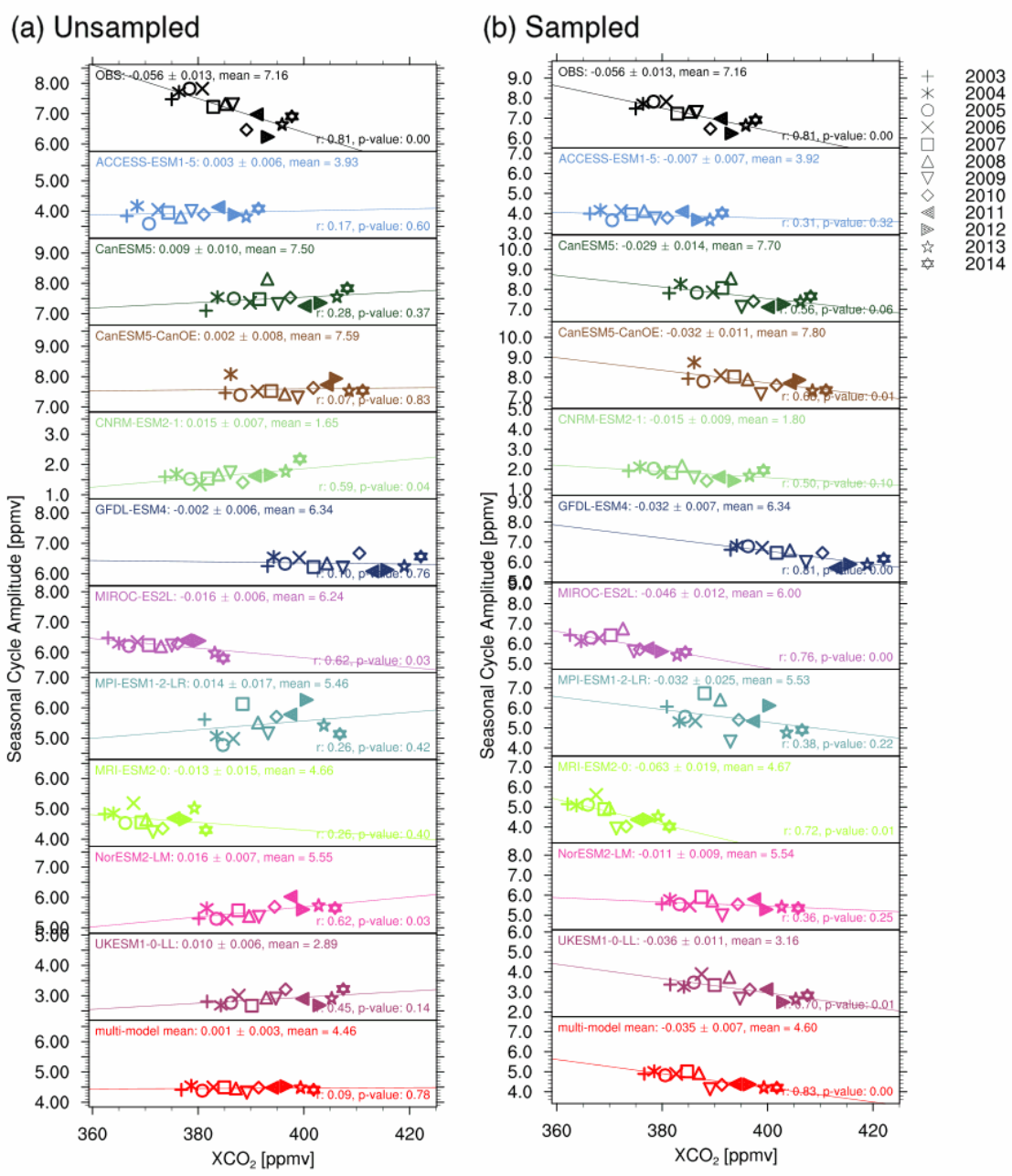

Figure ~~8~~7: Trend of SCA with XCO_2 2003–2014 for the northern mid-latitudes (30–60° N), including a linear regression with slope and mean SCA given on the top left of each panel and the Pearson correlation coefficient as well as the p-value on the bottom right. Symbols denote the different years and model colors are consistent with previous figures. The left panels (a) show unsampled CMIP6 models, while CMIP6 models sampled according to the satellite data are shown on the right (b). Note that the y-axis range for each plot is the same and only differs by a shift.

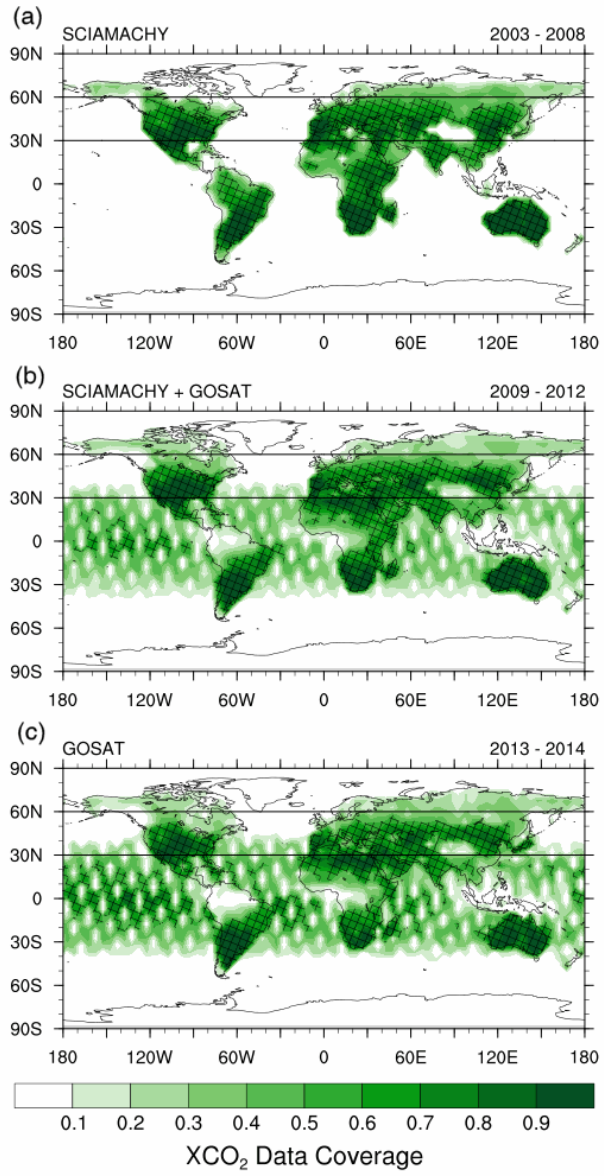

Figure ~~98~~: Data Coverage of the satellite observations for (a) 2003–2008, containing only SCIAMACHY data, (b) 2009–2012 containing the overlap of SCIAMACHY and GOSAT data, and (c) 2013–2014 containing only GOSAT data. The patterned area highlights values above 0.5.

1390

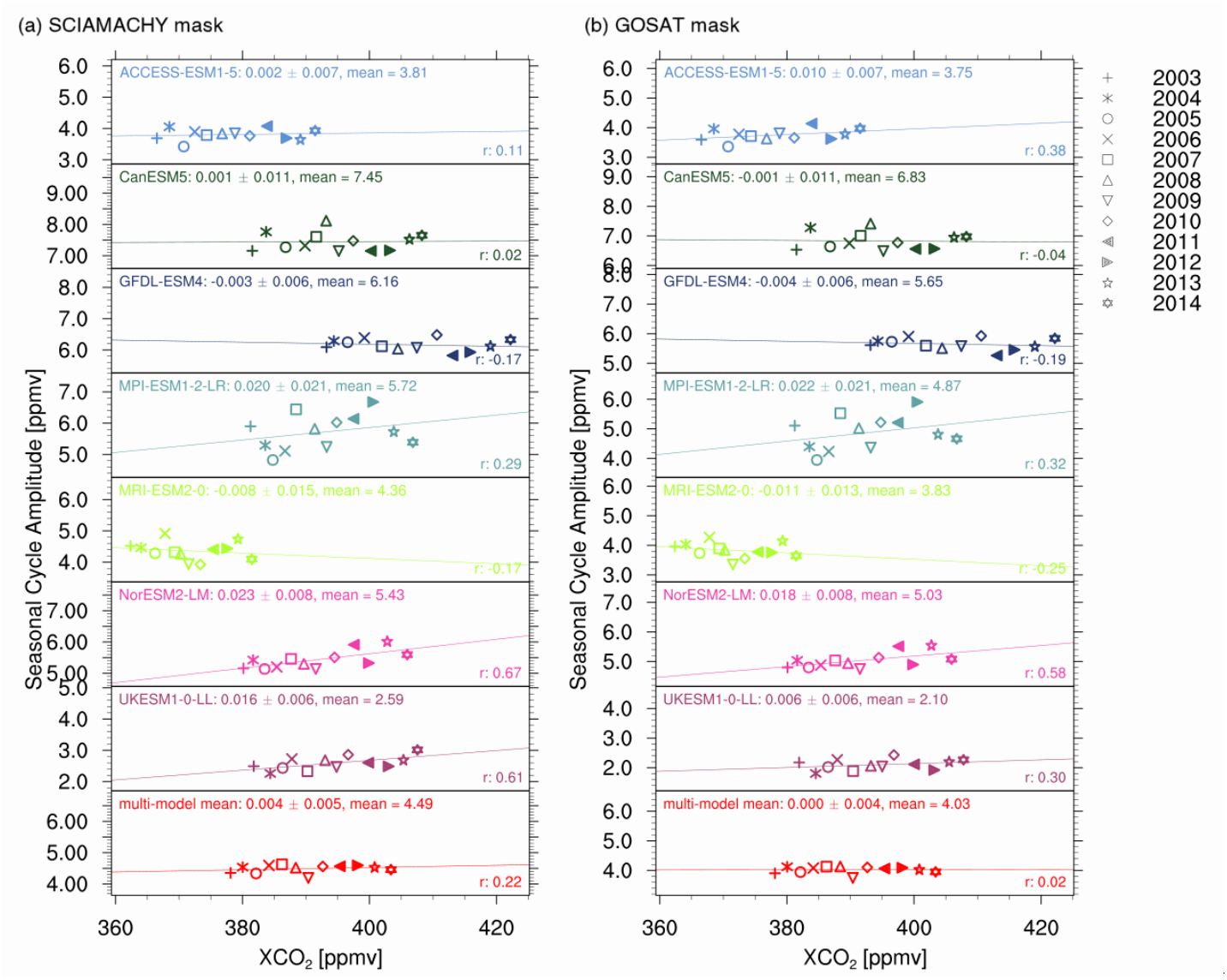
(a) SCIAMACHY mask
(b) GOSAT mask
ACCESS-ESM1-5: 0.002 ± 0.007, mean = 3.81
r: 0.11
CanESM5: 0.001 ± 0.011, mean = 7.45
r: 0.02
GFDL-ESM4: -0.003 ± 0.006, mean = 6.16
r: -0.17
MPI-ESM1-2-LR: 0.020 ± 0.021, mean = 5.72
r: 0.29
MRI-ESM2-0: -0.008 ± 0.015, mean = 4.36
r: -0.17
NorESM2-LM: 0.023 ± 0.008, mean = 5.43
r: 0.67
UKESM1-0-LL: 0.016 ± 0.006, mean = 2.59
r: 0.61
multi-model mean: 0.004 ± 0.005, mean = 4.49
r: 0.22
ACCESS-ESM1-5: 0.010 ± 0.007, mean = 3.75
r: 0.38
CanESM5: -0.001 ± 0.011, mean = 6.83
r: -0.04
GFDL-ESM4: -0.004 ± 0.006, mean = 5.65
r: -0.19
MPI-ESM1-2-LR: 0.022 ± 0.021, mean = 4.87
r: 0.32
MRI-ESM2-0: -0.011 ± 0.013, mean = 3.83
r: -0.25
NorESM2-LM: 0.018 ± 0.008, mean = 5.03
r: 0.58
UKESM1-0-LL: 0.006 ± 0.006, mean = 2.10
r: 0.30
multi-model mean: 0.000 ± 0.004, mean = 4.03
r: 0.02
2003
2004
2005
2006
2007
2008
2009
2010
2011
2012
2013
2014
Seasonal Cycle Amplitude [ppmv]
XCO2 [ppmv]
360
380
400
420

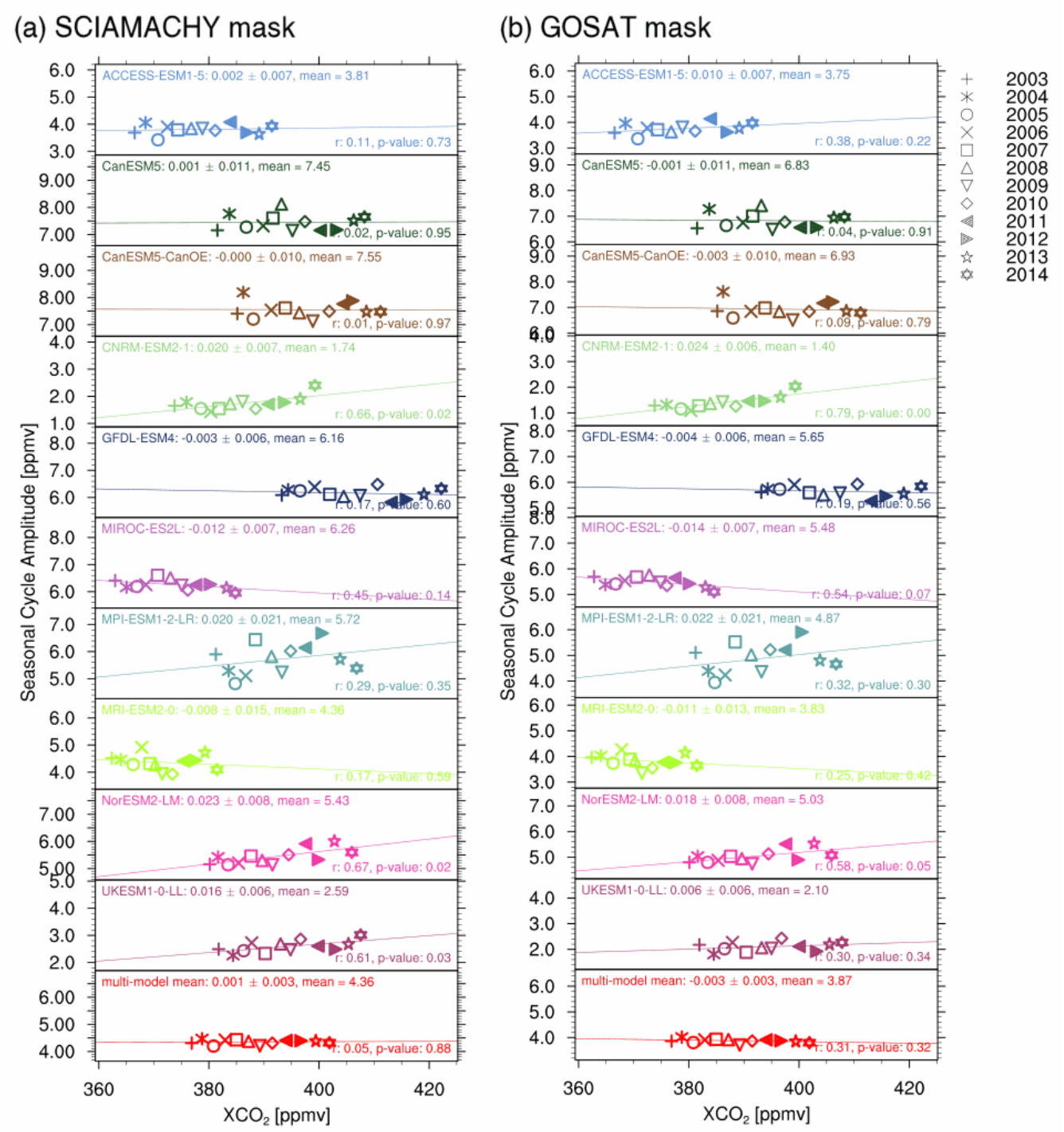

Figure ~~9~~10: Same as Figure ~~8~~7, but with CMIP6 models masked using (a) the SCIAMACHY mask and (b) the GOSAT mask, with the masks derived from Figure ~~9~~8, masking out points with less than 50% coverage in those time periods.

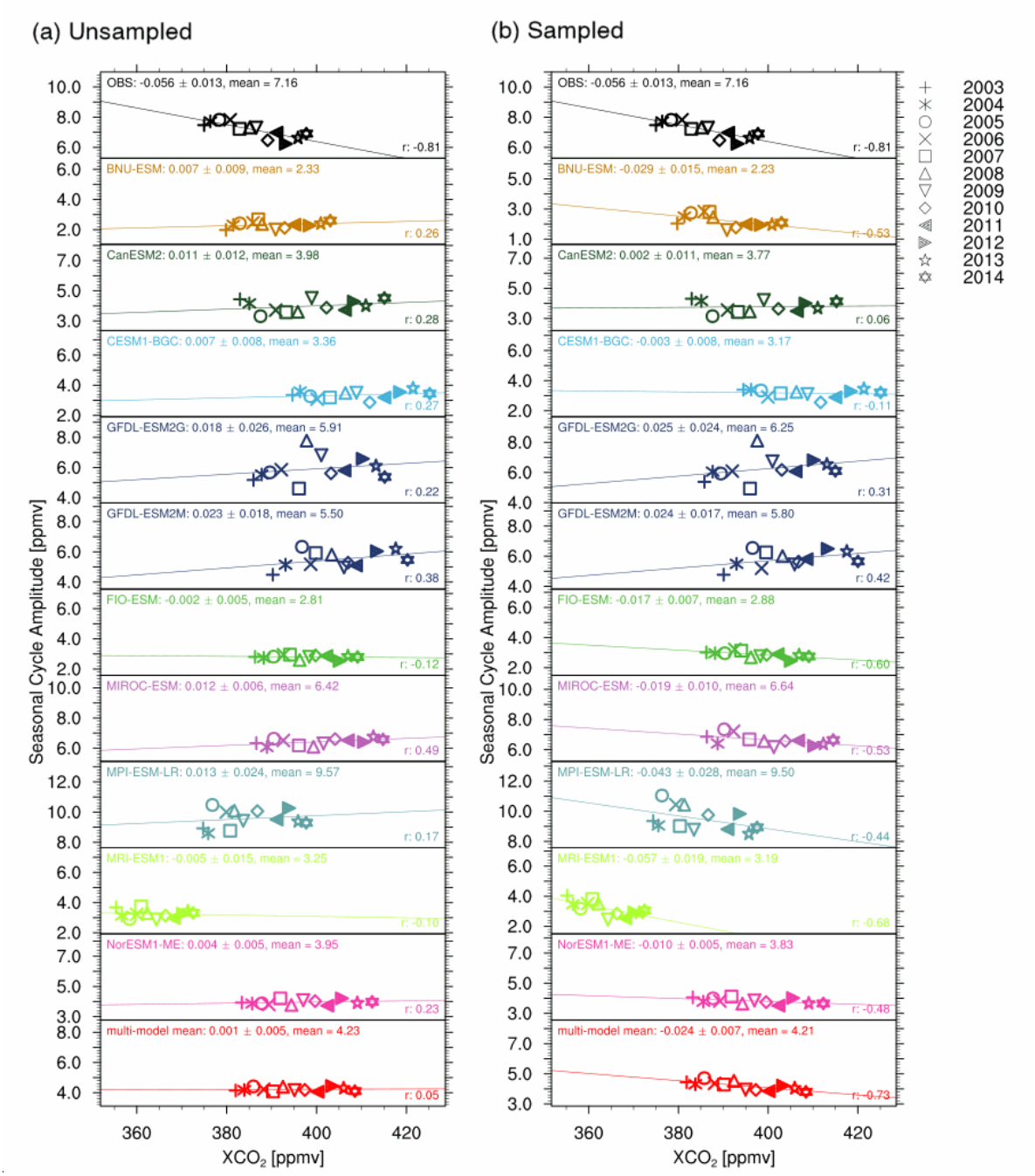
(a) Unsampled
(b) Sampled
OBS: -0.056 ± 0.013, mean = 7.16
r: -0.81
BNU-ESM: 0.007 ± 0.009, mean = 2.33
r: 0.26
CanESM2: 0.011 ± 0.012, mean = 3.98
r: 0.28
CESM1-BGC: 0.007 ± 0.008, mean = 3.36
r: 0.27
GFDL-ESM2G: 0.018 ± 0.026, mean = 5.91
r: 0.22
GFDL-ESM2M: 0.023 ± 0.018, mean = 5.50
r: 0.38
FIO-ESM: -0.002 ± 0.005, mean = 2.81
r: -0.12
MIROC-ESM: 0.012 ± 0.006, mean = 6.42
r: 0.49
MPI-ESM-LR: 0.013 ± 0.024, mean = 9.57
r: 0.17
MRI-ESM1: -0.005 ± 0.015, mean = 3.25
r: -0.10
NorESM1-ME: 0.004 ± 0.005, mean = 3.95
r: 0.23
multi-model mean: 0.001 ± 0.005, mean = 4.23
r: 0.05
BNU-ESM: -0.029 ± 0.015, mean = 2.23
r: -0.53
CanESM2: 0.002 ± 0.011, mean = 3.77
r: 0.06
CESM1-BGC: -0.003 ± 0.008, mean = 3.17
r: -0.11
GFDL-ESM2G: 0.025 ± 0.024, mean = 6.25
r: 0.31
GFDL-ESM2M: 0.024 ± 0.017, mean = 5.80
r: 0.42
FIO-ESM: -0.017 ± 0.007, mean = 2.88
r: -0.60
MIROC-ESM: -0.019 ± 0.010, mean = 6.64
r: -0.53
MPI-ESM-LR: -0.043 ± 0.028, mean = 9.50
r: -0.44
MRI-ESM1: -0.057 ± 0.019, mean = 3.19
r: -0.68
NorESM1-ME: -0.010 ± 0.005, mean = 3.83
r: -0.48
multi-model mean: -0.024 ± 0.007, mean = 4.21
r: -0.73
Seasonal Cycle Amplitude [ppmv]
XCO2 [ppmv]
2003
2004
2005
2006
2007
2008
2009
2010
2011
2012
2013
2014

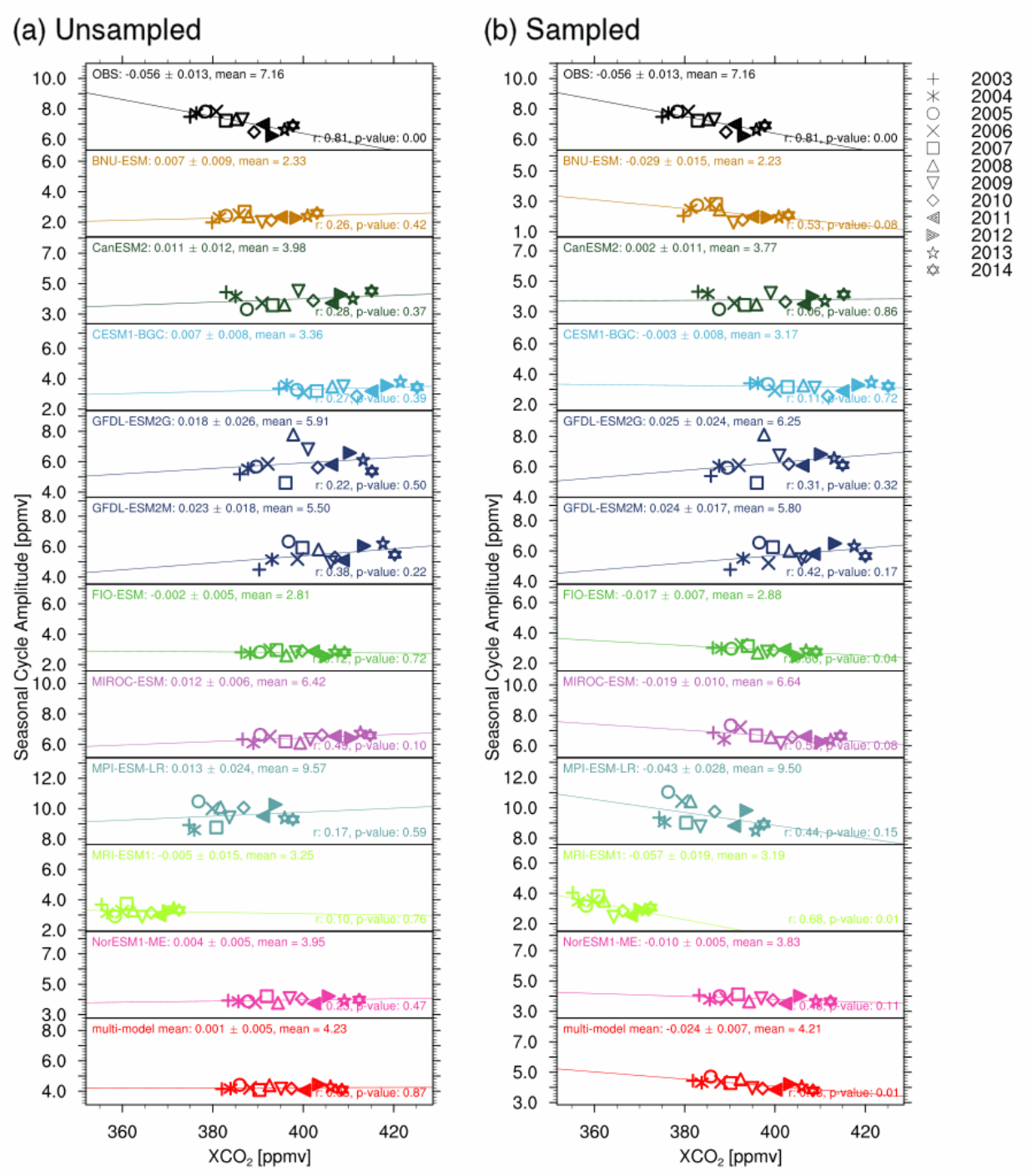

Figure B1: Same as Figure ~~8~~7 but for CMIP5 models. The left panels (a) show unsampled models, while models sampled according to the satellite data are shown on the right (b). Note that the y-axis range is the same and only differs by a shift.

1400

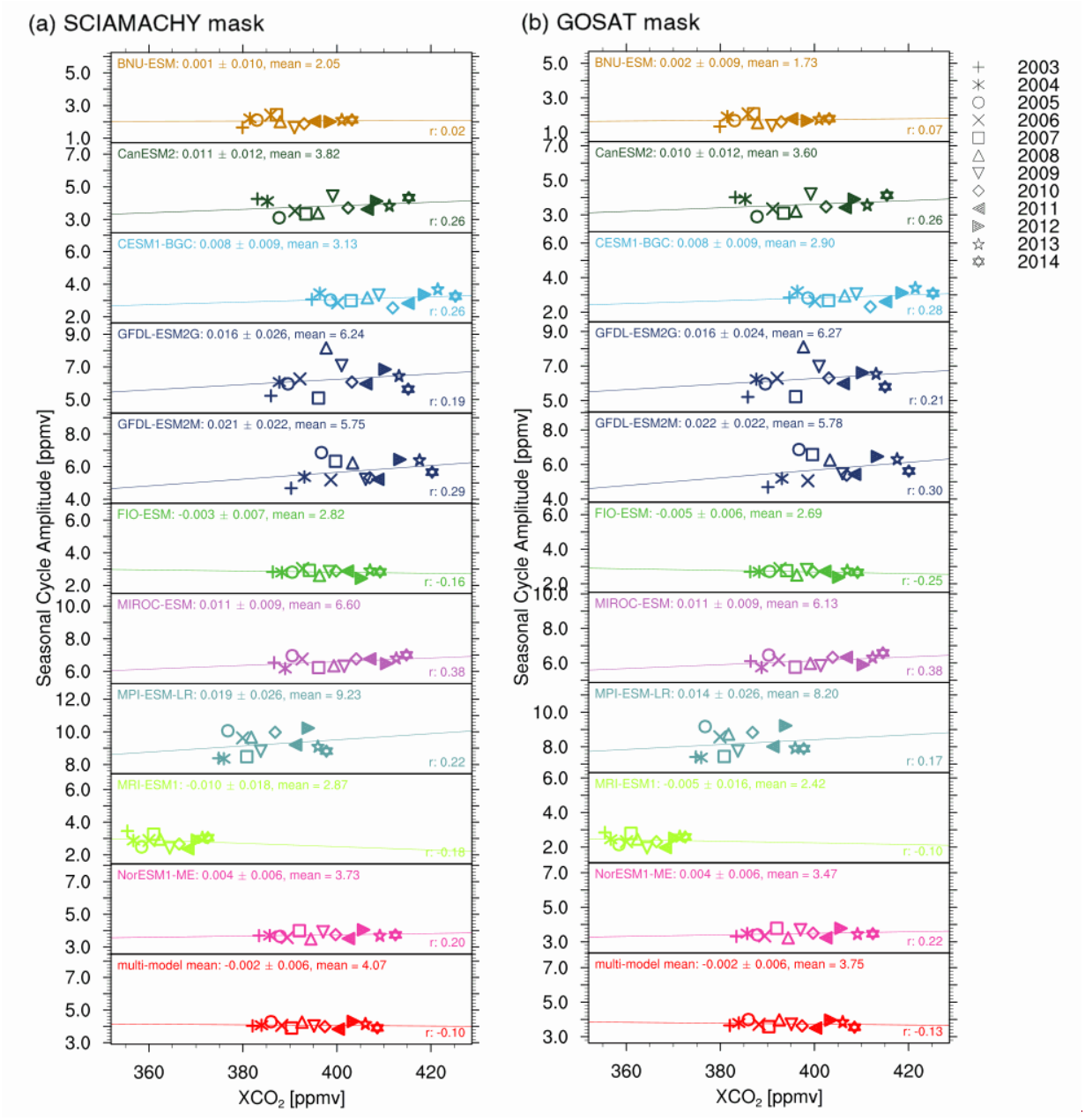
(a) SCIAMACHY mask
(b) GOSAT mask
BNU-ESM: 0.001 ± 0.010, mean = 2.05
r: 0.02
CanESM2: 0.011 ± 0.012, mean = 3.82
r: 0.26
CESM1-BGC: 0.008 ± 0.009, mean = 3.13
r: 0.26
GFDL-ESM2G: 0.016 ± 0.026, mean = 6.24
r: 0.19
GFDL-ESM2M: 0.021 ± 0.022, mean = 5.75
r: 0.29
FIO-ESM: -0.003 ± 0.007, mean = 2.82
r: -0.16
MIROC-ESM: 0.011 ± 0.009, mean = 6.60
r: 0.38
MPI-ESM-LR: 0.019 ± 0.026, mean = 9.23
r: 0.22
MRI-ESM1: -0.010 ± 0.018, mean = 2.87
r: -0.18
NorESM1-ME: 0.004 ± 0.006, mean = 3.73
r: 0.20
multi-model mean: -0.002 ± 0.006, mean = 4.07
r: -0.10
BNU-ESM: 0.002 ± 0.009, mean = 1.73
r: 0.07
CanESM2: 0.010 ± 0.012, mean = 3.60
r: 0.26
CESM1-BGC: 0.008 ± 0.009, mean = 2.90
r: 0.28
GFDL-ESM2G: 0.016 ± 0.024, mean = 6.27
r: 0.21
GFDL-ESM2M: 0.022 ± 0.022, mean = 5.78
r: 0.30
FIO-ESM: -0.005 ± 0.006, mean = 2.69
r: -0.25
MIROC-ESM: 0.011 ± 0.009, mean = 6.13
r: 0.38
MPI-ESM-LR: 0.014 ± 0.026, mean = 8.20
r: 0.17
MRI-ESM1: -0.005 ± 0.016, mean = 2.42
r: -0.10
NorESM1-ME: 0.004 ± 0.006, mean = 3.47
r: 0.22
multi-model mean: -0.002 ± 0.006, mean = 3.75
r: -0.13
Seasonal Cycle Amplitude [ppmv]
XCO2 [ppmv]
2003
2004
2005
2006
2007
2008
2009
2010
2011
2012
2013
2014

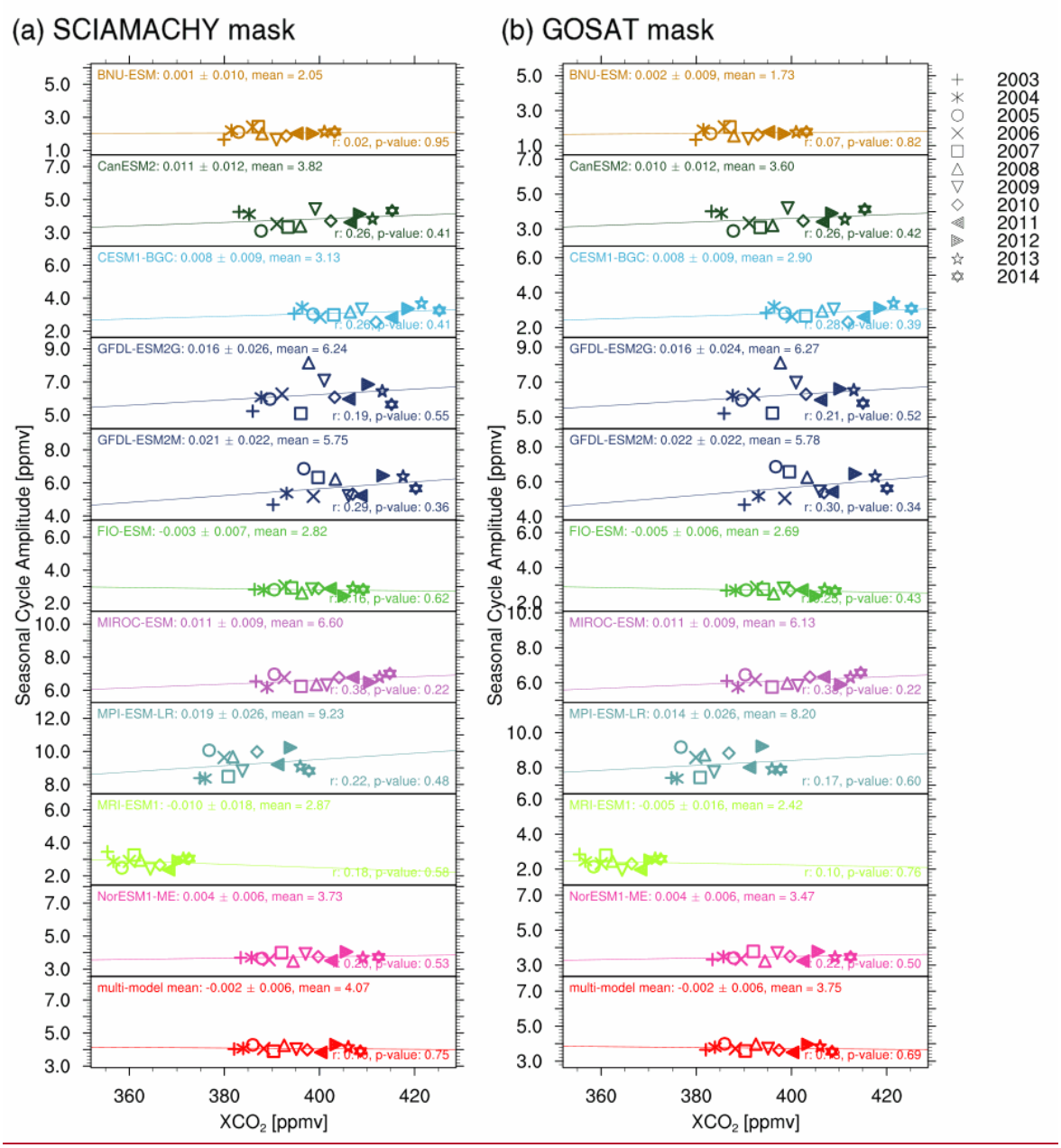

Figure B2: Same as Figure B1, but with CMIP5 models masked using (a) the SCIAMACHY mask and (b) the GOSAT mask, with the masks derived from Figure ~~98~~, masking out points with less than 50% coverage in those time periods.

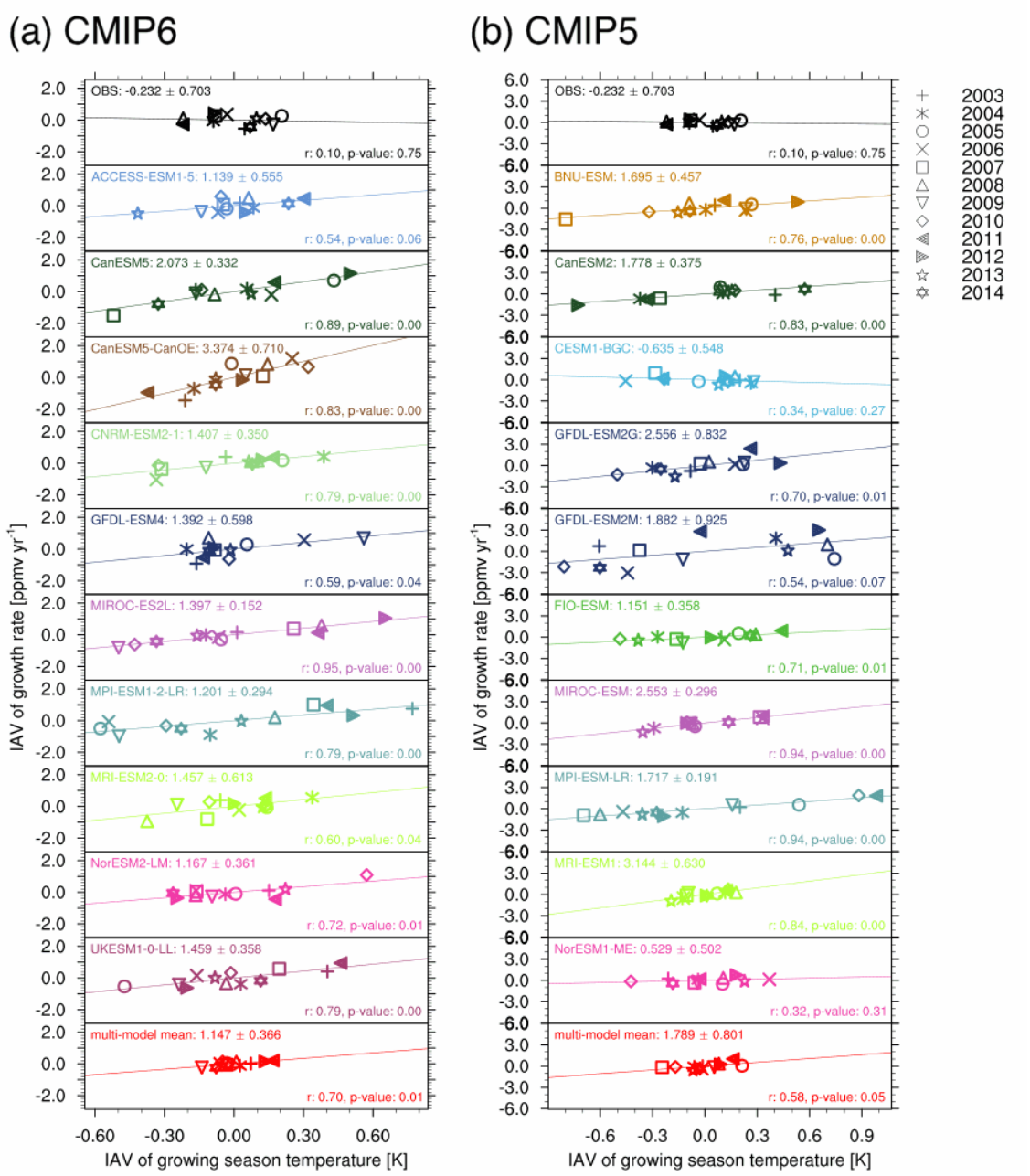

Figure C1: Sensitivity of the interannual variability of the XCO_2 growth rate in the tropics (30° S–30° N) to the interannual variability of tropical growing season temperature for CMIP6 models (a) and CMIP5 models (b). The observational temperature taken from the GIStemp temperature anomaly map, while the models use their own simulated temperature. A linear regression is performed on the data for each dataset. Model colors are the same as in Figure 3, and symbols denote the years. In the top left of each panel the regression coefficient and its uncertainty is shown, while the bottom right states the Pearson correlation coefficient and p-value.